

Floating Gate Metal-Oxide-Semiconductor Based Gas Sensor

By

Md. Obaej Tareq

A thesis submitted to the faculty of graduate studies of the University of Manitoba in partial fulfilment of the requirements of the degree of

Masters of Science

Department of Electrical and Computer Engineering

University of Manitoba

Winnipeg

Abstract

A semiconductor based gas sensor was developed by integrating a gas sensitive polymer with a floating-gate metal-oxide-semiconductor (FGMOS). The integration of the gas sensitive polymer with a semiconductor device enables the design of a large sensor array in a single chip for electronic sensing application. A new FGMOS structure was designed to reduce the number of post-processing steps during electrochemical polymer deposition. In this new design, the top metal layer of a standard CMOS process was used as an extended sensor pad which was connected to the floating gate. A sensor chip was designed using a standard 0.35 μm CMOS process. A polymer film was selectively deposited on the top metal layer (sensor pad) of a FGMOS using two post processing steps. The sensor response was measured by exposing the sensor in different concentration of water and methanol vapor. A short pulse measurement technique was introduced to measure the sensor response which was not affected by the measurement parameters.

Acknowledgements

First and foremost, I would like to express my deep sense of gratitude to my supervisor, Dr. Douglas A. Buchanan for his thoughtful guidance, patience supervision and encouragement. Without his support, it would be impossible for me to come this far in my research. His critical thinking ability and scientific approaches of thinking helped me to overcome many issues during my research and thesis writing. I learned a lot from him both in academic and personal level. I hope this help me in my future career.

I would like to sincerely thank Dr. Freund for his valuable suggestions and advice during my work with polymer deposition and sensor characterization. His post-doctoral fellow Dr. M Ramesh Kumar and PhD student, Akin Iyogun were always there to help me with any problem during polymer deposition. I want to thank both Dr. Ramesh and Akin Iyogun for their support.

The research work was supported by Natural Science and Engineering Research Council of Canada (NSERC), the Canadian Foundation of Innovation (CFI) and Canadian Microelectronics Corporation (CMC).

I would also like to appreciate Dr. Douglas J. Thomson, for his valuable suggestion and time during the sensor characterization. Our cleanroom supervisor Dwayne Chrusch helped me a lot during my cleanroom work. Our lab technician Daryl Hamelin was always there wherever I have some problem with any equipment software. Our information system coordinator Guy Jonatschick helped me a lot during my chip design and software problems. I want to thank them all for all their support.

I would also like to thank our graduate student advisor Amy Dario. During my time here in campus, she was always nice, helpful, and supportive with any issue. I also want to thank all my friends and colleagues for their support and make life enjoyable here.

I want to thank my parents and brother, who was always there for me. Finally I want remember my elder sister. Without her encouragement and support I would not be here today. I miss her every day in my life.

Table of Contents

Abstract.....	I
Acknowledgements.....	II
Table of Contents.....	IV
List of Figures.....	VII
List of Tables.....	XIV
List of Symbols.....	XV
List of Abbreviation and Acronyms.....	XVII
1 Introduction.....	1
1.1 Motivation.....	1
1.2 Thesis Outline.....	4
2 Chapter 2 – Floating Gate Metal Oxide Semiconductor (FGMOS).....	7
2.1 Charge Injection.....	9
2.1.1 Fowler-Nordheim Tunnelling.....	9
2.2 Effect of Floating Gate Charge on FGMOS.....	11
2.3 Charge Erasure from the Floating Gate.....	14

3	Chapter 3 – Design of a FGMOS Gas Sensor	16
3.1	New FGMOS Sensor Design.....	17
3.2	Modeling of a FGMOS Sensor.....	18
3.3	Design of a Sensor Array.....	25
3.3.1	Output Amplifier.....	28
4	Chapter 4 – FGMOS Sensor Characterization	31
4.1	Charge Injection onto the Floating Gate.....	31
4.2	Removing Charge from the Floating Gate.....	33
4.3	I-V Measurement Results	34
4.4	Scanning Electron Microscope (SEM) image of the FGMOS Cross section .	38
5	Chapter – 5 Post Processing	40
5.1	Electroless Gold Disposition	42
5.2	Gold Deposition Using Lift-Off	45
5.3	Polymer Deposition	47
6	Chapter 6 – Sensor Characterization	50
6.1	Sensor Response without any Polymer on the Sensor Pad.....	50
6.2	I-V Characteristics of Sensors	52

6.2.1 I-V Measurement Setup	54
6.2.2 I-V Measurement Results.....	55
6.3 Time and Field Dependent Sensor Response	60
6.3.1 Measurement Steps and Results.....	60
6.3.2 Pulse Measurement	63
6.3.3 I_{DS} Measurement as a Function of Pulse Interval	66
6.3.4 I_{DS} Measurement as a Function of Pulse Width.....	68
6.4 Short Pulse Measurement	71
6.4.1 Short Pulse Measurement Setup	71
6.4.2 Short Pulse Measurement Results.....	72
6.5 Sensor Characterization using a Short Pulse	74
6.6 Electrical Refreshing	77
6.7 Pulse Measurement with Electrical Refreshing.....	79
6.8 Sensor Responses in Continuous, Reverse and Random Order	82
7Chapter 7 – Conclusions and Future Work	84
7.1 Future work.....	85
References.....	88

List of Figures

Figure 1.1. Schematic structure of a (a) Metal-oxide-semiconductor field effect transistor (MOSFET) and (b) Floating gate metal oxide semiconductor.	3
Figure 2.1. Schematic diagram of a floating gate metal oxide semiconductor (FGMOS).....	7
Figure 2.2. Energy band diagram of FN tunnelling in a floating gate FET.	10
Figure 2.3. Schematic view of an equivalent capacitance model of a FGMOS.	12
Figure 2.4. The FGMOS threshold voltage shifts from V_{TH1} to V_{TH2} after charge tunnelling.....	14
Figure 2.5. Energy band diagram of charge erasing in a FGMOS.	15
Figure 3.1. Schematic view of a FGMOS sensor with an extended sensor pad. The “poly1” (poly crystalline silicon) is used as a metallic floating gate and is extended to act as a sensor pad.....	16
Figure 3.2. Schematic design of a FGMOS sensor. In this design, the top metal layer is used as a sensor pad and connected to the floating gate.	18
Figure 3.3. Schematic diagram of a capacitive equivalent model of a FGMOS sensor.	19

Figure 3.4. (a) Floating gate charge density (Q_{FG}) vs. the threshold voltage (V_{CGTH}).
(b) Floating gate charge density (Q_{FG}) vs. source- drain saturation current (I_{dsat}).
.....22

Figure 3.5. The control gate vs the source-drain current for different charge density on
the floating gate.23

Figure 3.6. (a) The total capacitance C_T vs. the threshold voltage (V_{CGTH}). (b) The
total capacitance C_T vs. source- drain saturation current (I_{dsat}).24

Figure 3.7. The control gate vs the source-drain current for different sensor pad
capacitance.25

Figure 3.8. The layout design of a FGMOS sensor with analog buffers for control gate
and floating gate voltage.26

Figure 3.9. A test sensor chip with n and p type 2D sensor array. The total chip size is
2 mm \times 4 mm.27

Figure 3.10. Schematic presentation of array addressing circuits of a sensor array. The
column and row addressing is used to select the individual device in the array.
The analog buffer is turned on by the addressing circuits and enables to apply an
analog voltage on the control gate and the floating gate.28

Figure 3.11. Output amplifier circuits of a sensor array. This amplifier converts the
 I_{DS} current of the FGMOS into a corresponding voltage scale.29

Figure 3.12. Output amplifier response of a sensor array. The input current range of the amplifier is 10^{-6} A to 10^{-10} A which produce a output voltage change from 0.7 V to 2.2 V	30
Figure 4.1. Ideal charge injection operation of a FGMOS sensor (a) n-type (b) p-type FGMOS.	32
Figure 4.2. Ideal I-V response of a FGMOS sensor response after charge injection onto the floating gate.	33
Figure 4.3. Ideal charge removing operation of a (a) n-type (b) p-type FGMOS.....	34
Figure 4.4. Ideal I-V response of a FGMOS sensor response after removing charge from the floating gate.	34
Figure 4.5. I_{DS} vs. V_{CG} measurement for a n-type FGMOS with a constant bias on the drain ($V_D = 1$ V) and sweeping the control gate voltage from 0 V to 20 V. a) Initial I-V measurement, b) I-V after applying $V_{CG} = +20$ V and $V_D = V_S = V_{SUB} = -10$ V, c) I-V after applying $V_{CG} = -20$ V and $V_D = V_S = V_{SUB} = +10$ V.....	35
Figure 4.6. I_{DS} vs. V_{CG} measurement for a p-type FGMOS with a constant bias on the drain ($V_D = -1$ V) and sweeping the control gate voltage from 0 V to -20 V. a) Initial I-V measurement, b) I-V after applying $V_{CG} = -20$ V and $V_D = V_S = V_{SUB} = +10$ V, c) I-V after applying $V_{CG} = +20$ V and $V_D = V_S = V_{SUB} = -10$ V.....	36
Figure 4.7. Expected charge removing from the floating gate onto the control gate during the ideal charge injection operation, (a) n-type and (b) p-type FGMOS	37

Figure 4.8. Charge injection from the control gate onto the floating gate, (a) n-type and (b) p-type FGMOS.....	38
Figure 5.1. Electrochemical polymer deposition on aluminum sample. The thickness of the aluminum was ~700 nm.	41
Figure 5.2. Aluminum sample, (a) after electroless gold deposition. (b) after electrochemical polymer deposition. Each aluminum strip was 100 μm wide and 100 μm spaced.....	43
Figure 5.3. Sensor chip after immersion gold and electrochemical polymer deposition.	44
Figure 5.4. An optical microscope image of a sensor chip after gold deposition using lift-off process.	47
Figure 5.5. Image of a FGMOS sensor after depositing sensing polymer (Polypyrrole) on the sensor pad.	48
Figure 5.6. I-V Characterization of FGMOS sensor before and after gold and polymer deposition. The control gate voltage was swept from 0V to 10 V with the drain was biased with a constant 1 V.....	49
Figure 6.1. I-V response of a FGMOS without any sensing polymer. The sensor was exposed to 25% H_2O and I-V responses were measured after every 10 minutes.	51

Figure 6.2. The I_{DS} current response of a FGMOS without any polymer on the sensor pad. The sensor was exposed to 50% methanol for 200 minutes. The I_{DS} response was measured using a short pulse of 0.5 second after every 5 minutes interval. The device was biased with $V_{CG} = 5$ V and $V_D = 1$ V during the 0.5 second pulse.....52

Figure 6.3. I-V measurement setup (S=Source, D=Drain, G=Control gate, Su=Substrate).55

Figure 6.4. Sensor response with 400 sccm N_2 flowing. Each curve was measured following a 10 minutes time interval.....57

Figure 6.5. I-V sensor response for a range of water vapour concentration, 5% - 25% in nitrogen. Each measurement was made after a 30 minutes exposure.58

Figure 6.6. I-V sensor response for a range of methanol vapour concentration, 5% - 25% in nitrogen. Each measurement was made after a 30 minutes exposure....59

Figure 6.7. Sensor response for water and methanol flow for 10 hours. Sensor responses were continuously measured throughout the measurement duration with a constant potential on the control gate ($V_{CG} = 5$ V) and drain ($V_D = 1$ V).62

Figure 6.8. (a) Measurement voltage pulse 0.5 second every 2 minutes ($V_{CG} = 5$ V and $V_D = 1$ V) (b) I_{DS} response for 300 sccm N_2 and 100 sccm for H_2O or CH_3OH64

Figure 6.9. (a) Applied pulse schematic with a constant pulse width (0.5 second) and the pulse interval ranging from 1, 2, and 5 minutes. (b) I_{DS} response for pulse voltage during exposure to 25% CH_3OH (100 sccm) and N_2 (300 sccm).....67

Figure 6.10. (a) Pulse measurement with increasing pulse width from 0.5, to 30 and 60 seconds with 2 minutes pulse interval. (b) I_{DS} response for 25% CH_3OH (100 sccm) with N_2 (300 sccm) exposures.69

Figure 6.11. Measurement setup for short pulse measurement.72

Figure 6.12. Short pulse measurement using 20 μ s, 40 μ s and 60 μ s pulse width and 2 minutes pulse interval.....73

Figure 6.13. Pulse measurement with 10%-50% methanol exposure with 10% increase in concentration.76

Figure 6.14. The sensor response (a) after 2 hours N_2 exposure (reference response), (b) after 30% methanol exposure, (c) After electrical refreshing with high control gate biasing.....78

Figure 6.15. Electrical refreshing by applying a constant high voltage on the control gate ($V_{CG}=30$ V) for 10 seconds.....79

Figure 6.16. Repeated sensor response from 10% to 50% CH_3OH in N_2 with 10% increment in the concentration. After each exposure the sensor was electrically refreshed.81

Figure 6.17. The gas concentration was changed in continuous order, the random order and reverse order.....83

Figure 7.1. Scanning electron microscope (SEM) image of the FGMOS cross section.
.....102

List of Tables

Table 2.1. Capacitance Equivalent Circuit Symbols.	12
Table 3.1. Design specification of the FGMOS sensor using TSMC 0.35 μ m technology.....	18
Table 5.1. Sputtering parameters for Titanium and gold deposition	46
Table 6.1. Comparison of the I_{DS} response between the ramped (after exposure) and pulsed (during exposure) measurement after a 30 minutes analyte exposure.	65

List of Symbols

Symbol	Description	Unit
m_{ox}^*	Electron effective mass	kg
ϕ_B	Interfacial barrier height	V
h	Planck's constant ($=6.626 \times 10^{-34} \text{Js}$)	Js
μ_{eff}	Effective carrier mobility	$\text{cm}^2/(\text{Vs})$
J_{FN}	Current density of the floating gate	A/cm^2
E	Electric field	MV/cm
$Q(t)$	Charge density on the floating gate	C/cm^2
C_{FC}	Capacitance between the control gate and the floating gate.	F
C_{FSUB}	Capacitance between the floating gate and the substrate,	F
C_{FD} and C_{FS}	Floating gate overlap capacitance	F
C_{CD} and C_{CS}	Gate overlap capacitance for the control gate	F
C_{PSUB}	Sensor pad capacitance	F
C_{T}	Total Capacitance	F/cm^2
V_{D}	Drain voltage	V
V_{S}	Source voltage	V
V_{SUB}	Substrate voltage	V
V_{CG}	Control gate voltage	V
V_{FG}	Floating gate voltage	V
Q_{FG}	Charge on the floating gate	C/cm^2

V_{FG}^{TH}	Threshold voltage with respect to floating gate	V
V_{CG}^{TH}/V_{TH}	Threshold voltage of the FGMOS	V
d1	Thickness of the ILD1 layer	μm
d2	Thickness of the ILD2 layer	μm
I_{DSAT}	Source-drain current at saturation	A

List of Abbreviation and Acronyms

CHEMFET	Chemical field effect transistor
SAW	Surface acoustic wave
CMOS	Complementary metal–oxide–semiconductor
FET	Field effect transistors
ISFET	Ion sensitive field effect transistors
WF-FET	Work function field effect transistors
MOSFET	Metal-oxide field-effect transistor
FGMOS	Floating gate metal-oxide-semiconductor
nMOS	n-type metal-oxide-semiconductor
pMOS	p-type metal-oxide-semiconductor
I-V	Current-Voltage
ILD	Inter-layer dielectric
CHE	Channel hot electron
FN	Fowler-Nordheim
TSMC	Taiwan Semiconductor Manufacturing Company
CMC	Canadian Microelectronics Corporation
UV	Ultra-violet
PPy	Polypyrrole

Introduction

1.1 Motivation

The sense of smell is a unique ability of humans and animals to perceive odors. This sense is so deeply rooted in human memory that this often dominates in our decision making process. In traditional food, beverage, cosmetic and tobacco industries, specially trained people determine the quality and taste of a product. This requires a large number of specially trained people to maintain the production quality and increases the production cost. Moreover, each person has a different sensitivity level for sensing the smell of an individual product. In the past several decades, researchers have been trying to design different types of chemical and electrical sensors to replace the human nose in many industrial applications. These types of sensors are often referred to as “Electric Nose” or “E-Nose”.

In the recent years, various types of devices for the sensing of individual chemicals have been investigated [1]. Several types of sensing concepts have been proposed using different types of sensing techniques for “E-Nose” applications. Among them, semiconductor based sensors have drawn particular interest for “sensor on chip” applications [2]. This type of sensor is more attractive because of their distinctive advantages, which include their small size, inexpensive fabrication and possible integration into a large sensor array. Especially, with the rapid advancement in semiconductor technology, these “sensor on chip” have become more realizable for “E-Nose” applications.

The physical and electrical properties of some polymers change in the presence of a gas or liquid analyte. In a resistive sensor, the analytes change the conductivity of the sensing polymers while in a capacitive sensor, the dielectric properties of the sensing polymers change [3,4]. With a surface acoustic wave (SAW) sensor, the sensing chemical absorbs the analytes molecules and changes the wave impedance of the device [5]. In a chemical transistor (CHEMFET), the chemical reaction between the sensing material and the analyte alters the charge density on the gate and produces a response by changing the source-drain (I_{DS}) current of the transistor [6]. Although different types of chemical sensors exist, recently CHEMFET chemical sensors have drawn particular interest because of their smaller size, lower production cost and their ability to be integrated with standard complementary metal–oxide–semiconductor (CMOS) process. Many sensor designs have been proposed that were based on a different CMOS device structure. These types of sensors like ion sensitive field effect transistors (ISFET), work function field effect transistors (WF-FET) and floating gate MOS sensors (FGMOS) have been investigated [7,8] and have shown significant development in electric sensors for e-nose applications. In an ISFET and WF-FET sensor, the gate material is replaced by a sensing polymer, which is not compatible with the silicon based fabrication process. However, FGMOS based sensors have no such limitation. The sensing polymer is deposited on the prefabricated sensor using several post processing steps. These types of sensors have been studied for e-nose application in recent years [9].

A metal–oxide–semiconductor field-effect transistor (MOSFET) is a four terminal device with a source (S), drain (D), gate (G) and substrate (Sub) as shown in Figure 1.1 (a). The top metallic gate (G) is isolated from the substrate by an insulating

layer. The potential applied to the gate (G) induces a conducting channel between the source and drain. The channel can contain electrons (nMOS) or holes (pMOS). The minimum gate voltage, required to create a conducting channel between the source and drain, is the “turn-on” voltage and is defined as the threshold voltage (V_{TH}). A floating-gate metal oxide semiconductor (FGMOS) is a standard MOSFET with an additional “floating” gate between the top gate (G) and the substrate. A schematic diagram of a FGMOS is shown in Figure 1.1 (b).

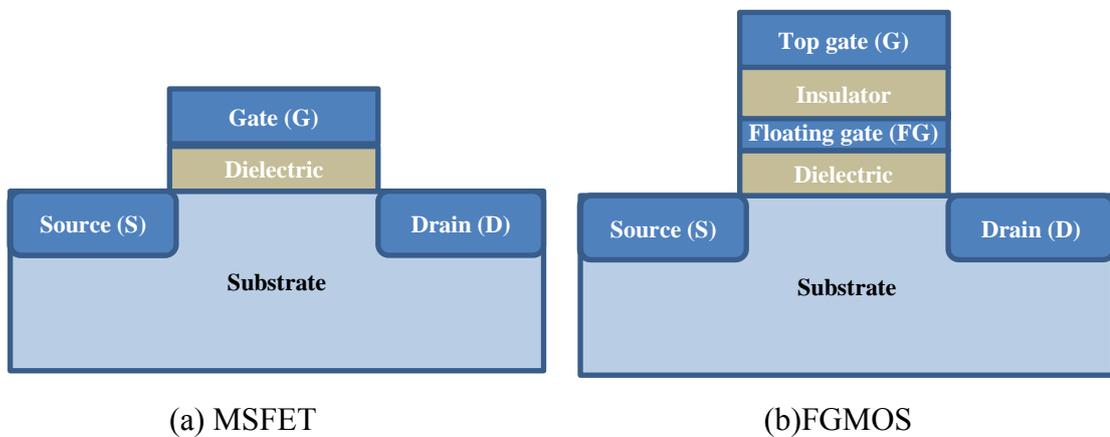


Figure 1.1. Schematic structure of a (a) Metal-oxide-semiconductor field effect transistor (MOSFET) and (b) Floating gate metal oxide semiconductor.

The floating gate (FG) is electrically isolated from the top gate (G) and from the substrate. As such its potential “floats” between the top gate and the substrate. During the device operation, a change in the charge density on the floating gate alters the electric field in the substrate, causing a shift in the threshold voltage and a change in the source-drain current of the FET. This device can be used for sensor applications if the change in the floating gate charge is initiated by exposure of a specific gas or liquid analyte. Several sensor structures have been proposed using the basic FGMOS

structure [9–12]. However, most of these sensors have been used to detect liquid analytes. Very few of these devices have been used as a gas sensor with a well-defined, standard CMOS-based device structure [13,14]. In most of these designs, the floating gate is exposed to the analyte by directly extending the floating gate from the gate region. However, in a standard CMOS process, the floating gate is buried under a thick oxide layer and requires additional post processing to expose the floating gate extension [15]. In the past several years, some designs have been proposed to increase the sensitivity by introducing new design ideas [14,16].

In this research, a new FGMOS based gas sensor has been proposed that utilizes a commercially available CMOS process. This sensor was designed to minimize the number of post processing steps, following the silicon chip fabrication. Each individual sensor is small, of the order of microns, which enables the design of a large sensor array. Different types of polymers can be selectively deposited on each sensor in the array to sense different types of volatiles using a single sensor chip.

1.2 Thesis Outline

The FGMOS is a charge sensitive device [17]. To understand the effect of charge on the FGMOS characteristic, the study of charge tunnelling mechanism is essential. The basic structure and working principle of a FGMOS are presented in Chapter 2. Fowler-Nordheim charge tunneling is introduced and studied to understand the charge injection, erasing and charge storage operation of a FGMOS. The schematic capacitive model of a FGMOS device is also presented in this chapter.

The design of a FGMOS as a sensor device is introduced in Chapter 3. The necessary structural changes of a FGMOS for sensor application are presented. The schematic capacitive model of a FGMOS sensor is introduced. A charge sharing mechanism is studied using this model. A mathematical model is presented to demonstrate the relationship between the floating gate charge and the source-drain current. Another model is presented to show the relationship between the source drain current and capacitance. Finally, the sensor chip and required driving circuits and output amplifier are presented in this chapter.

The FGMOS devices are most commonly used in semiconductor based memory applications. In a FGMOS memory device, charge is injected onto the floating gate. These injected charge shifts the threshold voltage and the source-drain current of the device. The basic structure and working principle of a FGMOS based memory device and sensor are similar. In a FGMOS sensor, charge is expected to be introduced onto the floating gate by exposing to a gas analyte. The effects of change on the FGMOS sensors were investigated by electrically injecting and removing charge onto the floating gate and are presented in Chapter 4. The source-drain current was measured after tunnelling charge onto the floating gate and after removing that charge from the floating gate.

Following an understanding of the behaviour of the FGMOS device under the controlled injection and removal of charge, the FGMOS was tested as a sensor. To act as a sensor, the sensing polymer needs to be deposited on the sensor pad of the FGMOS. Several post processing steps are required to deposit the sensing polymer on the sensing pad. The electrochemical polymer deposition process is well documented

and very selective deposition technique. Therefore, this technique was tested and is presented in Chapter 5. Initially, the direct electrochemical deposition of polymer on the sensor pad was tested. Then, a thin layer of gold was deposited on the sensor pad. Two gold deposition techniques were performed and results are presented in this chapter. Finally, the polymer was selectively deposited using the electrochemical process on the gold coated sensor pad and details are presented in this chapter.

Following the post processing steps to deposit sensing polymer on the FGMOS, the sensor was characterized as a sensor by exposing to different analyte gases and results are presented in Chapter 6. The I-V sweep (measure the source-drain current with increasing gate voltage) measurements were performed to observe any threshold voltage and I_{DS} current shift due to the gas exposure. Several experiments were performed to observe the time and field dependent sensor response. These experiments provided the proper measurement parameters that were required to measure the actual sensor responses. Finally, the sensor responses were measured using a short pulse and exposing in increasing, decreasing and random order of gas concentration and results are presented in this chapter.

In the last chapter, this work is summarized and conclusions are presented. Based on the measurement results, a guideline is presented for future work.

Chapter 2 – Floating Gate Metal Oxide Semiconductor (FGMOS)

The floating gate metal oxide semiconductor (FGMOS) device was first introduced by D. Kahng and S.M. Sze in 1967 for application as a non-volatile memory cell [17]. The basic structure of an n-type FGMOS device is shown in Figure 2.1. In this figure, “metal1” and “metal2” are two “metallic” gates that are separated by a thick insulating layer (ILD2). In the present work, the upper gate ‘metal2’ is referred to as the ‘control gate’. Beneath ILD2, the “floating gate” (metal1) is separated from the substrate by a thin insulating layer (ILD1). Since metal1 is electrically isolated from both the substrate and metal2, it is referred to as the floating gate and this device is therefore called as a floating gate metal-oxide-semiconductor (FGMOS).

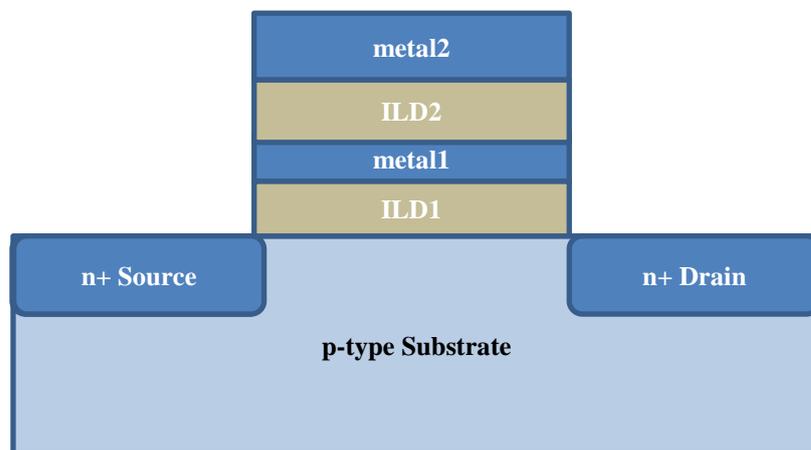


Figure 2.1. Schematic diagram of a floating gate metal oxide semiconductor (FGMOS).

To act as a memory device, the FGMOS may be operated in three distinct operational modes, (1) writing (tunneling charge onto the floating gate), (2) reading (measure source-drain current at a fixed bias condition, or sense device threshold voltage) and (3) erasing (removing charge from the floating gate). During the charging operation, charge is injected from the substrate through the thin gate oxide layer onto the floating gate. The injected charge shifts the threshold voltage of the device which results in a significant change in the source-drain current, either or both of which may be sensed during a “read” operation. The charge state of the FGMOS is typically measured by biasing the device in the sub-threshold region with the appropriate control gate, source, drain and substrate voltages and measuring the source-drain current of the device. The charge stored on the floating gate may be removed or erased via the same injection mechanism with an opposite biasing voltage on the control gate, source, drain and substrate.

In a FGMOS sensor, a layer of sensing polymer may be deposited on the floating gate to perform as a sensor. This polymer interacts with the analyte gases and produces a change of the potential on the floating gate or permittivity of the polymer while the sensor is exposed to the analyte gases. In an ideal case, any change in the charge or the capacitance on the floating due to analyte exposure alters the threshold voltage and causes a shift in the source-drain current. As such, the operation of a FGMOS sensor device is similar to a FGMOS memory device. In this work, the operation of a FGMOS memory device has been studied to enable the design of a FGMOS based sensor.

2.1 Charge Injection

Several injection mechanisms have been developed to introduce charge onto the floating gate of a FGMOS device. For a typical FGMOS, channel hot electron tunnelling (CHE) or Fowler-Nordheim tunnelling (FN tunnelling) are widely used to inject charge onto the floating gate [18]. In Channel Hot Electron (CHE) tunneling, a lateral high electric field between the source and drain is created by applying a high potential difference between the source and drain. When this lateral electric field becomes high due to the applied potential and reaches approximately 100 KV/cm [19], electrons gain enough energy from the applied field such that they no longer 'reside' at the bottom of the conduction band. In this condition electrons are referred to as "hot electron". Some electrons may gain enough energy to surmount oxide barrier height. Due to transverse electric field between the substrate and gate arising from the applied gate bias, those hot electrons may tunnel through the thin oxide layer and become trapped onto the floating gate. However, the presence of such carriers in the oxide, may trigger physical damages in the oxide and can reduce the device lifetime [20]. In this work, the effect of placing charge on the floating gate was investigated by injecting charge on the floating gate using FN tunneling.

2.1.1 Fowler-Nordheim Tunnelling

In semiconductor devices, band diagram are often used to explain tunnelling mechanisms. An energy band diagram represents the band structure of energy versus distance of the device. The energy band diagram of an n-type FGMOS during FN tunnelling is shown in Figure 2.2 [17]. In this figure, d_1 is the gate oxide thickness between the substrate and the floating gate (ILD1). The floating gate and the control

gate are separated by a thick (d_2 in Figure 2.2) inter layer dielectric (ILD2) material. In a FGMOS memory device, Fowler-Nordheim tunnelling (FN tunnelling) may occur when electrons from the substrate tunnel through the top portion of the oxide potential barrier onto the floating gate.

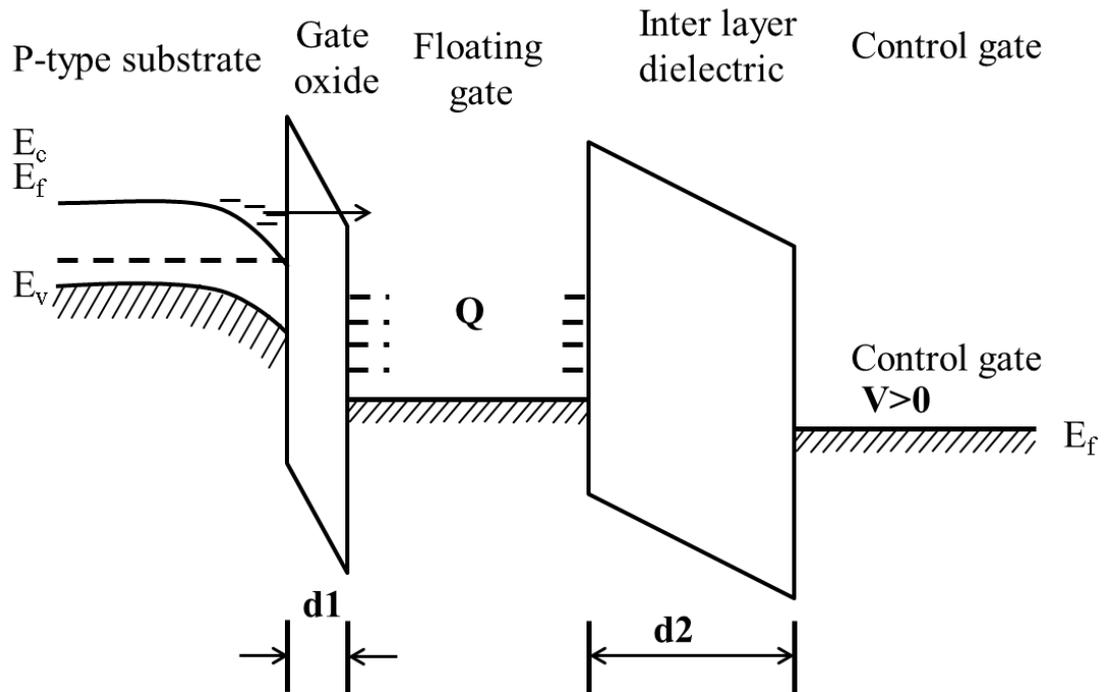


Figure 2.2. Energy band diagram of FN tunnelling in a floating gate FET.

When a high positive potential is applied to the control gate (metal2), electrons (Q) from the substrate may gain significant energy and tunnel through a triangular barrier of the oxide potential barrier. The carrier in the semiconductor induces an opposite image charge in the metal and reduces the barrier height. In the simplest case, when the effects of the temperature (kT) and image force barrier lowering are ignored, the FN tunnelling current density, J_{FN} , is given by [21],

$$J_{FN} = AE^2 \exp(-B/E) \quad (2.1)$$

where $A = \frac{q^3}{16\pi^2 h^2 \phi_B}$ and $B = \exp[4(2m_{ox}^*)^{1/2} \phi_B^{3/2} / 3hq]$

and m_{ox}^* is the electron effective mass, ϕ_B is the interfacial barrier height and h is Planck's constant. The electrons, which tunnel through the gate oxide, reside on the floating gate. The stored charge on the floating gate Q_{FG} , as a function of time, is given by [21]

$$Q_{FG}(t) = \int_0^t J_{FN} dt \quad (2.2)$$

For a constant electric field E , the current density remains the same and the charge density on the floating gate increases with time.

2.2 Effect of Floating Gate Charge on FGMOS

To model the potential, and charge distribution on a FGMOS device, a capacitive equivalent circuit of a FGMOS device was used and is shown in Figure 2.3.

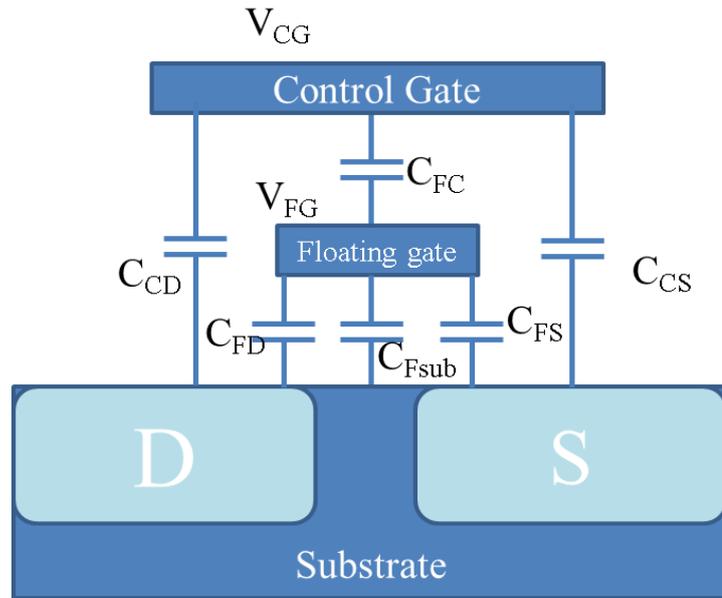


Figure 2.3. Schematic view of an equivalent capacitance model of a FGMOS.

Table 2.1. Symbols used in the capacitance equivalent model of a FGMOS.

C_{FC}	Capacitance between the control gate and the floating gate
C_{Fsub}	Capacitance between the floating gate and the substrate
C_{FD} and C_{FS}	Floating gate overlap capacitance
C_{CD} and C_{CS}	Gate overlap capacitance for the control gate
V_D	Drain voltage
V_S	Source voltage
V_{SUB}	Substrate voltage
V_{CG}	Control gate voltage
V_{FG}	Floating gate voltage

The net charge on the floating gate may be related to the capacitances connected with the floating gate and the voltage across those capacitances [22] and may be given by,

$$Q_{FG} = C_{FC}(V_{FG} - V_{CG}) + C_{FSUB}(V_{FG} - V_{SUB}) + C_{FD}(V_{FG} - V_D) + C_{FS}(V_{FG} - V_S) \quad (2.3)$$

Under typical operating conditions, the source is set to $V_S = 0$ V and the substrate is grounded. The control gate and the floating gate voltages can be calculated using equation (2.3) and can be expressed as [22],

$$V_{CG} = \frac{1}{C_{FC}}(C_T V_{FG} - C_{FD} V_D - Q_{FG}) \quad (2.4)$$

$$V_{FG} = \frac{1}{C_T}(C_{FC} V_{CG} + C_{FD} V_D + Q_{FG}) \quad (2.5)$$

where, $C_T = C_{FC} + C_{FSUB} + C_{FS} + C_{FD}$.

The threshold voltage of a FGMOS can be expressed as [22],

$$V_{CG}^{TH} = \frac{1}{C_{FC}}(C_T V_{FG}^{TH} - C_{FD} V_D - Q_{FG}) \quad (2.6)$$

$$\Delta V_{CG}^{TH} \approx \frac{\Delta Q_{FG}}{C_{FC}} \quad (2.7)$$

where V_{FG}^{TH} is the threshold voltage with respect to the floating gate and V_{CG}^{TH} is the threshold voltage of the FGMOS. All the capacitances in Equation (2.6) are constant and are related to the design of the device. Only the charge on the floating gate changes and it is that change which shifts the threshold voltage of the FGMOS. An example of a shift in the threshold voltage is shown in Figure 2.4. In this figure, when the floating gate charge state is changed (ΔQ_{FG}) the threshold voltage of the FGMOS is shifted from V_{TH1} to V_{TH2} .

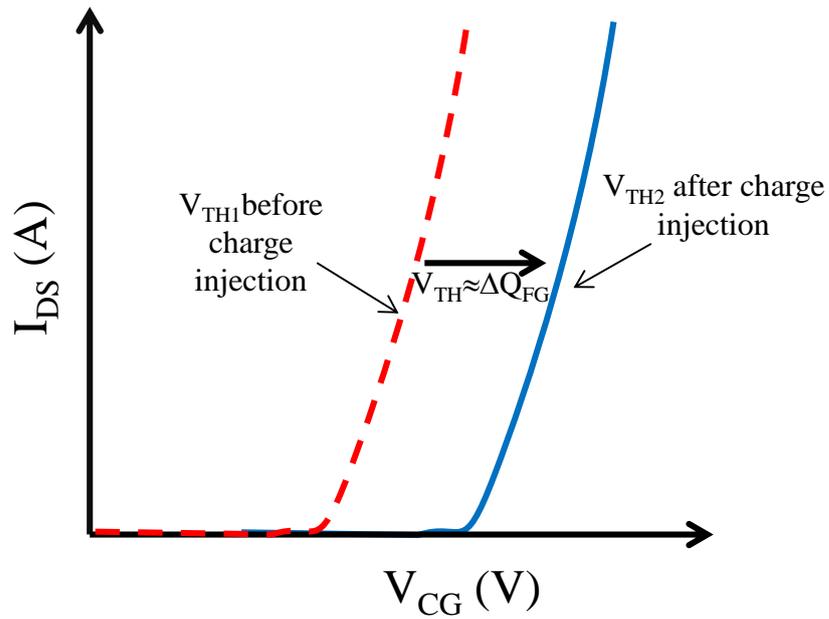


Figure 2.4. The FGMOS threshold voltage shifts from V_{TH1} to V_{TH2} after charge tunnelling.

2.3 Charge Erasure from the Floating Gate

In a standard n-type FGMOS device, charge erasing is done by FN tunnelling of electrons from the floating gate to the substrate. From a charge prospective, this is the same as holes tunneling from the substrate to the floating gate. The energy band diagram showing a FN tunnelling erasing mechanism of an n-type FGMOS device is illustrated in Figure 2.5.

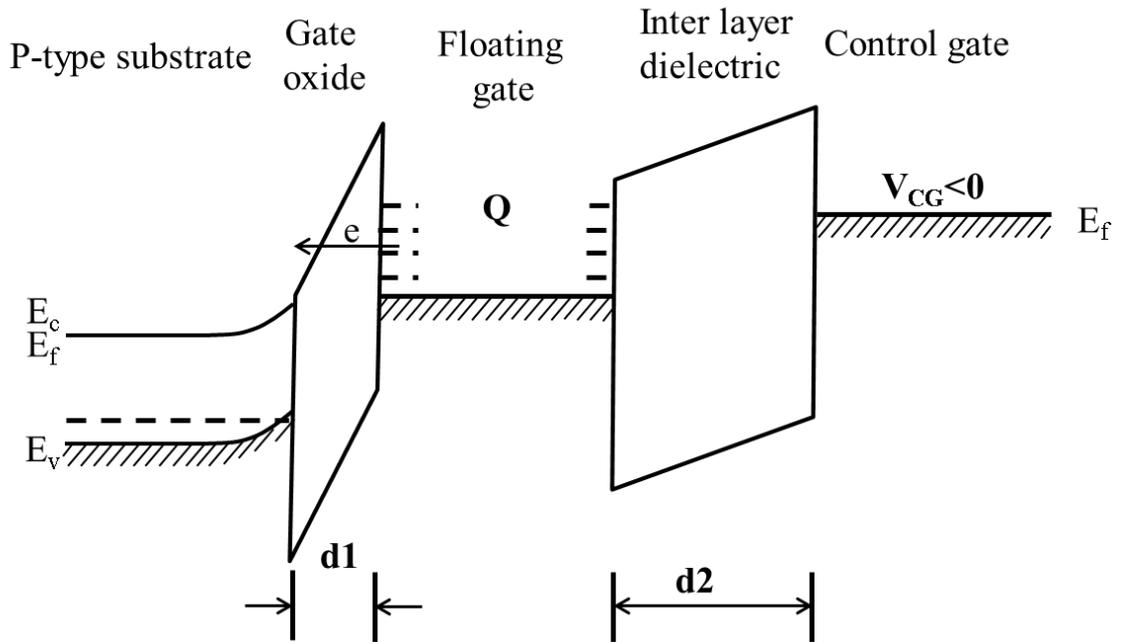


Figure 2.5. Energy band diagram of charge erasing in a FG MOS.

In this figure, Q is the stored charge on the floating gate. A high negative potential is applied to the control gate to create a positively charged inversion layer on the substrate surface. The electrons on the floating gate may gain significant energy from the strong electric field and tunnel through the triangular barrier of the oxide potential barrier into the substrate.

Chapter 3 – Design of a FGMOS Gas Sensor

The floating gate of a FGMOS device is sandwiched between the control gate and substrate and is separated by dielectric layers. In order to use the “floating gate” as a sensor, the floating gate area needs to be able to be exposed to a gas analyte. In many sensor designs, this was done by directly extending the floating gate from the gate stack region as shown in the schematic diagram in Figure 3.1 [22][23].

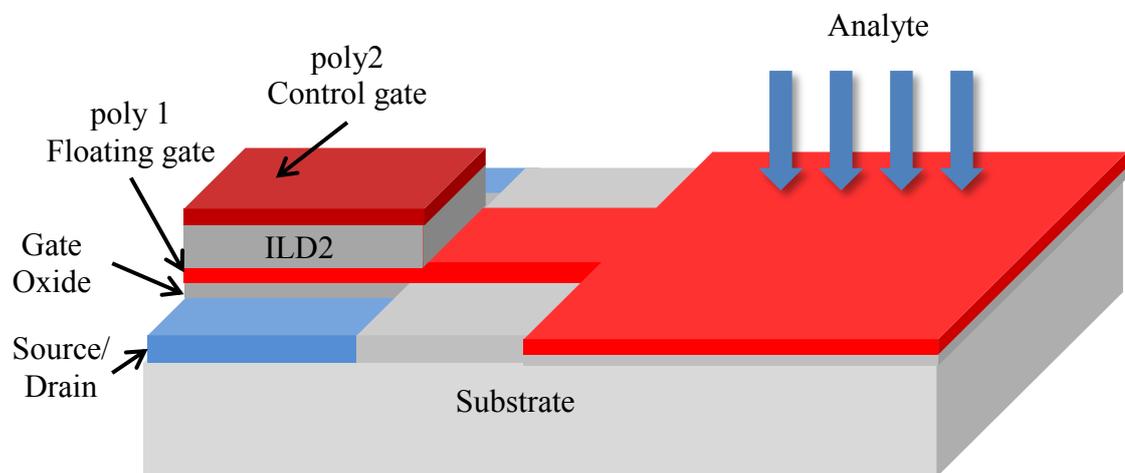


Figure 3.1. Schematic view of a FGMOS sensor with an extended sensor pad. The “poly1” (poly crystalline silicon) is used as a metallic floating gate and is extended to act as a sensor pad.

In Figure 3.1, the layers ‘poly1’ and ‘poly2’ were used as the floating gate and the control gate respectively. In the process used, both ‘poly1’ and ‘poly2’ are highly doped poly crystalline silicon. In the typical semiconductor fabrication process, ‘poly1’ is used as the metallic gate in MOS devices and ‘poly2’ is used to design resistors and capacitors. In the process that was used to design the FGMOS device in

the current work, ‘poly1’ was used as a floating gate and was buried under several layers of inter-layer dielectrics (ILDs) and metals [24]. To use a direct extension of the ‘poly1’ layer (the floating gate) from the gate stack region as the sensor pad, would require many post processing steps to remove the many ILDs and metal layers and allow polymer deposition on the sensor pad. In a previous study, it was found that exposure of the thin ‘poly1’ sensor pad was very difficult to achieve [24]. Therefore, a new sensor structure was designed which eliminates many of these post-processing steps.

3.1 New FGMOS Sensor Design

In the fabrication process that was used for the FGMOS sensor, the top metal layer ‘metal4’ is left exposed at the top level of the chip allowing it to be used as the sensor pad and avoid the aforementioned post-processing steps. This top metal layer was connected to the “poly1”, floating gate through several metal to metal interconnection process called “via” and poly-silicon to metal interconnection process called “contact”. Since both the top metal layer, interconnecting layers and the ‘poly1’ layer are highly conductive, the top metal acts as a direct extension of the floating gate. A schematic diagram of the new FGMOS sensor is shown in Figure 3.2.

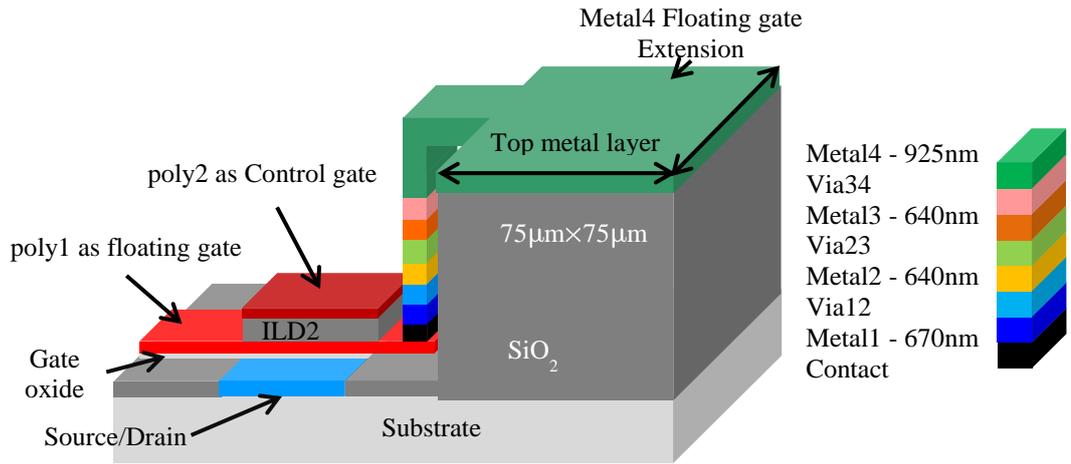


Figure 3.2. Schematic design of a FGMOS sensor. In this design, the top metal layer is used as a sensor pad and connected to the floating gate.

The detailed design specifications of the FGMOS sensor are shown in Table 3.1.

Table 3.1. Design specification of the FGMOS sensor using TSMC 0.35µm technology.

Control gate length/width	3 µm/12 µm
Floating gate length/width	1 µm /10 µm
Gate oxide between the substrate and the floating gate (ILD1)	7.5 nm
Inter layer dielectric (ILD2) between the control gate and the floating gate.	~37 nm
Sensor pad area	75×75 µm

3.2 Modeling of a FGMOS Sensor

An equivalent capacitive model of the designed FGMOS sensor was studied to

understand the effect of charge on the floating gate and is shown Figure 3.3. In this model, C_{PSUB} is the sensor pad capacitance. All of the other parameters remained the same as an ideal FMOS device that was presented in the previous section in Table 2.1.

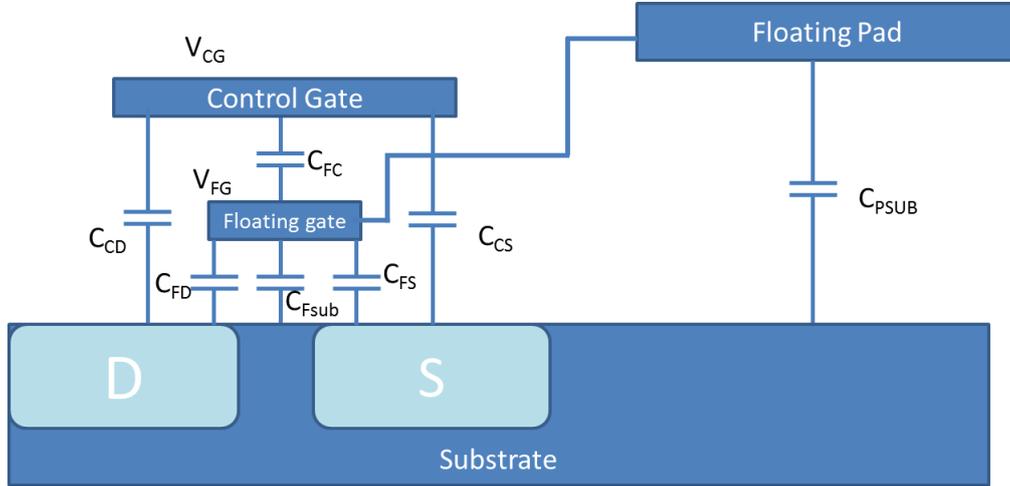


Figure 3.3. Schematic diagram of a capacitive equivalent model of a FGMOS sensor.

The net charge on the floating gate Q_{FG} is the sum of the charge on each capacitor connected to the floating gate and can be expressed as,

$$Q_{FG} = C_{FC}(V_{FG} - V_{CG}) - C_{FSUB}(V_{FG} - V_{SUB}) + C_{FD}(V_{FG} - V_D) + C_{FS}(V_{FG} - V_S) + C_{PSUB}(V_{FG} - V_{SUB}) \quad (3.1)$$

Under ideal operating condition, the source is biased with 0 V and the substrate is connected to ground. Therefore, the control gate and the floating gate voltage can be calculated from Equation ((3.1),

$$V_{CG} = \frac{1}{C_{FC}} (C_T V_{FG} - C_{FD} V_D - Q_{FG}) \quad (3.2)$$

$$V_{FG} = \frac{1}{C_T} (C_{FC}V_{CG} + C_{FD}V_D + Q_{FG}) \quad (3.3)$$

where C_T is the sum of all capacitances and can be written as,

$$C_T = C_{FC} + C_{FSUB} + C_{PSUB} + C_{FS} + C_D. \quad (3.4)$$

The threshold voltage of this device can be expressed as,

$$V_{CG}^{TH} = \frac{1}{C_{FC}} (C_T V_{FG}^{TH} - C_{FD}V_D - Q_{FG}) \quad (3.5)$$

$$\Delta V_{CG}^{TH} \approx \Delta Q_{FG} \quad (3.6)$$

where V_{FG}^{TH} is the threshold voltage with respect to the floating gate and V_{CG}^{TH} is the threshold voltage of the FGMOS. Any change in the capacitances in Equation ((3.4) or charge Q_{FG} in Equation ((3.5) will initiate a change in the threshold voltage of the FGMOS. The drain saturation current of the device also changes due to the threshold voltage shift and can be written as [25],

$$I_{dsat} = \mu_{eff} C_{GS} \frac{W}{2LC_T} (C_{FC}V_{CG} + C_{FD}V_D + Q_{FG} - V_{FG}^{TH})^2 \quad (3.7)$$

where μ_{eff} is the effective carrier mobility and C_{GS} is the total gate stack capacitance.

Some polymers change their physical and electrical properties when they are exposed to certain gases [1]. This type of polymer can be deposited on the sensor pad of the FGMOS. When the sensor is exposed to analyte gases, those sensing polymer may absorb or react with the gas molecules and may change their properties. These changes in the polymer can alter the sensor pad capacitance (C_{PSUB}) or the charge density onto the floating gate (Q_{FG}). As shown in Equation ((3.5) and ((3.7), any

change in the total capacitance C_T (due to a change C_{PSUB}) or the floating gate charge (Q_{FG}) alters the threshold voltage V_{CG}^{TH} and subsequently changes the source-drain (I_{DS}) current of the FGMOS.

A model was developed in Mat Lab using Equation ((3.5) and ((3.7) to investigate the effect of the floating gate charge change and the sensor pad capacitance change on the threshold voltage and drain saturation current of the FGMOS. For simplicity, the modeling was performed only for n-type devices. The similar results can be obtained for p-type devices with a change in the appropriate parameters. The threshold voltage (V_{CG}^{TH}) and the drain saturation current (I_{dsat}) were calculated by changing the charge density on the floating gate (Q_{FG}). The calculated results are shown in Figure 3.4. For an n-type FGMOS device, the charge change on the floating gate (Q_{FG}) shifts the threshold voltage (V_{CG}^{TH}) of the device (see Equation (3.5)) as shown in Figure 3.4 (a). If the device is biased in the sub-threshold region ($V_{CG} = 5$ V, $V_D = 1$ V), the source-drain saturation current decreases with the increasing threshold voltage and is shown in Figure 3.4 (b). The source-drain current I_{DS} as a function of the control gate (V_{CG}) for different charge densities on the floating gate was also extracted using this model and are shown Figure 3.5. This demonstrates that when the charge density on the floating gate is increased by more than 1×10^{-7} C/cm², the source-drain current and threshold voltage are changed significantly as seen the Figure 3.4.

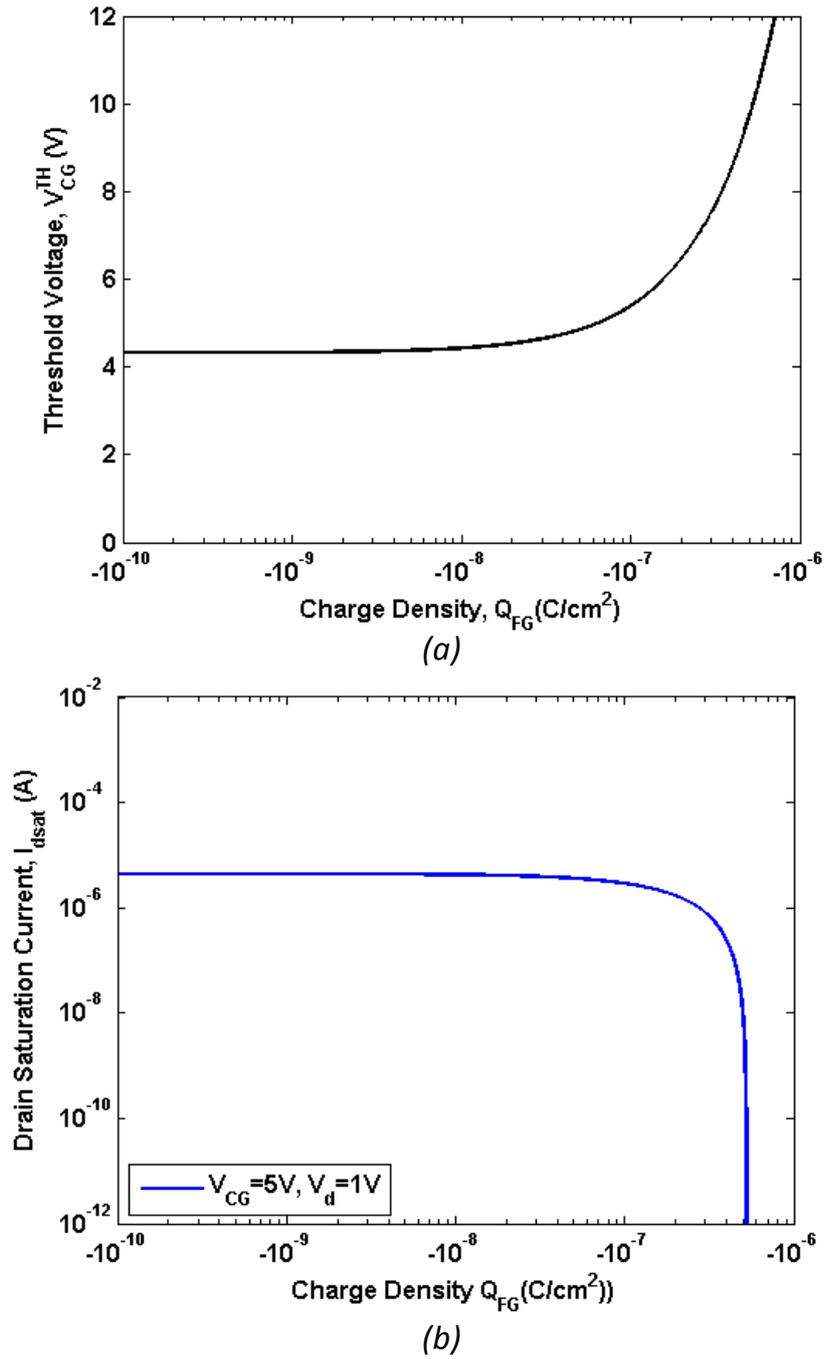


Figure 3.4. (a) Floating gate charge density (Q_{FG}) vs. the threshold voltage (V_{CG}^{TH}). (b) Floating gate charge density (Q_{FG}) vs. source- drain saturation current (I_{dsat}).

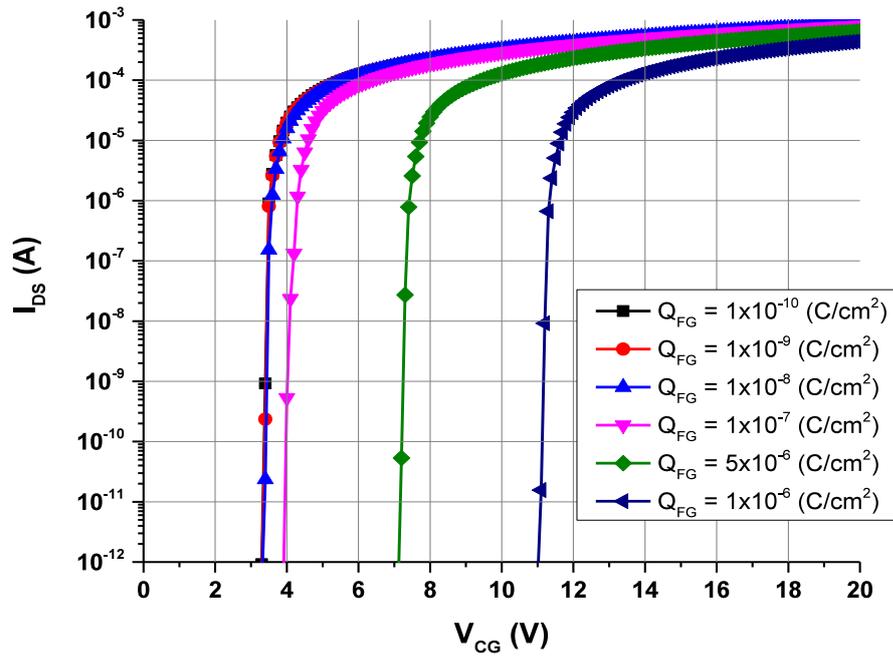
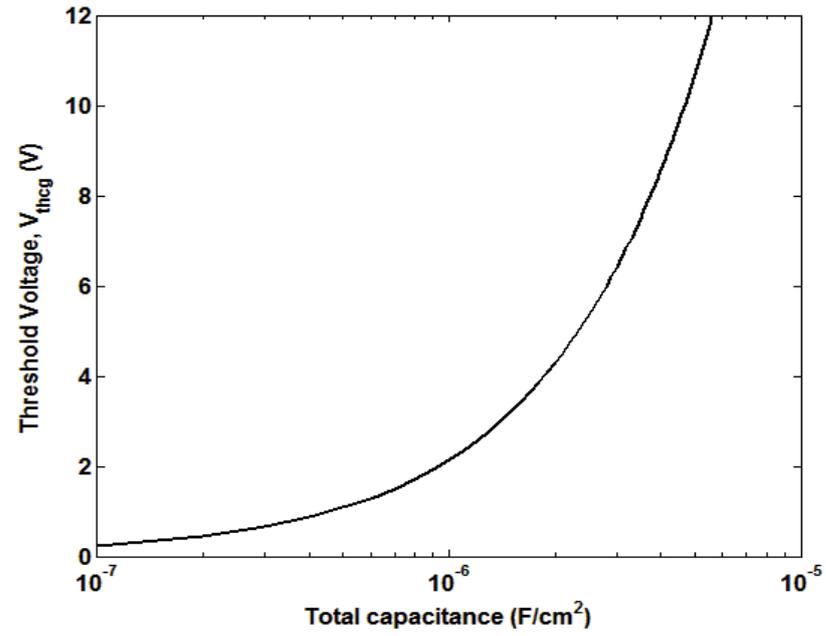
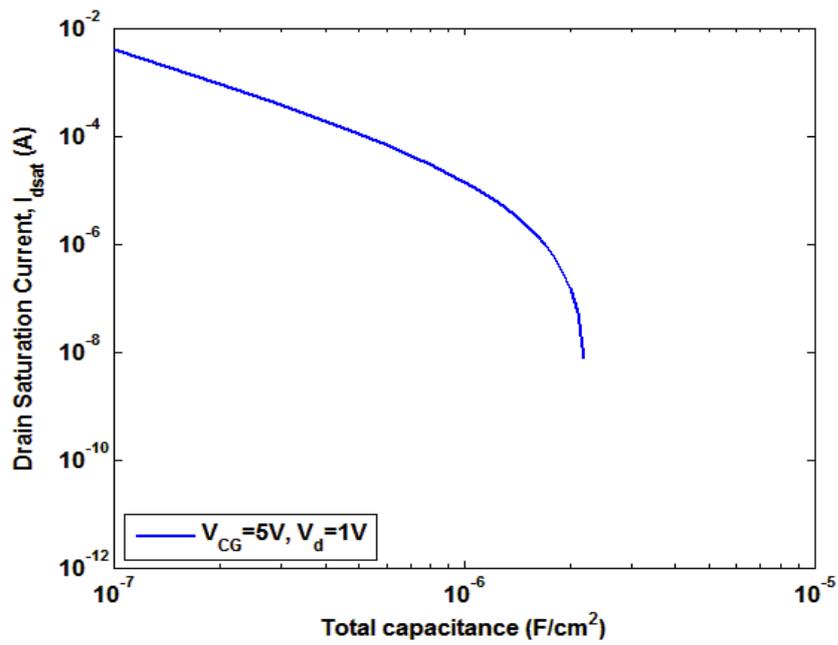


Figure 3.5. The source-drain current I_{DS} as a function of the control gate voltage, V_{CG} for different charge density on the floating gate.

The threshold voltage (V_{CG}^{TH}) and the drain saturation current (I_{dsat}) were also calculated as a function of the total capacitance (C_T) and the results are shown in Figure 3.6. The threshold voltage of the device increased with the sensor pad capacitance as predicated by Equation ((3.5), and is shown in Figure 3.6 (a). As the threshold voltage increases, the source-drain saturation current keeps decreasing as shown in Figure 3.6 (b).



(a)



(b)

Figure 3.6. (a) The total capacitance C_T vs. the threshold voltage (V_{CG}^{TH}). (b) The total capacitance C_T vs. source- drain saturation current (I_{dsat}).

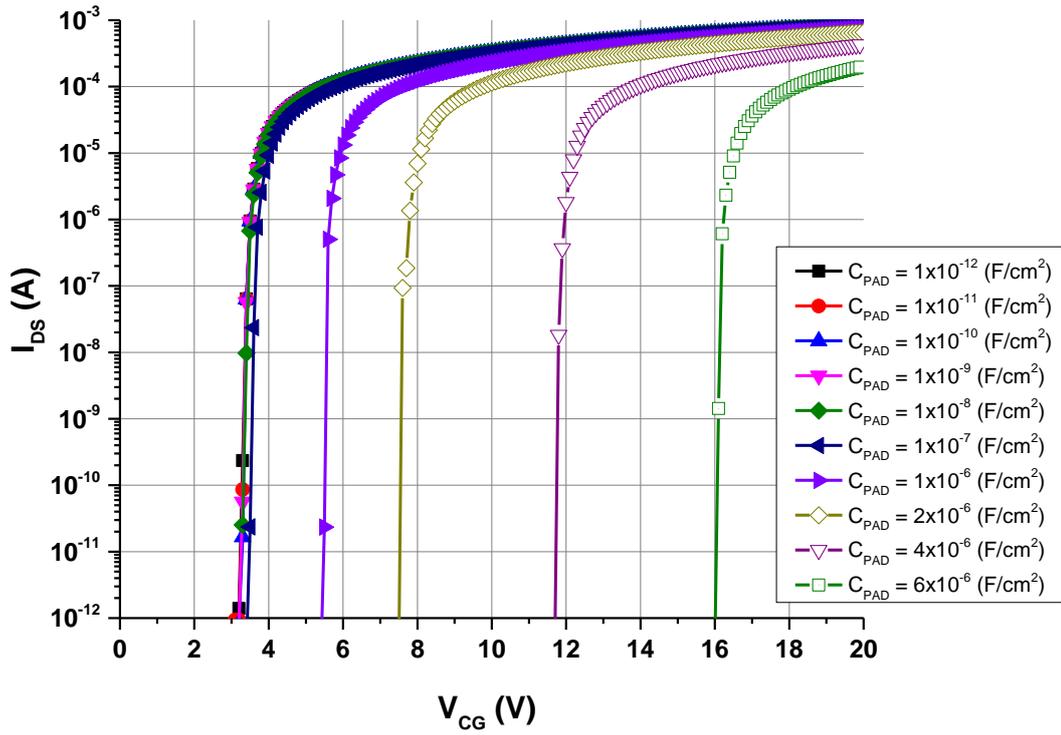


Figure 3.7. The source-drain (I_{DS}) as a function of the applied control gate voltage (V_{CG}) for different sensor pad capacitance.

The source-drain (I_{DS}) as a function of the applied control gate voltage (V_{CG}) for different sensor pad capacitance (C_{PAD}) was also calculated using this model and is shown in Figure 3.7. This analysis demonstrates that if the sensor pad capacitance increases more than $1 \times 10^{-6} \text{ F/cm}^2$, both the threshold voltage and the source-drain current can change significantly. The calculated sensor responses will be compared with the measured sensor responses in Section 4.3 and 6.2.2.

3.3 Design of a Sensor Array

A FGMOS sensor with extended sensor pad using the top metal layer is shown

in Figure 3.8. Due to the design limitation in TSMC 0.35 μm technology, a maximum allowed dimension of a metal4 pad was $35 \times 35 \mu\text{m}$ [26]. To create a larger sensor pad, four separate ‘metal4’ pads were connected together to design a large sensor pad. A 2-D sensor array was designed using these sensors and the array chip layout is shown in Figure 3.9.

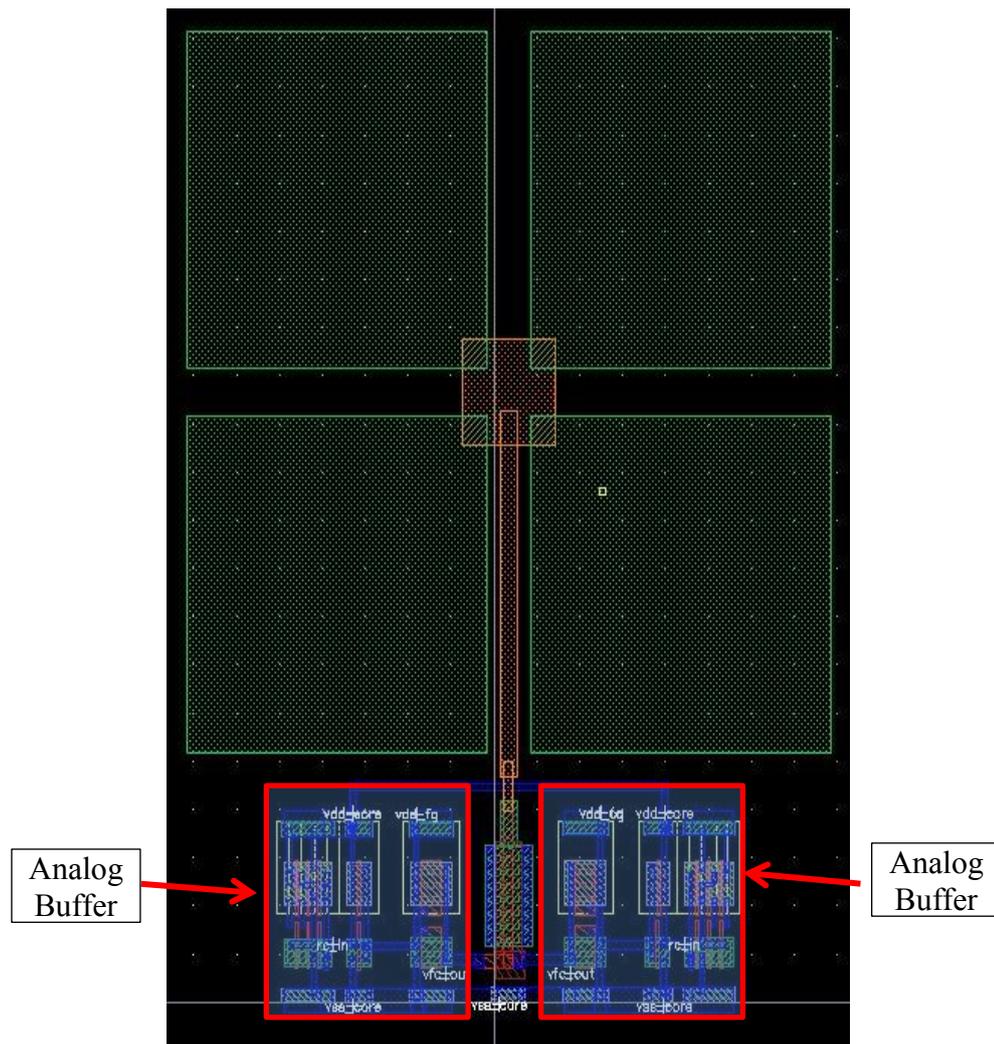


Figure 3.8. The layout design of a FG MOS sensor with analog buffers for control gate and floating gate voltage.

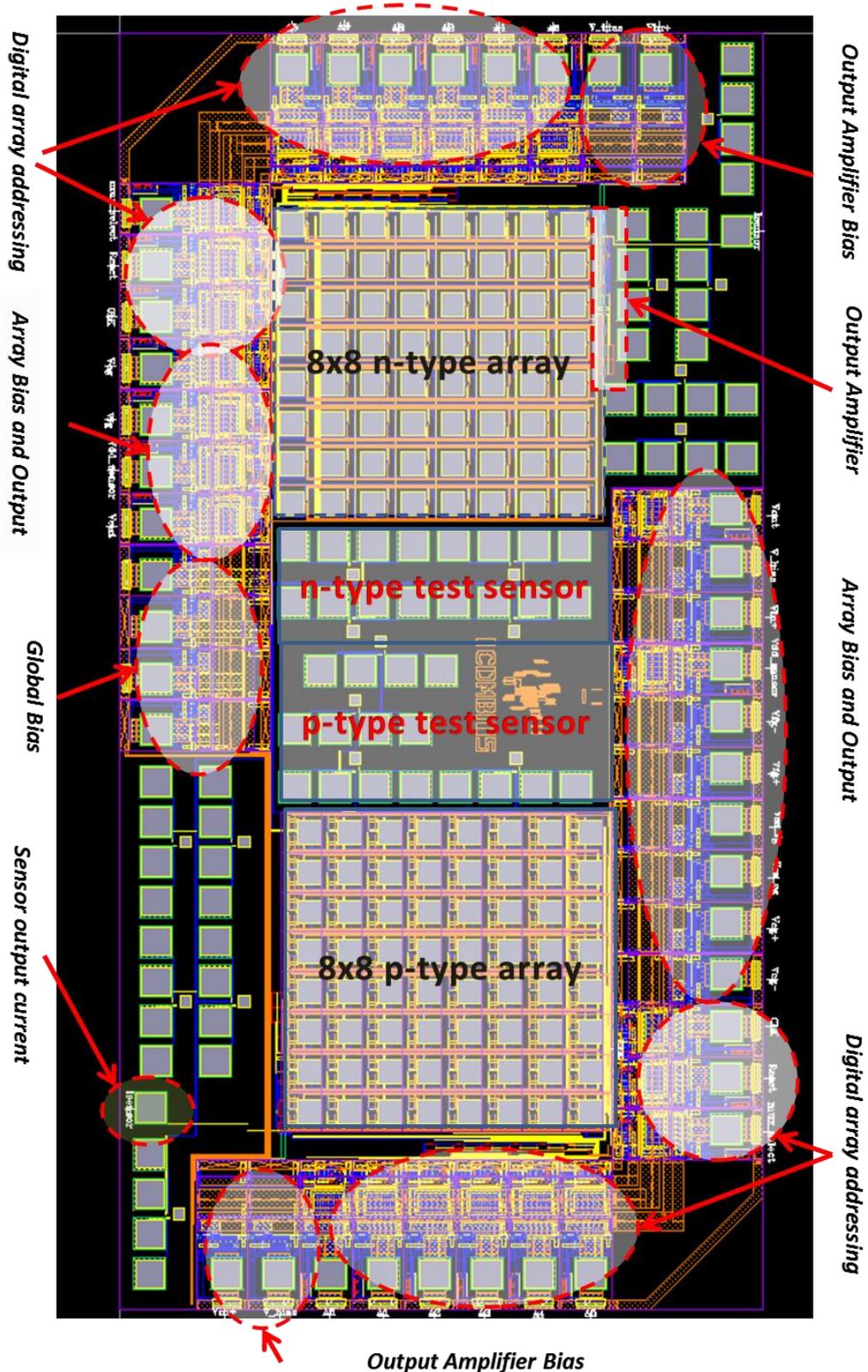


Figure 3.9. A test sensor chip with n and p type 2D sensor array. The total chip size is 2 mm × 4 mm.

This chip contains a few individual n and p-type test sensor and one n-type and one p-type sensor array (8×8). Digital array addressing circuits and an output amplifier for each array were included on the same chip. The digital array addressing circuit selects an analog buffer which delivers the required driving voltages to the device (Figure 3.8). A schematic diagram of the array addressing circuit is shown in Figure 3.10.

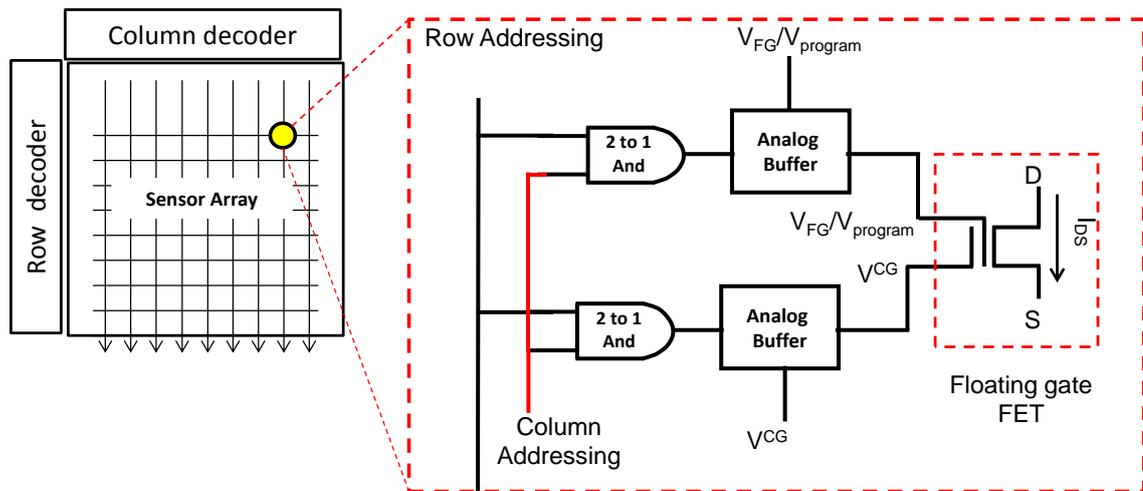


Figure 3.10. Schematic presentation of array addressing circuits of a sensor array. The column and row addressing is used to select the individual device in the array. The analog buffer is turned on by the addressing circuits and enables to apply an analog voltage on the control gate and the floating gate.

3.3.1 Output Amplifier

In an ideal FGMOS sensor operation, the device is biased in the sub-threshold region with appropriate bias voltage to the control gate, source, drain and substrate. In the sub-threshold region, a small change in the floating gate charge or capacitance creates a significant change in the source-drain current. This current is then converted

into the corresponding voltage level using an output amplifier. The circuit diagram of the output amplifier is shown in Figure 3.11.

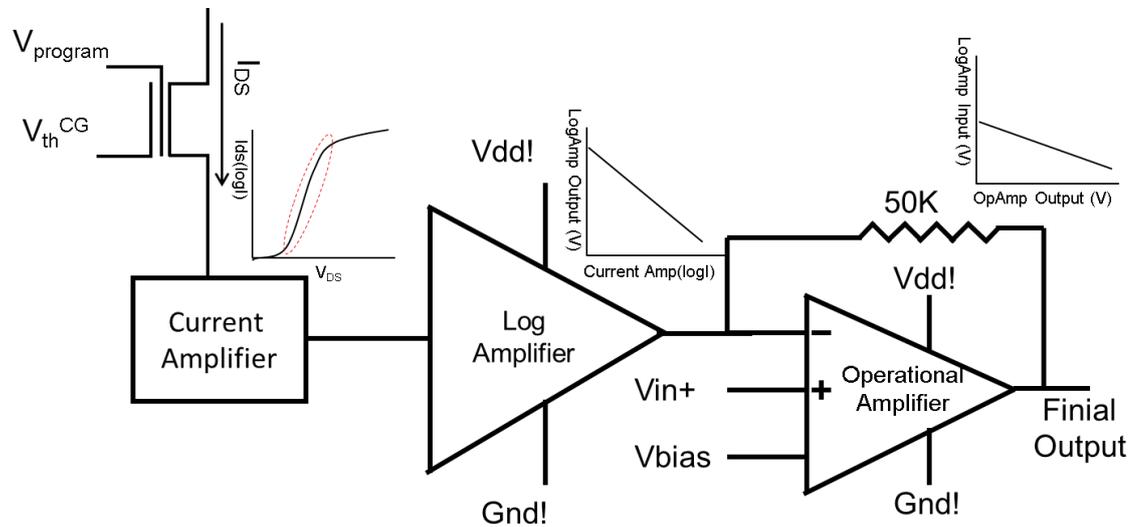


Figure 3.11. Output amplifier circuits of a sensor array. This amplifier converts the I_{DS} current of the FGMOS into a corresponding voltage scale.

In the sub-threshold region of a FGMOS transistor, the source-drain current can change from a few pico-amps (10^{-12} A) to a few milliamps (10^{-3} A). The log amplifier converted the log of the output current of the FGMOS to a linear voltage level. However, the output of the log amplifier was very small. An operational amplifier was used to increase this small voltage to reasonable value. The simulation results of the output amplifier are shown in Figure 3.12 and demonstrate that the output voltage was changing from 0.8 V to 2.2 V for currents from 10^{-6} A to 10^{-10} A. However, the output current of the designed FGMOS changes from 10^{-3} A to 10^{-12} A and this amplifier does not cover that full current range; and therefore a new output amplifier needs to be designed for a future design.

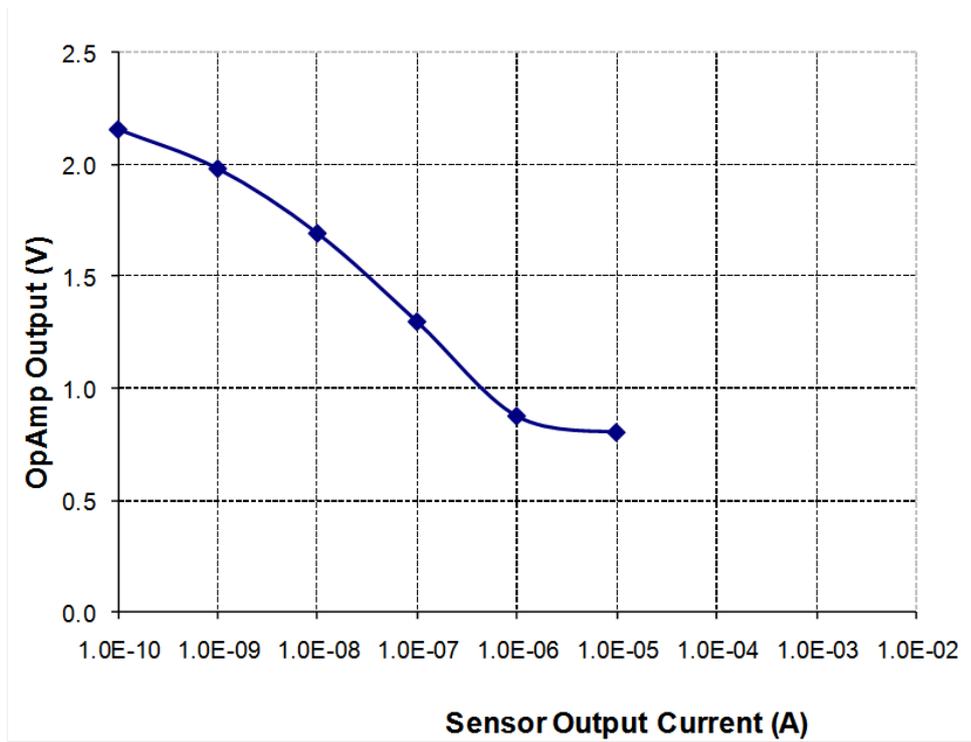


Figure 3.12. Output amplifier response of a sensor array. The input current range of the amplifier is 10^{-6} A to 10^{-10} A which produce a output voltage change from 0.7 V to 2.2 V

Chapter 4 – FGMOS Sensor Characterization

The FGMOS sensor chip was fabricated by Taiwan Semiconductor Manufacturing Company (TSMC) using their 0.35 μm technology that was facilitated through CMC Microsystems. In general, the FGMOS structure is widely used in non-volatile memory applications. The working principle and device structure of a FGMOS sensor and a FGMOS memory device are similar and have been discussed in Chapter 2 and 3. In a FGMOS memory device, charge is injected onto the floating gate by tunneling whereas, in a FGMOS sensor, charge change on the floating gate is expected result from the interaction between the sensing polymer and analyte gas. The effect of charge on the FGMOS sensor can be studied by characterizing the device as a FGMOS memory device. The FGMOS sensor was tested by electrically injecting charge onto the floating gate and measuring the resultant change in the current characteristic. The injected charge was removed from the floating gate and the source-drain current (I_{DS}) characteristic was measured again. These two operations are referred as “writing” and “erasing” for a floating gate memory device.

4.1 Charge Injection onto the Floating Gate

The dielectric thickness between the control gate and substrate of the designed FGMOS sensor was 44 nm (7 nm between the substrate and the floating gate and 37 nm between the floating gate and the control gate). When the potential difference between the control gate and substrate is more than 22 V, the electric field across the gate dielectric exceeds 5 MV/cm and in an n-type FGMOS the electrons tunnel from

the substrate via Fowler-Nordheim tunneling onto the floating gate. In a p-type device, energy band offset or barrier height is greater than for electrons. Therefore, a higher control gate voltage is required ($V_{CG} = -28 \text{ V}$) to tunnel the holes from the substrate onto the floating gate. These tunnelling mechanisms for the n type and p-type FGMOS sensor are shown in Figure 4.1. For the n-type device, the source, drain and substrate were connected together and biased at -10 V and the control gate was biased at $+20 \text{ V}$, which created a sufficient electric field ($<5 \text{ MV/cm}$) between the control gate and substrate to initiate electron tunneling onto the floating gate from the substrate. For a p-type device, these biases were set to $+10 \text{ V}$ and -20 V respectively to initiate hole tunneling from the substrate onto the floating gate (electron tunneling from floating gate to substrate). After the charge injection onto the floating gate, the threshold voltage of the FGMOS should increase and should shift the “I-V” curve in the right side for both n and p-type devices as shown in Figure 4.2.

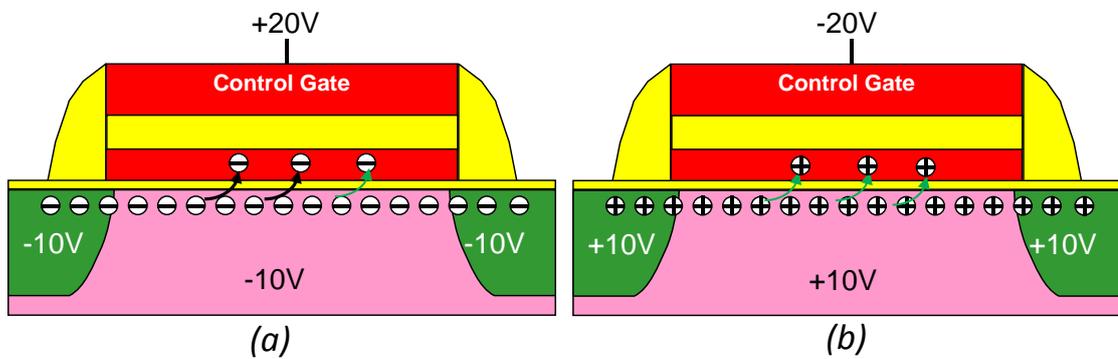


Figure 4.1. Ideal charge injection operation of a FGMOS sensor (a) n-type (b) p-type FGMOS.

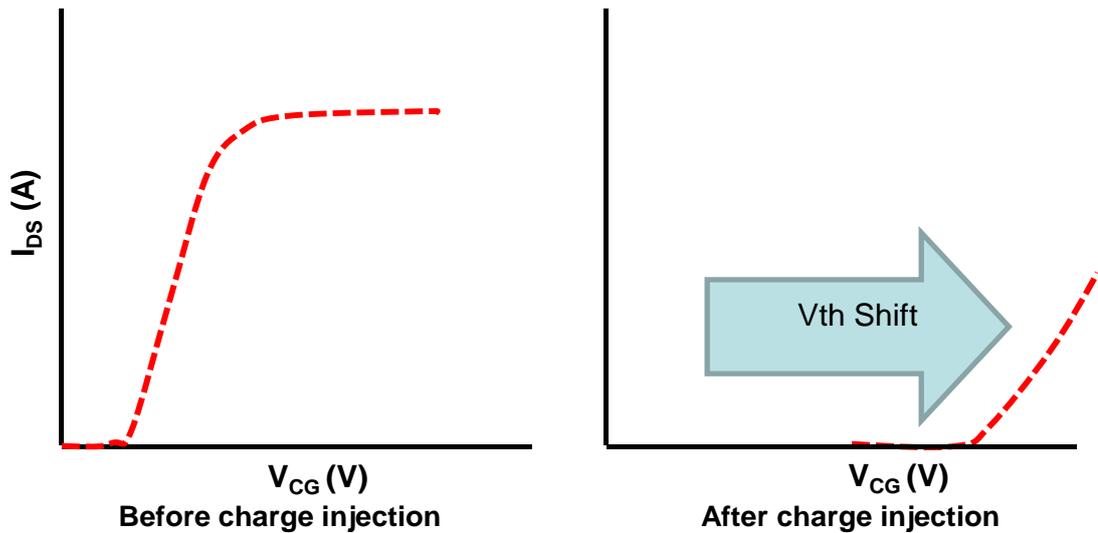


Figure 4.2. Ideal I-V response of a FGMOS sensor response after charge injection onto the floating gate.

4.2 Removing Charge from the Floating Gate

To remove the charge from the floating gate, an opposite biasing voltage was applied across the device. For the n-type device, the control gate voltage was set to $V_{CG} = -20$ V and the source drain and substrate were biased at +10 V. Due to higher negative potential on the control gate and positive potential on the substrate, the stored negative charge onto the floating gate should gain enough energy and tunneled through the thin gate oxide layer (between the floating gate and substrate) to the substrate. Similarly, for a p type device, the control gate was biased at $V_{CG} = +20$ V and the source, drain and substrate were connected together to -10 V. It was expected that due to higher positive bias on the control gate the stored positive charge onto the floating gate should tunnel to the negatively charged substrate. This should shift the threshold voltage back to the initial uncharged condition. The tunnelling mechanisms during charge removal from the floating gate are shown in Figure 4.3. The source-

drain (I_{DS}) current response after removing charge from the floating gate is shown in Figure 4.4.

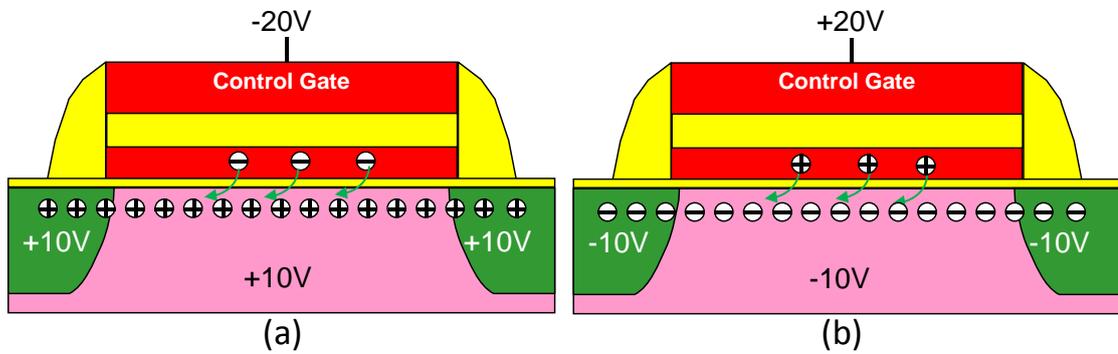


Figure 4.3. Ideal charge removing operation of a (a) n-type (b) p-type FGMOS

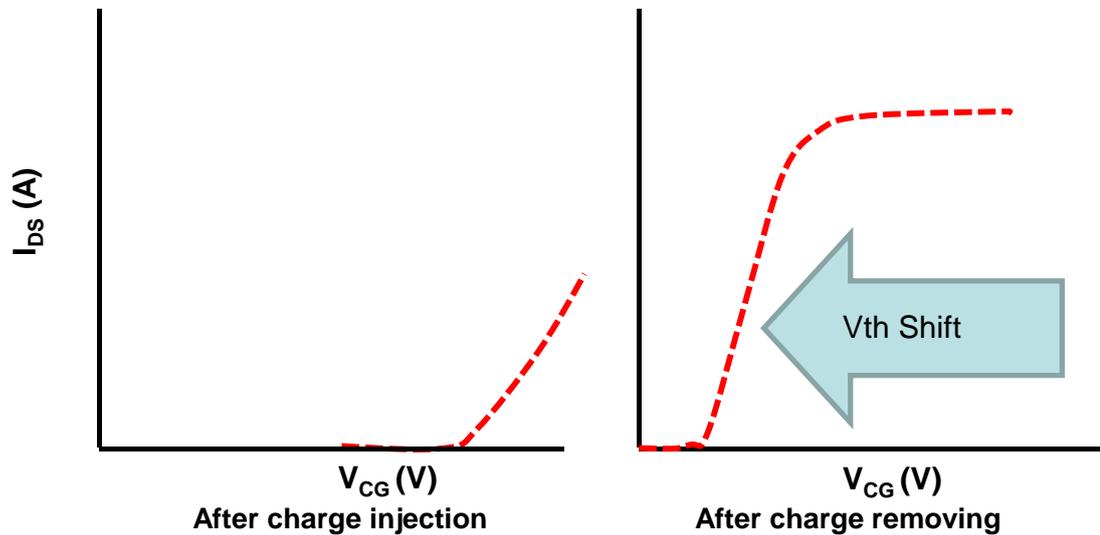


Figure 4.4. Ideal I-V response of a FGMOS sensor response after removing charge from the floating gate.

4.3 I-V Measurement Results

In the current vs voltage (I-V) measurement, the control gate voltage (V_{CG}) was changed over a predefined range with a constant voltage bias applied to the drain, source and substrate during which the corresponding source-drain current (I_{DS}) was

measured. In this experiment an Agilent HP parameter analyzer (4146C) was used to apply the voltage bias on the source, drain, control gate and substrate and measure the corresponding currents. The control gate voltage was ramped from 0 to 20 V for an n-type device (0 to -20 V for p-type) with a 1 V/s ramp step. The drain and source were biased with a constant bias voltage $V_D = 1$ V, ($V_D = -1$ V for p-type) and $V_S = 0$ V respectively and the substrate was grounded. The source-drain (I_{DS}) current was measured before and after the charge tunneling to observe the threshold voltage and I_{DS} current shifts.

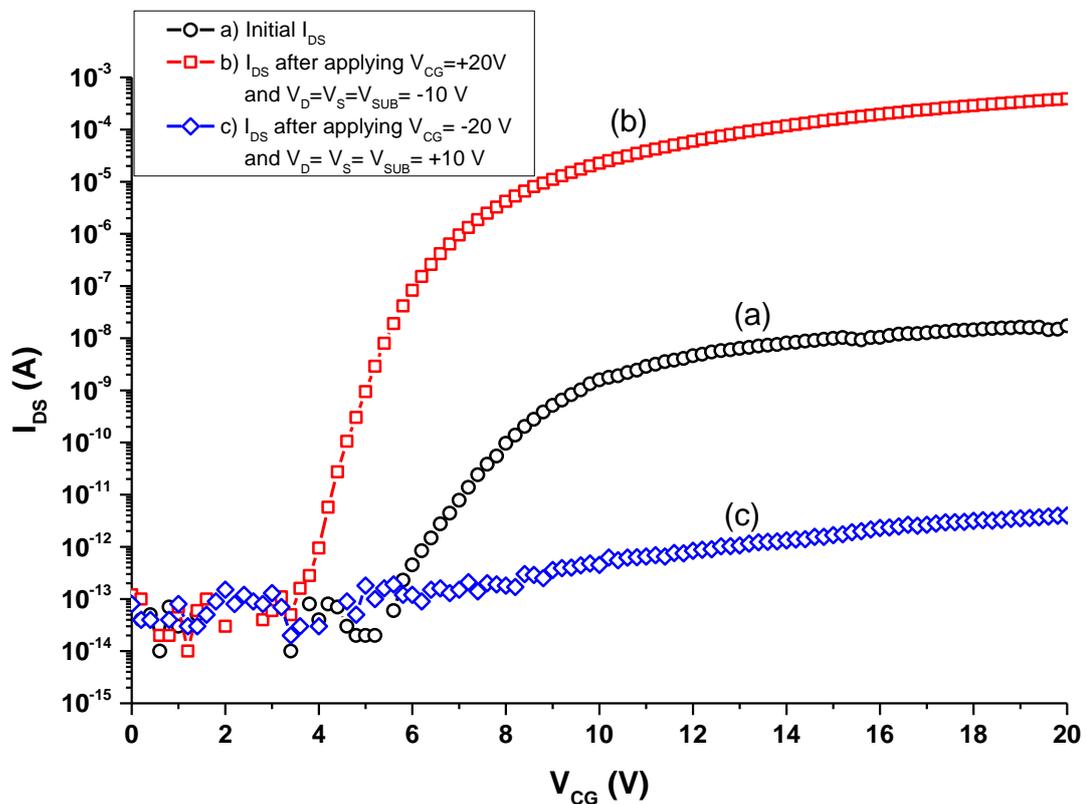


Figure 4.5. I_{DS} vs. V_{CG} measurement for a n-type FGMOS with a constant bias on the drain ($V_D = 1$ V) and sweeping the control gate voltage from 0 V to 20 V. a) Initial I-V measurement, b) I-V after applying $V_{CG} = +20$ V and $V_D = V_S = V_{SUB} = -10$ V, c) I-V after applying $V_{CG} = -20$ V and $V_D = V_S = V_{SUB} = +10$ V.

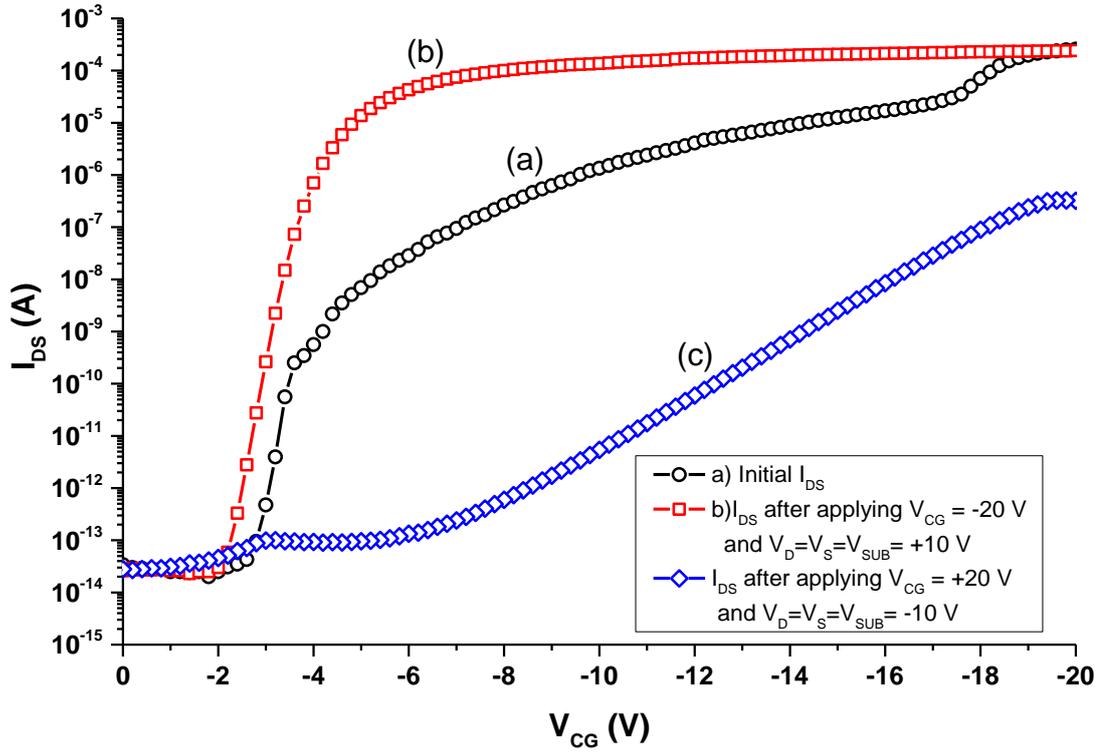


Figure 4.6. I_{DS} vs. V_{CG} measurement for a p-type FGMOS with a constant bias on the drain ($V_D = -1$ V) and sweeping the control gate voltage from 0 V to -20 V. a) Initial I-V measurement, b) I-V after applying $V_{CG} = -20$ V and $V_D = V_S = V_{SUB} = +10$ V, c) I-V after applying $V_{CG} = +20$ V and $V_D = V_S = V_{SUB} = -10$ V.

The I-V responses of the n-type and p-type devices after charge injection and charge removal are shown in Figure 4.5 and

Figure 4.6 respectively. The experimental results shown in Figure 4.5 demonstrate that for an n-type FGMOS, the threshold voltage was decreasing after applying $V_{CG} = +20$ V and $V_D = V_S = V_{SUB} = -10$ V. The ideal characteristic that was discussed in Section 3.2 demonstrate that after applying this biasing condition, the charge from the substrate might tunnel onto the floating gate. If this happens, the threshold voltage

should increase (Figure 3.5). However, the measurement result shows that the threshold was decreasing instead of increasing (see Figure 4.5 (b)). Similarly, when the control voltage was set to $V_{CG} = -20$ V and the source, drain and substrate was biased to +10 V, in ideal condition, that should decrease the threshold voltage (see Figure 4.4). The measurement result shown in Figure 4.5 (c) demonstrated that after applying this biasing condition the threshold voltage was increasing. The similar characteristic was observed for p-type sensor and shown in

Figure 4.6.

The clear understanding of these types of responses requires more study of the FG MOS sensor. However, decrease in the threshold voltage in the first case (when $V_{CG} = +20$ V and $V_D = V_S = V_{SUB} = -10$ V for a n-type FG MOS), suggest that instead of injecting charge onto the floating gate, it might remove the pre-stored charge from the floating gate as shown in Figure 4.7 (a). Similarly, when the bias was set to $V_{CG} = -20$ V and $V_D = V_S = V_{SUB} = +10$ V for an n-type FG MOS, the charge might injected onto the floating gate from the control gate as shown in Figure 4.8 (a). Similar, tunneling might happen in a p-type device and shown in Figure 4.7 (b) and Figure 4.8 (b).

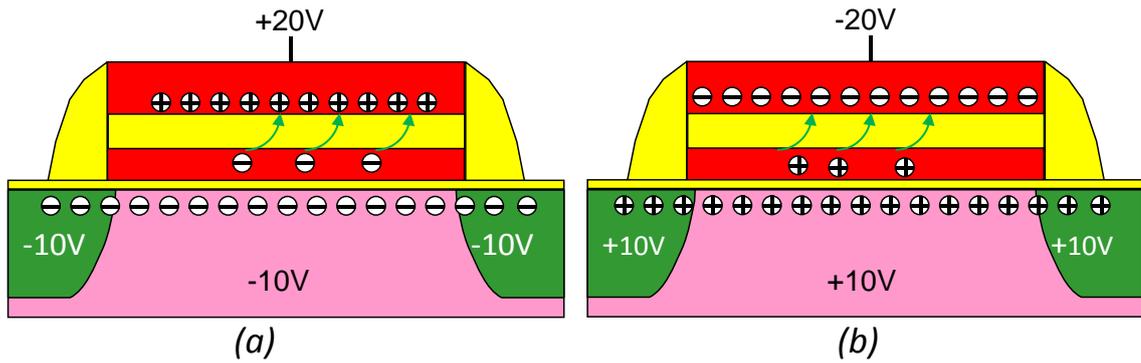


Figure 4.7. Expected charge removing from the floating gate onto the control gate during the ideal charge injection operation, (a) n-type and (b) p-type FGMOS

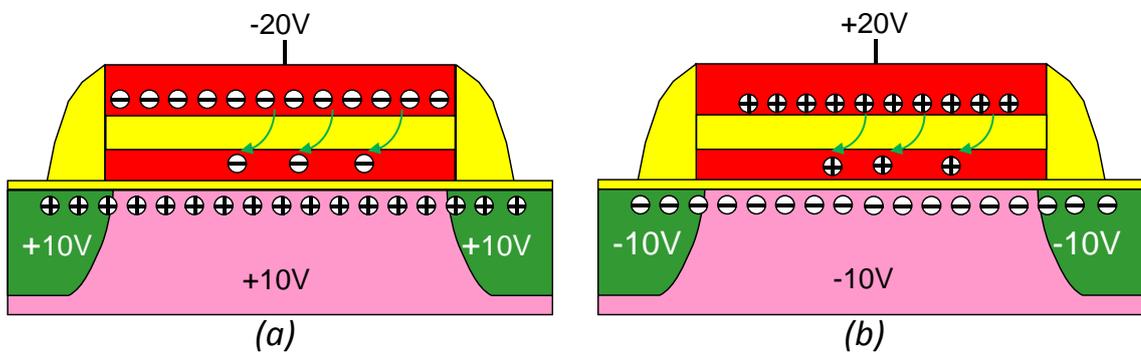


Figure 4.8. Charge injection from the control gate onto the floating gate, (a) n-type and (b) p-type FGMOS

4.4 Scanning Electron Microscope (SEM) image of the FGMOS Cross section

The FGMOS responses that are presented in the last section (see Figure 4.5 and Figure 4.6) were significantly different than an ideal FGMOS shown in Figure 3.5 and Figure 3.7. To investigate those responses, it was important to have a clear idea about physical structure of the device. Therefore, a scanning electron microscope (SEM) image of the fabricated FGMOS cross section was taken and shown in Figure 4.9.

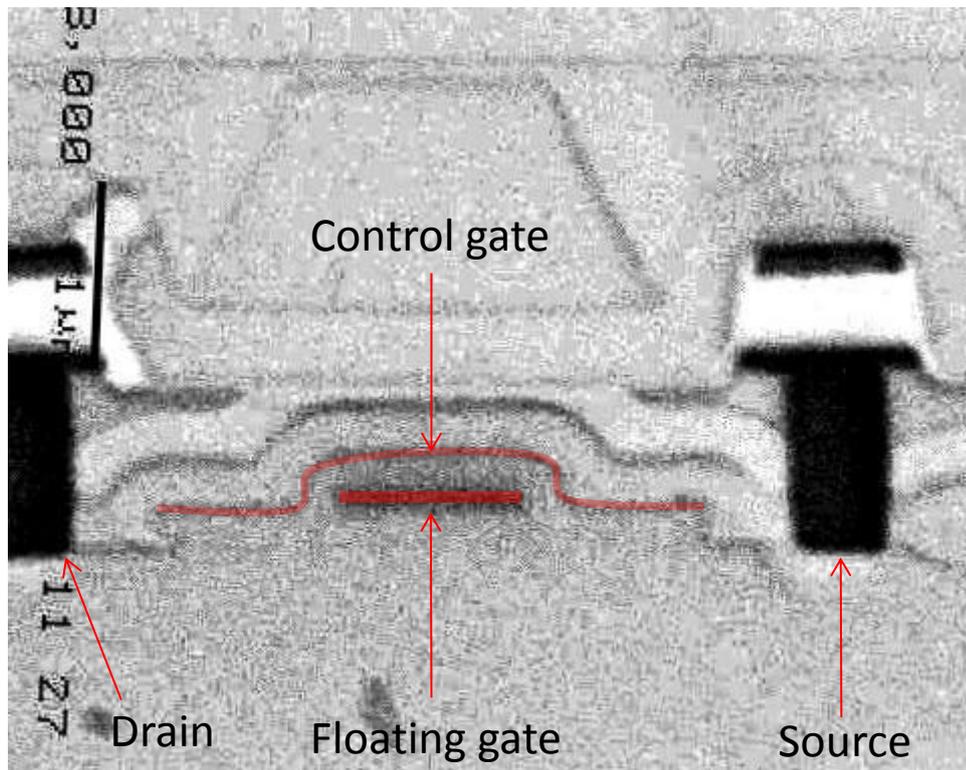


Figure 4.9 Scanning electron microscope (SEM) image of the FGMOS cross section.

The location of the control gate and the floating gate is shown in this figure and demonstrates that the control gate surrounds around the floating gate and reaches close to the substrate surface, likely separated by only the gate oxide. This image suggested that the actual device structure was significantly different than an ideal FGMOS. Therefore, the model presented previously, based on an ideal FGMOS structure is insufficient to fully characterize the FGMOS. The proper understanding of this FGMOS would require either a new model based on the actual device structure or a device structure that more closely resembled the ideal device.

Chapter – 5 Post Processing

In this FGMOS design, only one post processing was required to deposit a sensing polymer on the sensor pad. The top metal layer 'metal4' was used as a sensor pad, which is a composite alloy of mostly aluminum (Al) with small amount of copper. Top metal (metal4) layer thickness was approximately 750 nm. Different techniques were tested to deposit polymer on this sensor pad. Due to the limited number of sensor chips to work with, a test sample was used to assess the polymer deposition onto the Al film, similar to that of metal 4, onto a glass substrate. The aluminum was deposited using a thermal evaporation technique and the deposited thickness was ~700 nm. The sensing polymer was deposited onto the test structures using an electrochemical deposition process [27]. A conventional three-electrode electrochemical setup was used for polymer deposition. In the three-electrode electrochemical process, a platinum electrode, a silver/silver chloride (Ag/AgCl) electrode and the Al sample were used as counter, reference and working electrodes respectively [28]. A solution of 0.25 M of pyrrole monomer and 0.25 M sulfuric acid (H₂SO₄) was prepared. All of the electrodes and the Al sample were submerged inside the solution. A DC bias was applied from -0.6 V to 1.5 V between the counter electrode and the sample for 10 minutes.

An optical microscope image of the samples, after deposition of the polymer film is shown in Figure 5.1. The image clearly shows that during the deposition process, instead of the polymer being deposited on the aluminum, the aluminum electrodes were etched by the electrochemical process. It was therefore resolved that,

a protective layer was required to protect the ‘metal4’ sensor pad during electrochemical polymer deposition process.

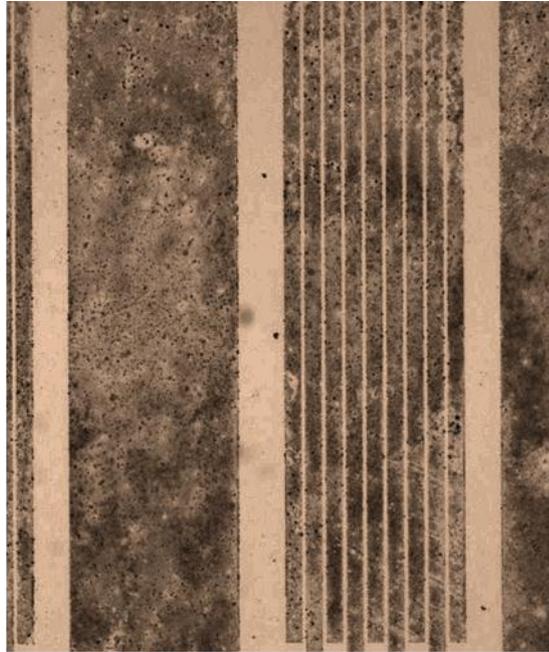


Figure 5.1. Electrochemical polymer deposition on aluminum sample. The thickness of the aluminum was ~ 700 nm.

Nobel metals such as platinum, gold and silver substrate are widely used as a substrate for the deposition of polymers using electrochemical process [28]. In this research, a gold film was used as the protective layer. Standard gold deposition techniques, like sputtering and thermal evaporation, are not selective and deposit gold over the entire surface of the sample. However, in the sensor chip, the gold needed to be selectively deposited only on the individual sensor pads and avoid any interconnection between the sensors. Selective gold deposition on the small sensor pads on a prefabricated chip required special technique which was investigated and presented in the next section.

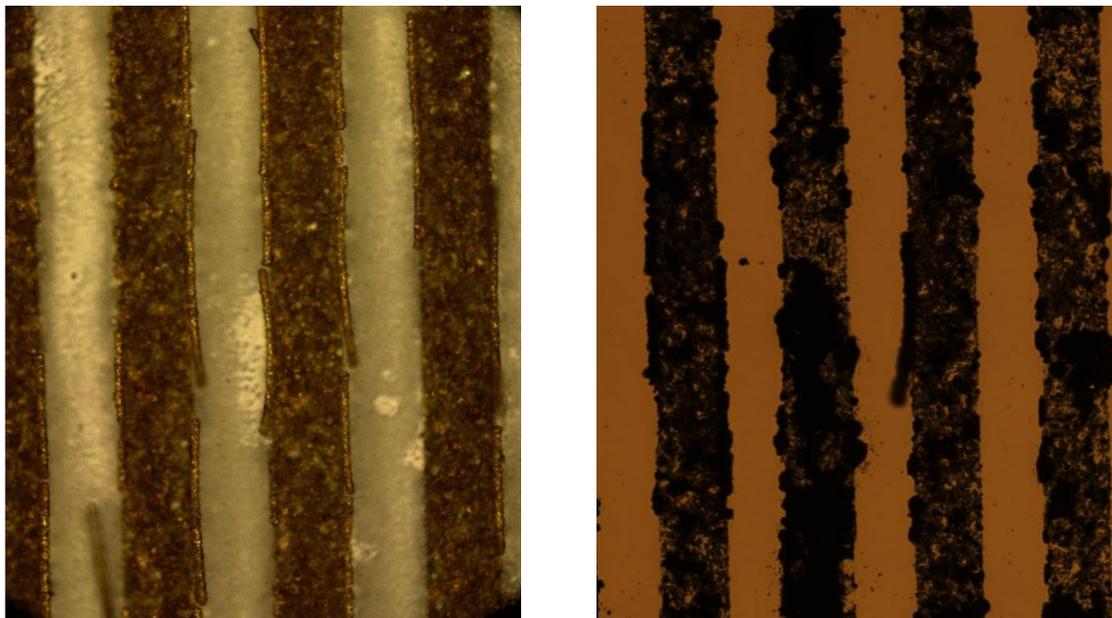
5.1 Electroless Gold Disposition

Selective gold (Au) deposition on a prefabricated chip has been reported by several researcher group [2–5]. Since, this is a chemical process, the gold is only deposited on the surface metal and makes it a selective gold deposition process. Moreover, a large number of chips can be processed in a single run which makes it an economical process. Therefore, in this experiment, an electroless gold deposition process was investigated. The chemical deposition of metal using electroless immersion solution was first invented by Brenner and Riddell to deposit nickel or cobalt on a steel surface without the use of an electric current [32]. Later, this process was developed to deposit gold on other metal such as steel, aluminum and copper [33–35].

Electroless gold deposition process involves three steps deposition, i) Zinc (Zn) deposition ii) Nickel (Ni) deposition, iii) Gold (Au) deposition. In the first step, a layer of zinc is deposited to protect the aluminum during nickel deposition. A layer of nickel is then deposited on top of zinc which provides a good interface between the gold and aluminum [36]. Immersion Zincate, Nিকেlex and Gold solutions from Transene Company Inc. were used in this deposition process. Several experiments were performed to find the optimized process for thin film gold deposition. The optimized deposition technique is presented in the next section.

The zincate solution (salt containing $\text{Zn}(\text{OH})_4^{2-}$) was heated at 80° C and the aluminum sample was immersed into this solution for 10 seconds. During this process, the native aluminum oxide layer was etched away and a layer of zinc was deposited on top of the aluminum electrodes. This zinc layer prevented the aluminum

to re-oxidize in the air and protected it during the nickel deposition process. The nickalex solution (a solution of nickel complex and hypophosphite (H_2PO_2^-)) was heated up to 95°C and the aluminum sample was then submerged into this solution for 1 minute. The sample was then cleaned with water and annealed at 400°C for 30 minutes. During this process, the Zn ions were replaced by Ni ions and deposited a layer of nickel on top of the aluminum film. Finally, the gold solution was heated up to $70\text{-}75^\circ\text{C}$ and the aluminum sample was immersed in this solution for 5 minutes. During this process, the top Ni ions were dissolved into the gold solution, and Au ions were deposited on top of the aluminum substrate [37].



(a)

(b)

Figure 5.2. Aluminum sample, (a) after electroless gold deposition. (b) after electrochemical polymer deposition. Each aluminum strip was $100\ \mu\text{m}$ wide and $100\ \mu\text{m}$ spaced.

An optical microscopy image of the aluminum test sample after gold deposition

is shown in Figure 5.2 (a). The image of the test sample shows that the surface of the deposited gold was rough and has some holes on the gold surface. The average gold thickness was 300 nm. Immersion gold deposition on nickel substrate using the similar technique presented by other group reported similar result [37]. After depositing gold, the layer of polymer film was deposited using electrochemical process. An optical microscopy image after polymer deposition is shown in Figure 5.2 (b). It can be seen from this figure that the deposited polymer layer was non-uniform and in some places the substrate aluminum was etched away.

A sensor chip was also tested to deposit polymer following the same technique and image of this chip is show in Figure 5.3. It can be seen from this figure that the polymer was deposited on some unwanted places. This demonstrates that the electroless gold deposition was not that reliable to selectively deposit a thin layer of gold and then electrochemically deposit a polymer layer on a small sensor chip. A new technique was studied and presented in the next section.

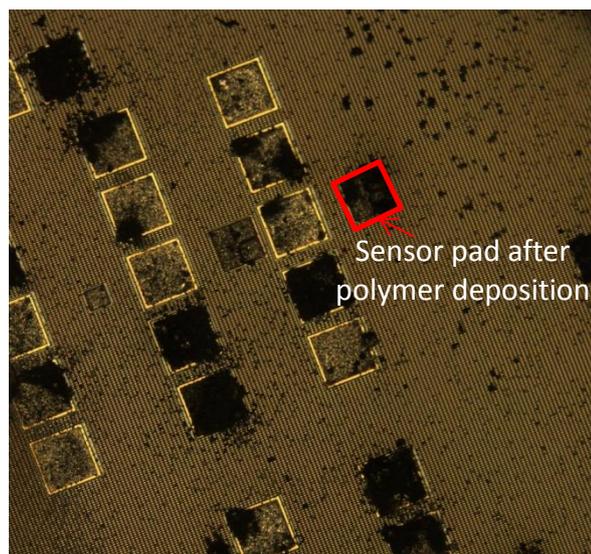


Figure 5.3. Sensor chip after immersion gold and electrochemical polymer deposition.

5.2 Gold Deposition Using Lift-Off

Even though, chemical gold deposition should be more preferable for mass production, it was found to be an unreliable technique for selective gold deposition. Lithography is a widely used process that allows fabrication of a small feature. Since gold is chemically inactive and hard to etch, lift-off is the most commonly used selective gold deposition process using lithography technique. In a standard lift-off process, the sample is spin coated with photoresist. The photoresist is then removed from the region where gold needs to be deposited. This is done by exposing those locations in ultra violet ray (UV) and washed in developer solution. The gold is deposited using sputtering or thermal evaporation technique. Finally, the unwanted gold from the chip is removed by immersing the sample in acetone using an ultrasonic cleaner.

Since the sensor chip is very small (4 mm × 2 mm), it was very hard to make a uniform photoresist layer on top of this chip using spin coating. Edge bead in four corners of the small rectangle chip is significantly high as compared to the center of the chip [38]. Different spin coating techniques was tested to reduce the edge beading as small as possible. It was found that spin coating for 1 minute with 3000 rpm produced less edge beading.

A positive photo mask was used to expose only the sensor pad area during the UV light exposure. The ABM 6 inches two sided mask aligner was used align the chip with mask. During this process, it was found to be very difficult to align the photo mask with the chip. In a positive mask, the only visible structures are the small opening for each sensor pad. Moreover, the microscope of the mask alignment system

can focus only on the top surface of the mask. Using this positive photo mask, it was difficult to see the bottom sensor chip and align it with the top photo mask. A new technique was used to make a perfect alignment between sensor chip and photo mask. In this technique, first the microscope was moved on the desired location of the mask. The sensor pad opening areas on the mask were marked on the microscope external display. Then the mask was removed from the top and the chip was brought up to the focus point of the microscope. The sensor pads on the chip were aligned with marked area on the microscope display. The chip was then lowered down without moving in x and y directions. Now the mask is placed again and sensor chip was brought up to align with the opening of the photo mask. After alignment, the chip was then exposed in the UV light for 10 seconds. The sensor chip was washed in a developer solution to remove the photoresist from the sensor pad area. The chip was baked in the oven at 120° C for 30 minutes to harden the photoresist. The gold was then deposited on the sensor chip using a sputtering system.

Gold (Au) sputtering is two steps process. Initially, a thin titanium (Ti) layer was deposited as an adhesion layer between the aluminum and gold. The sputtering parameters for titanium and gold deposition are presented in Table 5.1.

Table 5.1. Sputtering parameters for Titanium and gold deposition

	Titanium (Step 1)	Gold (Step 2)
Base pressure	5×10^{-5} torr	5×10^{-5} torr
Sputtered pressure	10 millitorr	10 millitorr
Sputtering time	2 minutes	2 minutes
Thickness	~80 nm	~200 nm

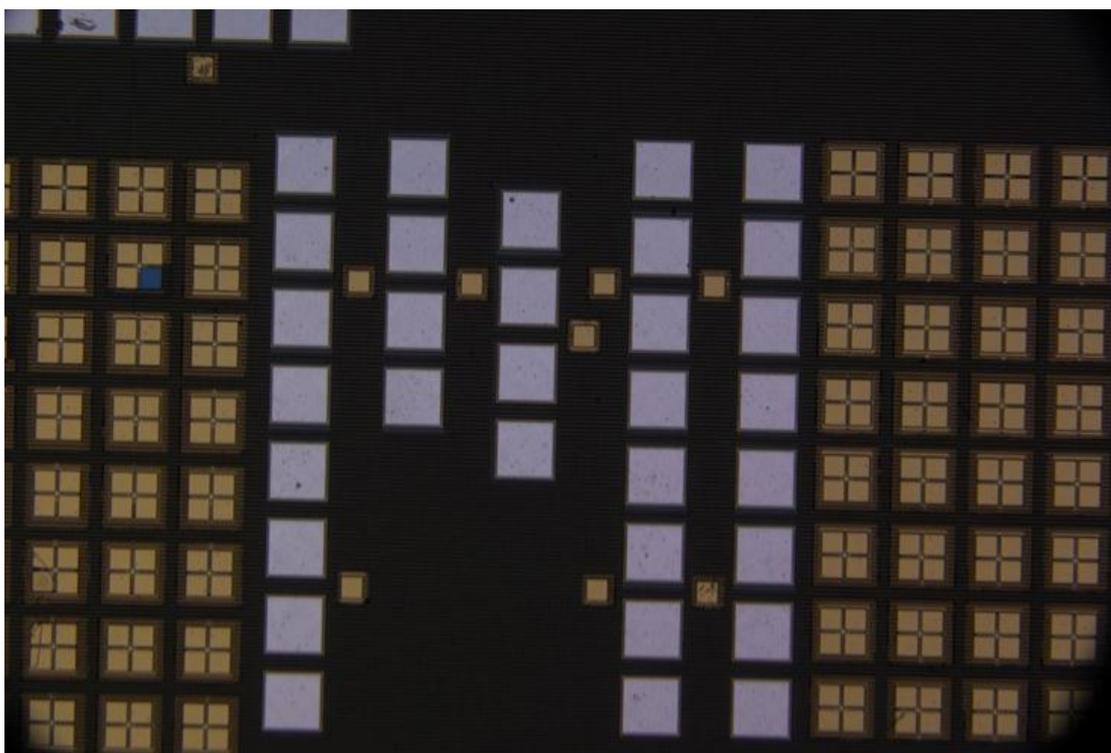


Figure 5.4. An optical microscope image of a sensor chip after gold deposition using lift-off process.

An optical microscope image of the sensor chip after gold deposition is shown in Figure 5.4. It can be observed from the image, that the gold was deposited only on the sensor pads area without making any overlapping with the adjacent structures. The deposited gold thickness was 200 nm. After this gold deposition, the sensor was ready for polymer deposition.

5.3 Polymer Deposition

The polymer film was deposited selectively on the sensor pad using an electrochemical deposition process [27]. Polymer deposition using other methods would be significantly more difficult on the relatively small sensor pad area. In

addition, the electrochemical method allows the flexibility to change the chemical and physical nature of the polymer (by changing the dopant or set potential) which alters its response to different analytes [39]. For this sensor experiment, polypyrrole (PPy) was used as polymer because of its extensive use for sensing in many gases and pH applications [1,40,41].

For electrochemical deposition, an electrolyte was prepared by a 0.1 M solution of a pyrrole monomer with a 0.5 M solution of H_2SO_4 . Platinum and Ag/AgCl were used as counter and reference electrodes respectively. The polymer was grown under potentiostatic conditions using CHI 760C potentiostat, and the thickness of the grown polymer was between 630-650 nm. A sensor chip after complete post processing is shown in Figure 5.5.



Figure 5.5. Image of a FGMOS sensor after depositing sensing polymer (Polypyrrole) on the sensor pad.

The source-drain current (I_{DS}) was measured as a function of the applied control gate bias (V_{CG}) before and after every post processing steps to observe any change in the device characteristic due to the post processing. During the I_{DS} measurement, the control gate voltage was swept from 0 to 10 V with 0.5 V steps and a constant 1 V was applied to the drain. The I_{DS} current responses are shown in Figure 5.6 and demonstrate that the post processing steps did not alter the device characteristic.

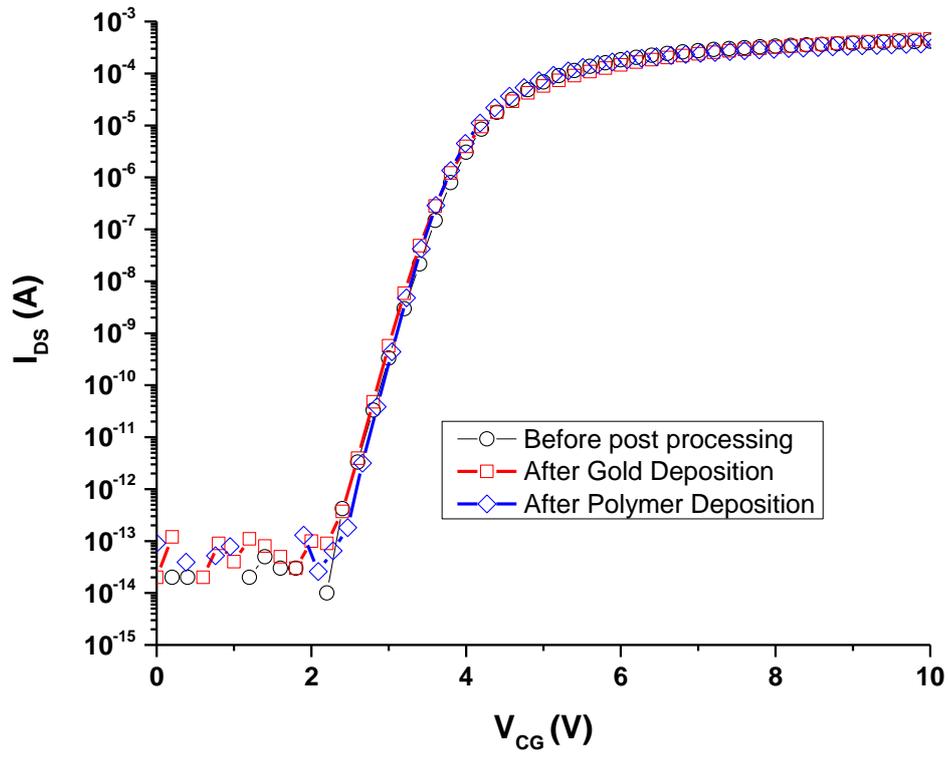


Figure 5.6. I-V Characterization of FGMOS sensor before and after gold and polymer deposition. The control gate voltage was swept from 0V to 10 V with the drain was biased with a constant 1 V.

Chapter 6 – Sensor Characterization

A polymer based FGMOS gas sensor translates the concentration of a gas analyte into a detectable signal through the change of the physical and/or electrical properties of the sensing polymer. The FGMOS data shown in Chapter 4, demonstrated that in a FGMOS sensor, any change in the floating gate charge or capacitance causes a change in the threshold voltage (ΔV_{TH}) and produces a shift in the source-drain (I_{DS}) current. These changes may be initiated due to the interaction between the sensing polymer and the analyte gas. In this chapter, the FGMOS sensor responses using different measurement techniques are presented.

6.1 Sensor Response without any Polymer on the Sensor Pad

Before starting the sensor experiment with a post processed FGMOS (FGMOS after polymer deposition) a FGMOS, without any post processing was tested by exposing to analyte gas. This experiment will demonstrate, if the FGMOS sensor without any polymer on the sensor pad can produce any response to the analyte gas or not. In this experiment, the FGMOS without any deposited polymer on the sensor pad was initialized by exposing to nitrogen for 2 hours. The FGMOS was then exposed to 25% water for 30 minutes and an I-V responses were measured after every 10 minutes while the gas was still flowing. The measured responses are shown in Figure 6.1. The measurement results demonstrate that the I-V responses were not shifting. Therefore, it can be assumed that any change that will be observed in the FGMOS with a

polymer on the sensor pad is only due to the interaction between the polymer and the analyte gases.

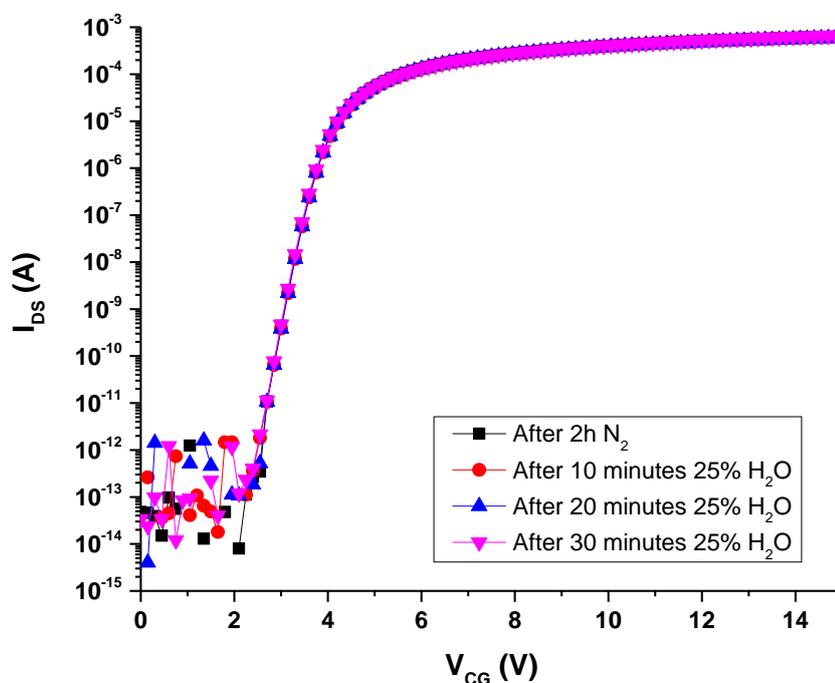


Figure 6.1. I-V response of a FGMOS without any sensing polymer. The sensor was exposed to 25% H₂O and I-V responses were measured after every 10 minutes.

To have a control in this experiment, the I_{DS} response of a FGMOS sensor, that did not have a polymer film deposited on the sensor pad, was measured after exposure to a high concentration, 50% of methanol. The FGMOS was initialized by applying a high potential on the control gate ($V_{CG} = 30$ V and $V_D = 1$ V). The sensor response was then measured with a fixed pulsed bias condition ($V_{CG} = 5$ V, $V_D = 1$ V) while it was exposed to 50% methanol for 200 minutes. The bias was applied on the control gate and drain for 0.5 seconds, every 5 minutes during which time, I_{DS} was measured.

The measurement results are shown in Figure 6.2 and demonstrate that the I_{DS} current remained relatively constant. This demonstrates that the initialization process ($V_{CG} = 30$ V and $V_D = 1$ V) is stable and that exposure to a sensor without a polymer film does not react to the analyte.

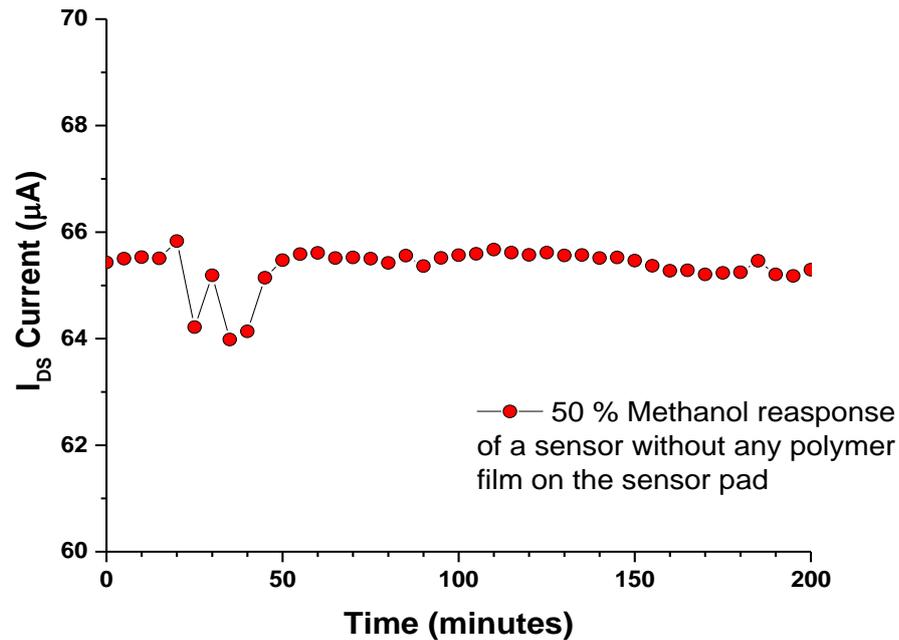


Figure 6.2. The I_{DS} current response of a FG MOS without a polymer film on the sensor pad. The sensor was exposed to 50% methanol for 200 minutes. The I_{DS} response was measured using a short pulse of 0.5 seconds every 5 minutes. The device was biased with $V_{CG} = 5$ V and $V_D = 1$ V during the 0.5 second pulse

6.2 I-V Characteristics of Sensors

Current voltage (I-V) characterization is one of the most widely used techniques to characterize semiconductor devices. The details of this technique have been

presented in Chapter 4, where this measurement was used to characterize the effect of the charge on the floating gate of the FGMOS response. A similar measurement was repeated after depositing sensing polymer on the sensor pad of the FGMOS. This time, instead of electrically injecting charge onto the floating gate, the sensor was exposed into an analyte gas.

It has been demonstrated in several studies, that the electrical and/or physical properties of the sensing polymer can be changed after exposure to certain gases [17–20]. In a FGMOS sensor, if any of those changes alter the charge density on the floating gate or change the capacitance connected to the floating gate, it will initiate a change in the threshold voltage (V_{TH}) and subsequently a change in the source-drain current (I_{DS}) (see section 3.2).

For the I-V characterization of the sensor, the source-drain current (I_{DS}) was measured as a function of the control gate voltage (V_{CG}) before and after exposing the sensor to a gas analyte for a certain period of time. It has been demonstrated before that the FGMOS is very sensitive to charge onto the floating gate. Charge that may have tunnelled onto the floating gate as a result of the applied measurement voltage might alter the sensor response and it could be difficult to separate the sensor response due to the gas exposure. Therefore, it was necessary to find the maximum measurement voltage at which the effect of any charge injection should be minimised. The maximum control gate voltage at which the Fowler–Nordheim (FN) tunneling starts can be calculated from the following equation [46],

$$E \approx \frac{V_{CG}}{d_{ox}} \quad (6.1)$$

where E is the electric field between the control gate and substrate, V_{CG} is the control gate voltage and d_{ox} is the distance between the control gate and the substrate. In the designed FGMOS, the total gate insulator thickness is 44 nm; 7 nm between the substrate and the floating gate and 37 nm between the floating gate and the control gate. These thickness were obtained from the TSMC design specification [47]. The FN tunneling starts when the electric field across the control gate and substrate exceeds ~ 5 MV/cm [46]. From the above equation, for an n-type FGMOS, when the control gate potential is less than 22 V ($V_D = 0$ V, $V_S = 0$ V and substrate is grounded), the electric field across the gate dielectric remains lower than 5 MV/cm. Therefore, in this work, V_{CG} was varied from 0 to 10 V and the V_{DS} was set to a constant 1 V during the sensing operation to maintain the electric field across the control gate and substrate less than 5 MV/cm.

6.2.1 I-V Measurement Setup

The experimental setup that was used for the I-V measurement is shown in Figure 6.3. The measurement system consisted of a probe station, a gas flow system, and a parameter analyzer. A computer was used to control the gas flow system and data acquisition during the measurement. The test chip was placed inside a Cascade Microtech probe station. This probe station has four probes with tungsten probe tips which were used to connect to the source, drain, substrate and control gate of the test device. The probe station was placed on a vacuum table and shielded inside a metallic box to reduce the vibration and electrical noise. Within the Plasmionique Flocon 09 flow system, nitrogen was flowed through a liquid water or methanol to produce a gaseous analyte. This system controlled the gas flow rate for a predefined time where

the pressure and temperature were kept constant throughout the measurement period. The analyte gas generated from the flow system was passed through a tube inside the probe station. The end of the tube was placed 10-20 mm above the device under test. An Agilent 4155C parameter analyzer was used to apply the voltage to the source, drain, substrate and control gate and measure the corresponding currents.

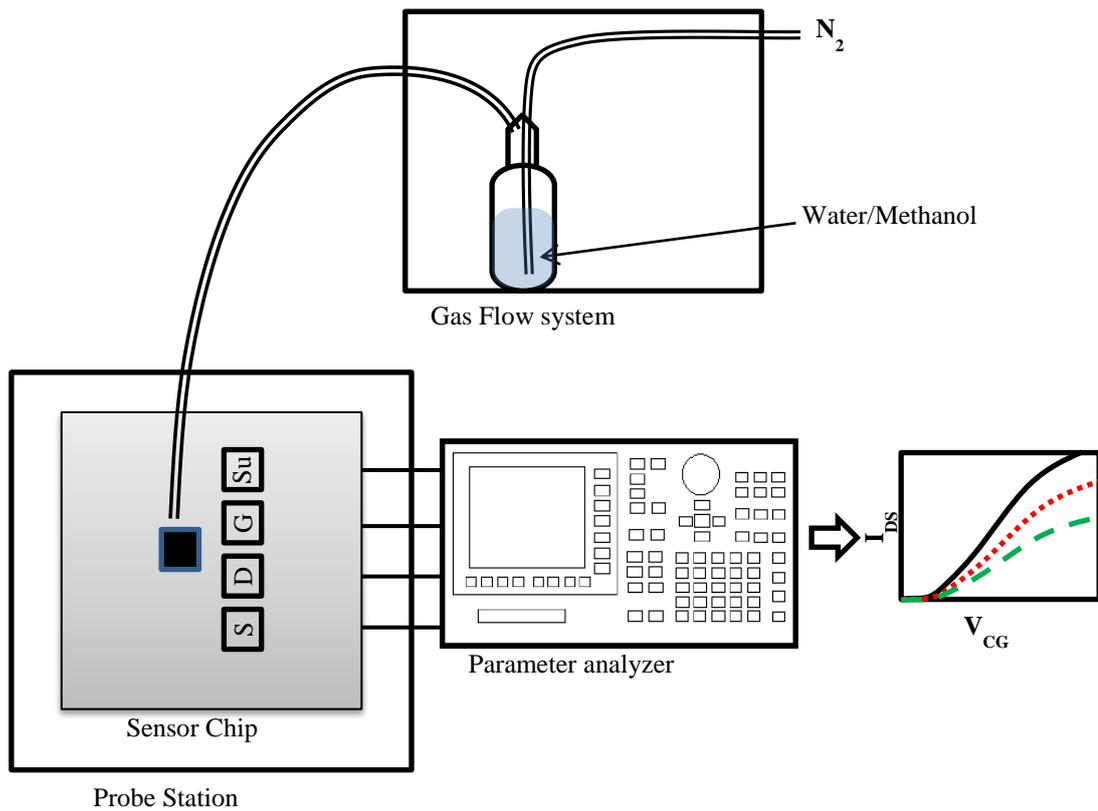


Figure 6.3. I-V measurement setup (S=Source, D=Drain, G=Control gate, Su=Substrate).

6.2.2 I-V Measurement Results

It is possible that the floating gate of a FGMOS could contain some residual charge resulting from the fabrication process. Before starting the gas exposure, the

sensor was initialized to remove any stored charge from the floating gate to ensure each experiment began in the same charge state. To initialize the sensor, a voltage higher than the normal potential ($V_{CG} = 30 \text{ V}$ and $V_D = 1 \text{ V}$) was applied on the control gate and the source, drain and substrate was grounded. The detail of this tunneling mechanism was presented previously in section 4.2.

Polypyrrole was used as a sensing polymer in this experiment which is known to absorb water molecules from the air at room temperature [48]. To ensure that the polymer was dry and no water molecules were left on the polymer, the sensor was exposed into a constant flow (400 sccm) of nitrogen (N_2). During this N_2 exposure, the source-drain current (I_{DS}) current was measured by changing the control gate voltage from 0 to 10 V with 0.5V step. This measurement was repeated several times with a 10 minutes interval. This ramped I-V data are shown in

Figure 6.4 and demonstrate that after 100 minutes of N_2 exposure the I_{DS} vs V_{CG} curves was shifting very slowly at 10 mV/s rates which could be considered as a relatively stable condition. Once this relatively stable condition was achieved, the device was assumed to be initialized and therefore ready for analyte exposure.

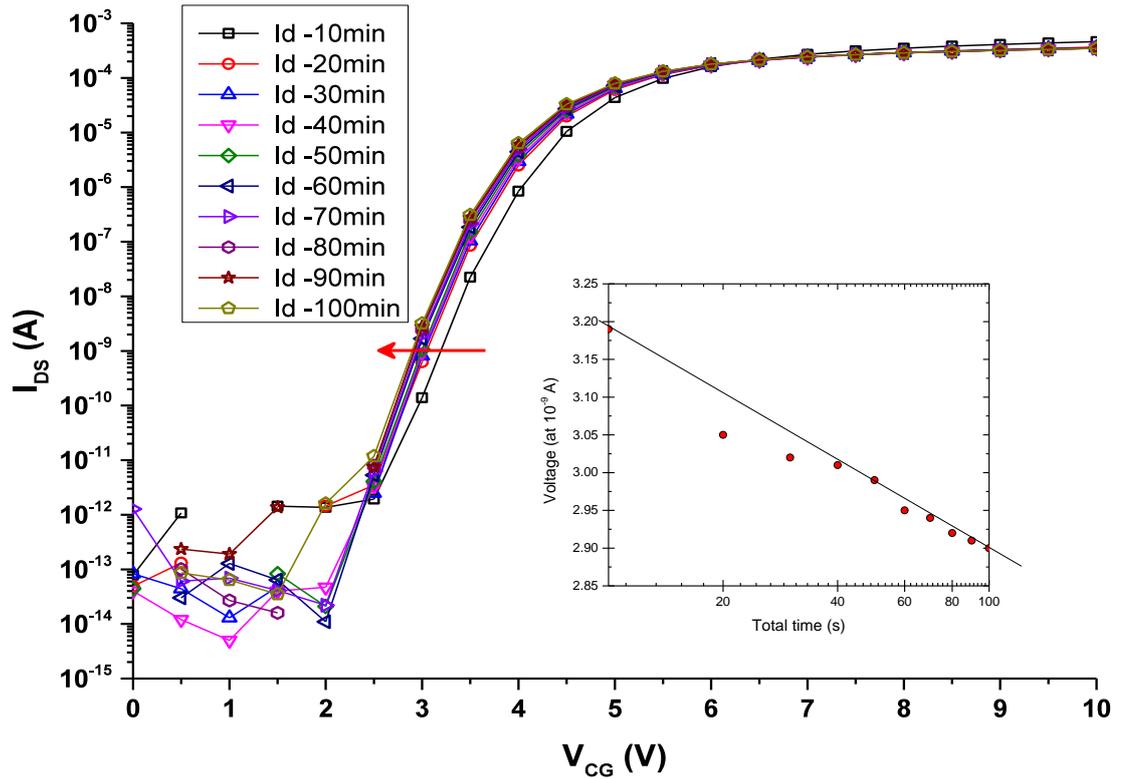


Figure 6.4. Sensor response with 400 sccm N₂ flowing. Each curve was measured following a 10 minutes time interval.

A FGMOS sensor with deposited polymer on it was then tested by exposing it to the gas analytes. The FGMOS sensor was first exposed to dry N₂ for two hours. After that, the source-drain current (I_{DS}) was measured while the N₂ was flowing. The sensor was then exposed to a mixture of water (H₂O) vapor, with a flow rate of 20 sccm and N₂ with a flow rate of 380 sccm for 30 minutes. At atmospheric pressure this results in a 5%/95% mixture of H₂O vapor/N₂. After 30 minutes, the source-drain current (I_{DS}) was measured while the gas was still flowing. After each I-V measurement, the sensor was electrically initialized (as discussed above) and exposed to N₂ for two hours. The H₂O vapor concentration was gradually increased in 5%

increments until 25% was obtained. A similar experiment was also undertaken using methanol (CH_3OH). The sensor responses to the H_2O vapor and CH_3OH are shown in

Figure 6.5 and Figure 6.6 respectively.

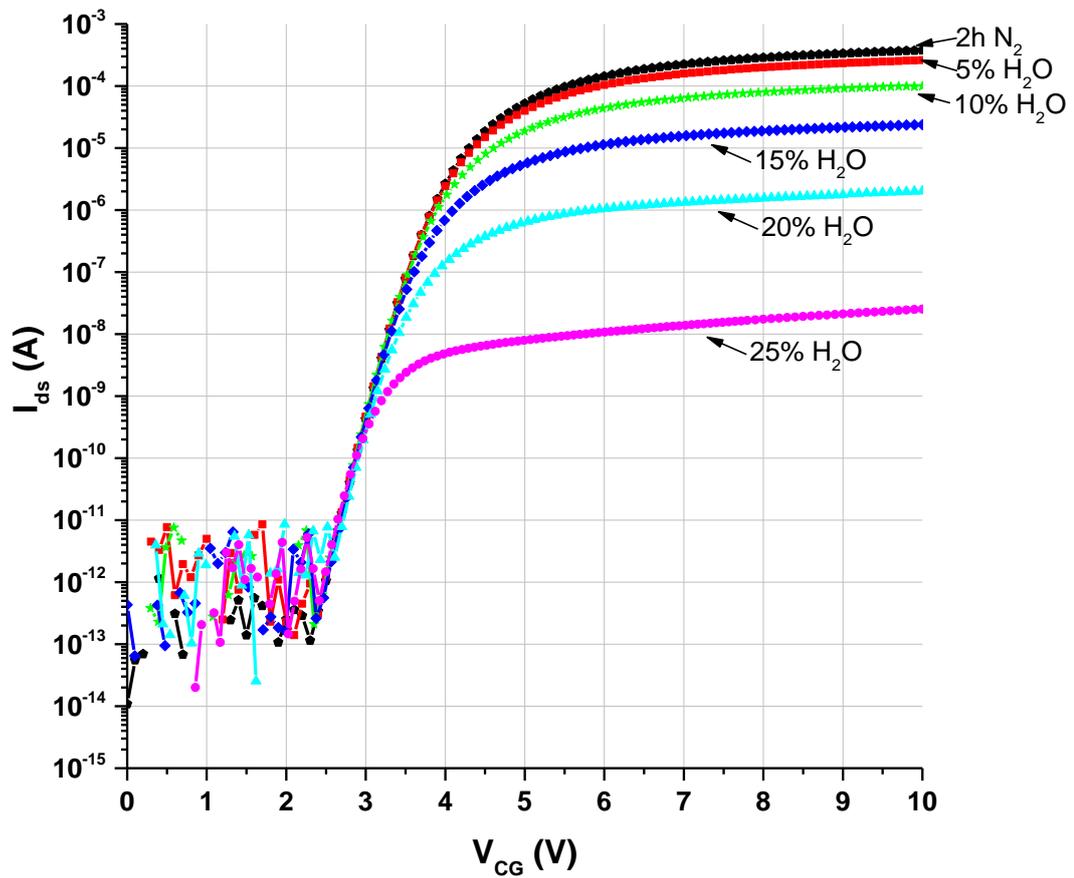


Figure 6.5. I-V sensor response for a range of water vapour concentration, 5% - 25% in nitrogen. Each measurement was made after a 30 minutes exposure.

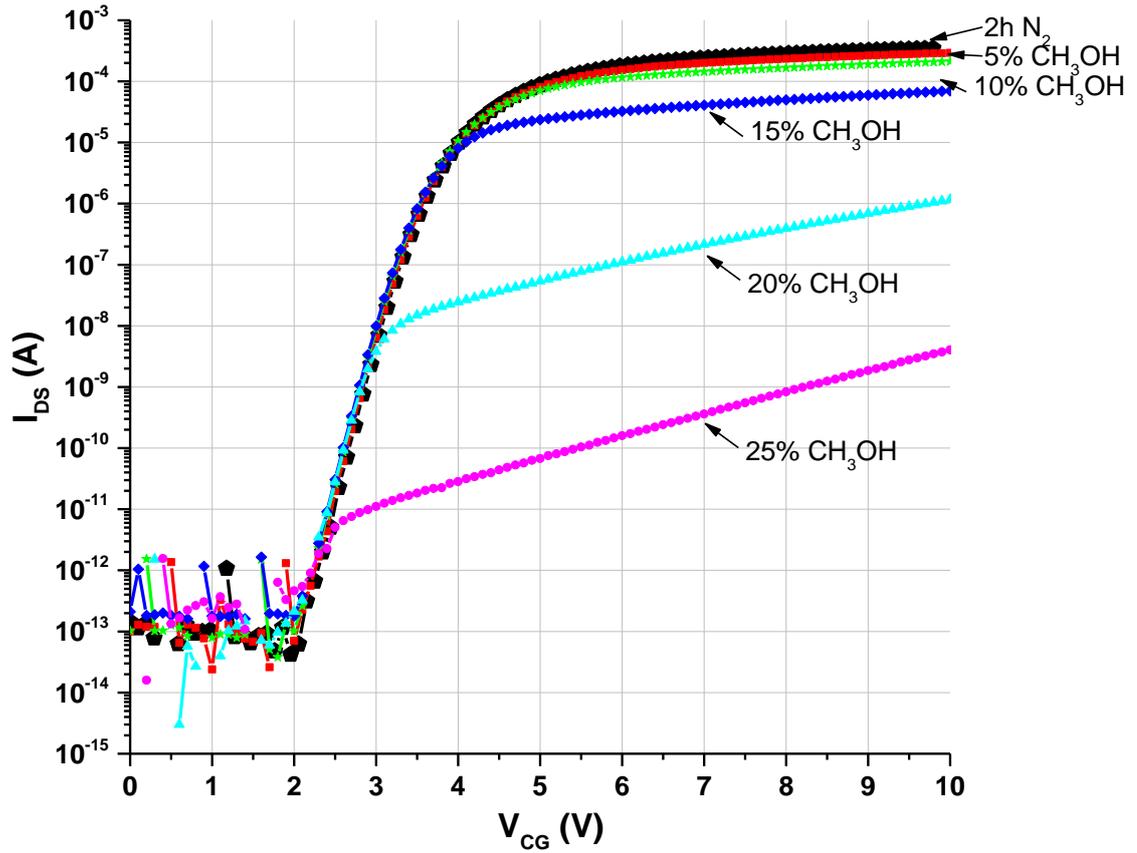


Figure 6.6. I-V sensor response for a range of methanol vapour concentration, 5% - 25% in nitrogen. Each measurement was made after a 30 minutes exposure.

From both of these data, it can be seen that the threshold voltage stays relatively constant, while there is a decreasing I_{DS} as a function of increasing concentration, for both water and methanol. As discussed previously in section 3.2, a change in either the charge on the floating gate or a change in the sensor pad capacitance should result a shift in both the threshold voltage as well as a change in the source-drain current (I_{DS}). After exposing the sensor to analyte gas, it was not able to produce any threshold voltage shift which suggested that the floating gate change or capacitance remain unchanged due to the analyte exposure. Further investigation is needed to have a better understanding of the device. However, in the following section, the

measurement time and electric field will be shown to have had a substantial effect of these measurements.

6.3 Time and Field Dependent Sensor Response

In the saturation region of a FGMOS, the effect of the control gate bias on the I_{DS} is very small. The results shown in

Figure 6.5 and Figure 6.6 demonstrated that the I_{DS} were increasing significantly with the control gate voltage at the saturation region while the gas was still flowing. It appears that there might be a causal relationship between the control gate voltage and the I_{DS} response. To investigate this relationship, a constant potential was applied to the control gate and change in the I_{DS} current was measured over 10 hours. The extended measurement period was chosen to observe the change in the I_{DS} current with a constant bias voltage on the control gate during exposure. The measurement setup was same as that used in the standard I-V measurement shown in Section 6.1.1. During the extended exposure time experiment, a constant voltage bias was applied to the source, drain, control gate and substrate and corresponding currents were measured. The voltage was applied to the control gate so that the device would be biased in the sub-threshold region. Since, in this regime, the current changes exponentially with gate bias, any small change in the threshold voltage should show a significant shift in the source-drain current.

6.3.1 Measurement Steps and Results

The source-drain current (I_{DS}) was continuously measured with a constant bias on the control gate ($V_{CG} = 5$ V), and drain ($V_D = 1$ V), while the sensor was exposed

to the analyte gas. The sequence of the experimental steps for this measurement is given below.

- i) The sensor was exposed to 400 sccm N_2 for 10 hours and I_{DS} was continuously measured with $V_{CG} = 5$ V and $V_D = 1$ V.
- ii) The sensor was then exposed to 20% H_2O vapor in N_2 and I_{DS} was continuously measured with same bias condition used in step (i).
- iii) The sensor was then reset to a known initial condition by applying $V_{CG} = 30$ V, $V_{DS} = 1$ V and exposed to N_2 for 2 hours.
- iv) The value of I_{DS} was again measured with 25% H_2O vapour in N_2 for 10 hours.

A similar experiment was repeated except the sensor was exposed to CH_3OH (25% in N_2) instead of H_2O vapour.

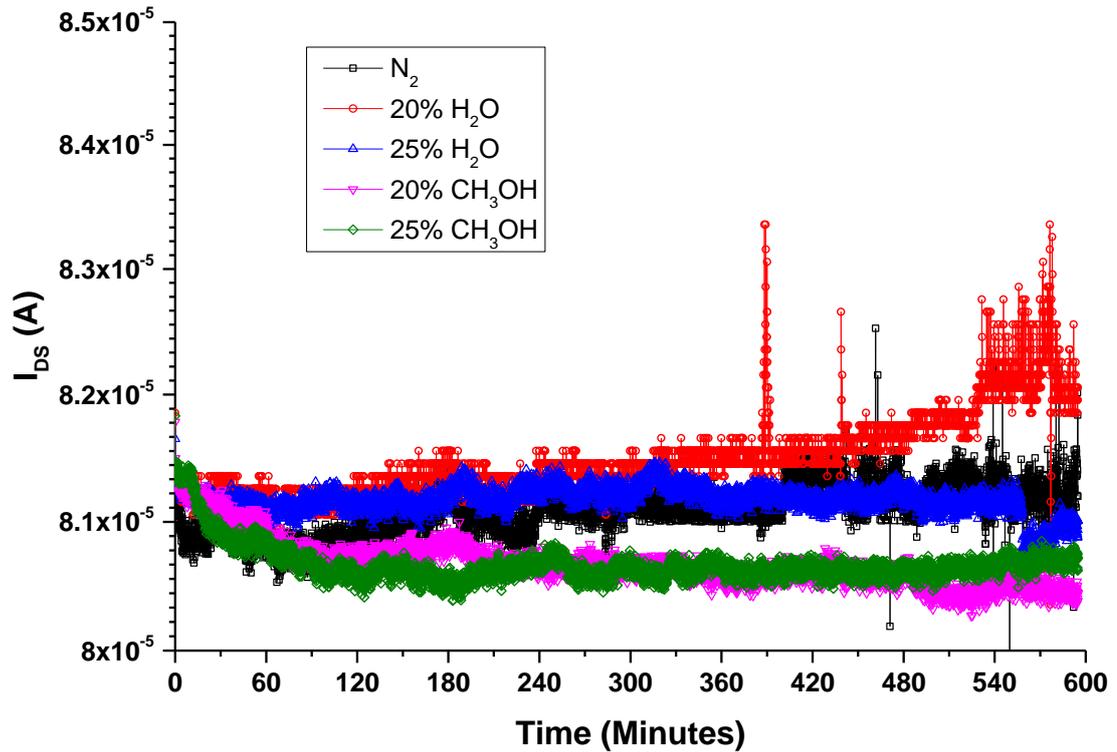


Figure 6.7. Sensor response for water and methanol flow for 10 hours. Sensor responses were continuously measured throughout the measurement duration with a constant potential on the control gate ($V_{CG} = 5 \text{ V}$) and drain ($V_D = 1 \text{ V}$).

For the 10 hours H_2O and CH_3OH exposure I_{DS} remained relatively constant. This is especially evident when the data of the

Figure 6.7 is compared to the previous results shown in

Figure 6.5 and Figure 6.6 The main difference between these two experiments is that in the second case, the bias was applied throughout the measurement. From these two experiments, it would appear that the applied potential has a pronounced effect on

the sensing capability of the polymer and the sensor. To more fully understand the effect of the applied bias, the sensor current were measured using a short voltage pulse on the control gate rather than a constant potential.

6.3.2 Pulse Measurement

To investigate the effect of the applied bias on the sensors capability, a voltage pulse of a short and defined duration and interval was applied to the source, drain, control gate and substrate while the sensor was continuously exposed to a gas analyte. The source-drain (I_{DS}) current was measured only during this short applied bias interval. The magnitude of the applied potential on the control gate and the drain was $V_{CG} = 5$ V and $V_D = 1$ V, respectively. The bias was applied to the control gate and drain for 0.5 second once every 2 minutes during which the source-drain current (I_{DS}) was measured. The schematic diagram illustrating the applied pulse on the control gate is shown in Figure 6.8 (a). The analyte gas concentration was set to 25% as the sensor showed maximum response with this concentration. The experimental sequence for this experiment is given below,

- i) The sensor was exposed in 400 sccm N_2 flow for 2 hours.
- ii) The initial sensor responses (I_{DS}) were measured continuously for 30 minutes while the N_2 gas was flowing.
- iii) The sensor was then exposed to 25% H_2O in mixed with N_2 . The source-drain current (I_{DS}) was measured with a 0.5 second duration voltage pulse to the control gate and drain ($V_{CG} = 5$ V and $V_D = 1$ V). The 0.5 second pulse was repeated every 2 minutes interval. The gas analyte remained flowing during the entire experiment.

iv) The experiment was repeated with same concentration of methanol.

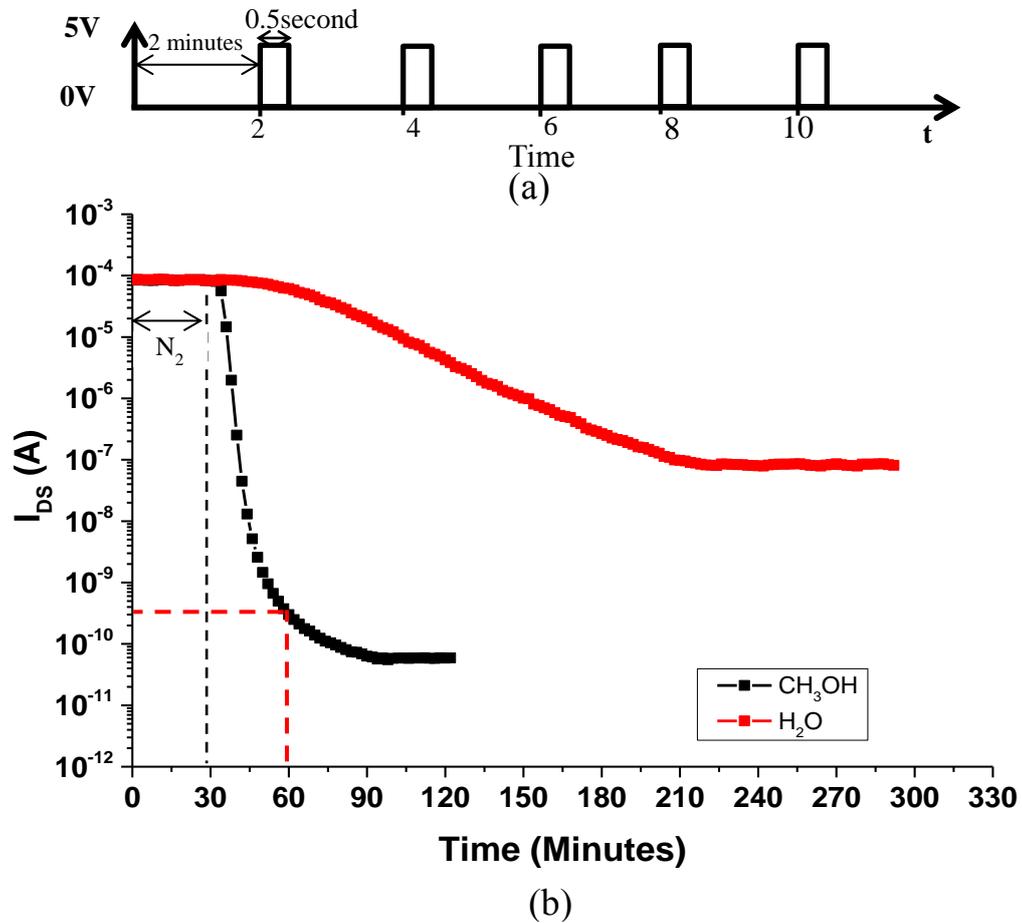


Figure 6.8. (a) Measurement voltage pulse 0.5 second every 2 minutes ($V_{CG} = 5$ V and $V_D = 1$ V) (b) I_{DS} response for 300 sccm N_2 and 100 sccm for H_2O or CH_3OH .

The change in the source-drain current (I_{DS}) as a function of time, for 25% H_2O and CH_3OH exposure is shown in Figure 6.8 (b). This pulse voltage data show that the source-drain (I_{DS}) current was decreased by several decades over the duration of this measurement. Even though the timescales were of the same order, the pulsed measurement results are substantially different to the relatively constant I_{DS} when the bias was applied continuously. The results

from the pulse measurement showed a large decrease in the source-drain current (I_{DS}) which was similar to the initial experiment (see

Figure 6.5 and Figure 6.6) where there was no applied bias during the analyte exposure. The current in this case was measured only at the end of the exposure time. It should be noted that while in both cases a substantial decrease in I_{DS} was observed, the absolute values of the current was not the same for these I-V measurement. A comparison of the absolute value of the ramped and pulsed data is shown in the Table 6.1.

Table 6.1. Comparison of the I_{DS} response between the ramped (after exposure) and pulsed (during exposure) measurement after a 30 minutes analyte exposure.

I_{DS} Measurement (A) after 30 minutes exposure at $V_{CG}=5$ V and $V_D=1$ V		
Analyte	Ramped I-V after exposure	Using Pulsed Voltage (after 30 minutes)
Water (25%)	8.2×10^{-9} A	6.2×10^{-5} A
Methanol (25%)	6.8×10^{-11} A	3.7×10^{-10} A

This variation in the current appears as if the applied bias (0.5 second pulse) was still affecting the sensor response during the analyte exposure. Moreover, this substantial difference in the I_{DS} current would suggest that the sensor response is not only affected by the control gate bias, but also the different molecule of the analyte gas. In the following experiments the pulse duration and measurement interval were changed to understand the effect of time and applied bias more clearly.

6.3.3 I_{DS} Measurement as a Function of Pulse Interval

To investigate the effect of the applied bias on the I_{DS} , in following experiment, the measurement pulse width (0.5 second) was kept constant and the measurement interval was changed from 1 to 2 then 5 minutes. The control gate voltage (V_{CG}) and the drain (V_D) were kept the same at 5 V and 1 V, respectively. During this 0.5 second pulse the source-drain (I_{DS}) current was measured. As the sensor responds faster when exposed to CH_3OH compared to H_2O , CH_3OH was chosen as the analyte to investigate this effect. The experimental steps for this experiment are given below,

- i) The sensor was exposed to N_2 for 2 hours. No bias was applied during this time. This established an initialization for all devices.
- ii) The sensor current I_{DS} was measured with a 0.5 second pulse once every minute while N_2 was flowing. This was repeated for 30 minutes.
- iii) The sensor was exposed to a 25% CH_3OH (100 sccm) in N_2 (300 sccm). The sensor response was measured with the same voltage pulse and timing as that in step (i).
- iv) The experiment procedure was repeated for I_{DS} measurement intervals of 2 and 5 minutes.

The schematic of the measurement pulses applied to the control gate for these three experiments are shown in Figure 6.9 (a) with the resultant data illustrated in Figure 6.9 (b).

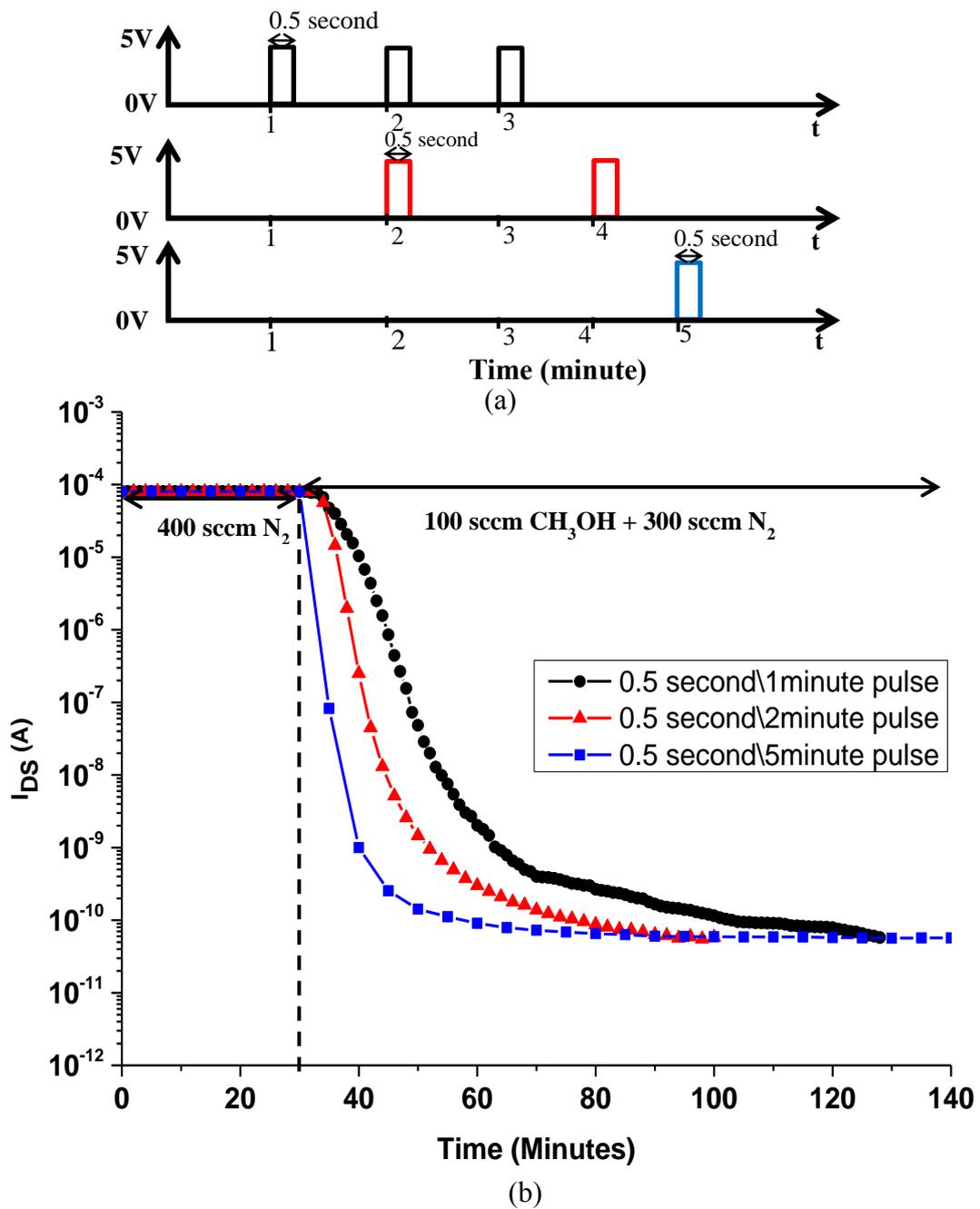


Figure 6.9. (a) Applied pulse schematic with a constant pulse width (0.5 second) and the pulse interval ranging from 1, 2, and 5 minutes. (b) I_{DS} response for pulse voltage during exposure to 25% CH_3OH (100 sccm) and N_2 (300 sccm).

The measurement data presented in Figure 6.9 (b) shows that as the pulse interval was increased, the current dropped to a lower value. For the shorter pulse

interval, the sensor did not appear to have enough time to respond completely between the pulses, leading a higher current value. This suggests that the sensor response is very sensitive to the applied potential, the duration over which it is applied and the interval between applications. To more fully investigate this effect of applied potential, in a subsequent experiment, the pulse width was varied (0.5, 30 and 60 seconds) with a fixed measurement interval (2 minutes).

6.3.4 I_{DS} Measurement as a Function of Pulse Width

In the following experiment, the pulse duration was adjusted for 3 pulse width; 0.5 to 30 and 60 seconds as demonstrated schematically in Figure 6.10 (a). The pulse interval was kept constant at 2 minutes.

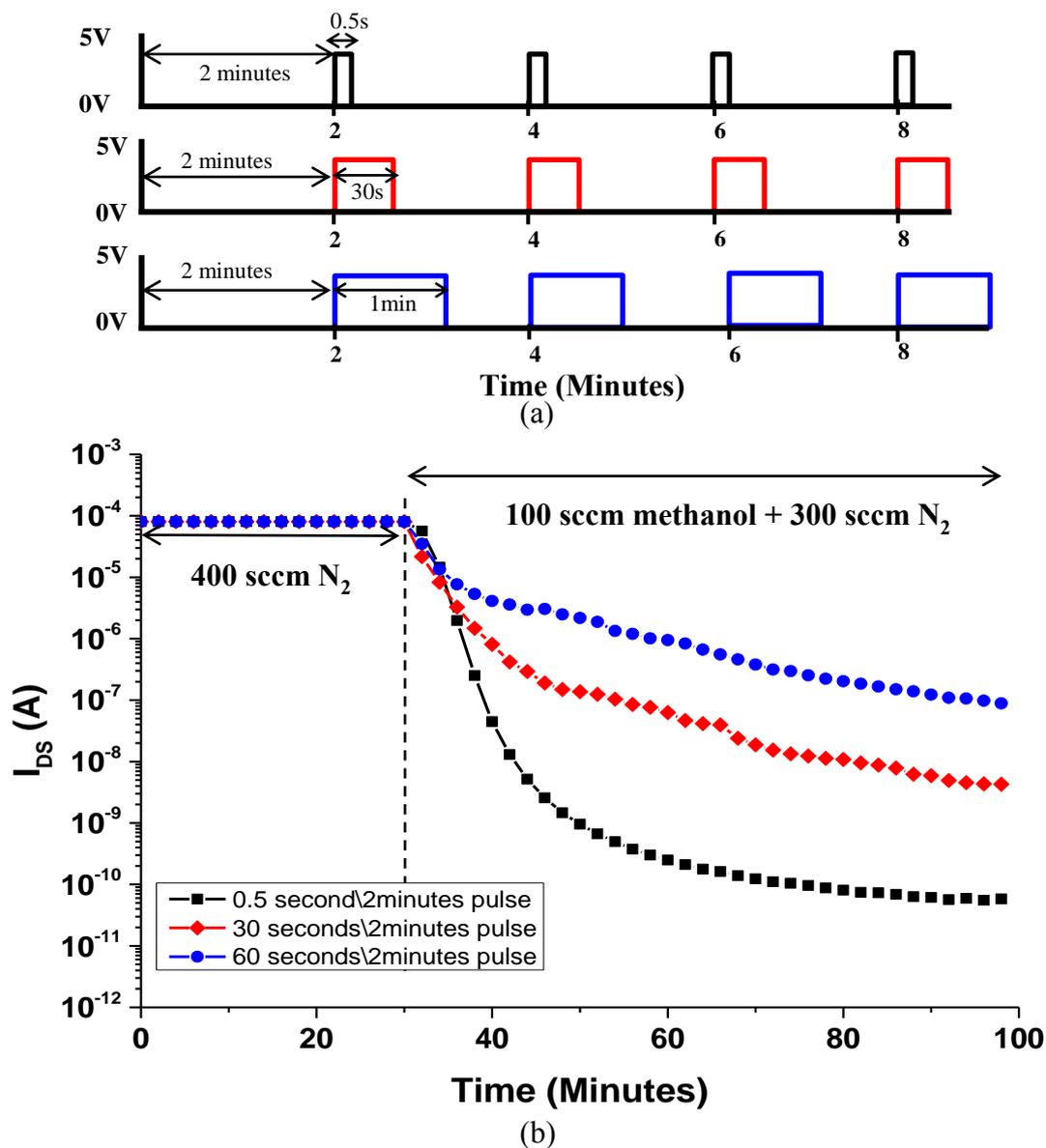


Figure 6.10. (a) Pulse measurement with increasing pulse width from 0.5, to 30 and 60 seconds with 2 minutes pulse interval. (b) I_{DS} response for 25% CH_3OH (100 sccm) with N_2 (300 sccm) exposures.

The measurement data shown in Figure 6.10 (b) demonstrates that as the pulse width was decreased, the current also decreased, for a given total exposure time. For the shortest pulse width, the largest decrease in I_{DS} was observed. From these last two experiments, the applied bias, duration and interval are shown to have a substantial

effect on the sensor response. To minimize the effect of the applied bias for the I_{DS} measurement, time during which the bias is applied should be minimized, while the interval between applications of the bias should be maximized.

Similar results showing the effect of an applied bias on a sensor response have been reported for work on conducting polymer based MOS sensors [49]. In this paper, the π -Conjugated poly (3,4-ethylenedioxythiophene) (PEDOT) based conducting polymer was used as the gate of a field-effect transistors. The doping of the polymer was achieved by partial oxidation of polymer by ferric p-toluenesulfonate (FTS). It was proposed that the effective doping in the polymer was reduced when a bias was applied during exposure in the water vapor. The polypyrrole was used as the sensing polymer in the FGMOS sensor design, which is also a conducting polymer and is also sensitive to humidity. The measurement data shown in Figure 6.7 (b) and Figure 6.8 (b), suggest that the polypyrrole might be similarly affected when a bias is applied during analyte gas exposure. For longer pulse widths and decreasing pulse intervals, the polypyrrole experiences a greater effect of the bias which might be reducing the doping level of the polymer and therefore the sensor response.

To minimize the effect of the applied bias and I_{DS} measurement on the sensor response, optimal times for both the pulse width and interval must be investigated. In the next experiment, the sensor response was measured with shorter pulses to find the minimum pulse duration required for I_{DS} measurement with minimal effect on the sensor analyte response.

6.4 Short Pulse Measurement

The previous measurement results showed a significant shift in the source-drain current (I_{DS}) as the pulse width and interval were changed. The pulses used in the previous experiments were still significant enough to alter the sensor response. To accurately measure the true sensor response, it is necessary to make sure that the effects of the measurement parameters are minimal. As such, determining the proper measure parameters was necessary to continue any further sensor response measurement. In this experiment, the sensor response was measured with even shorter pulses than the previous measurement.

6.4.1 Short Pulse Measurement Setup

The parameter analyzer used in the last few experiments could only produce a pulse of 0.5 second. As this pulse was found to affect the sensor response, a different measurement system, with a capability for shorter pulses was used to measure the sensor response. An arbitrary waveform generator (TGA1244) was used to generate pulses down to 20 μs with an interval of 1 minute. Two channels of this pulse generator were used to generate pulses for the control gate and the drain simultaneously. The drain voltage was also reduced to minimize its effect on the sensor. The applied potential on the control gate and drain was set to $V_{CG} = 5 \text{ V}$ and $V_D = 0.5 \text{ V}$ respectively. A Keithley 428 programmable current amplifier was used to measure the current from the source of the FGMOS. This current amplifier can convert currents down to few nano-amperes with a time constant of 10 microseconds. The output of the amplifier is a voltage which is proportional to the current. This output was displayed on an oscilloscope to measure I_{DS} . An Agilent oscilloscope

(DSO5014A) was used to display and measure this voltage which was proportional to I_{DS} .

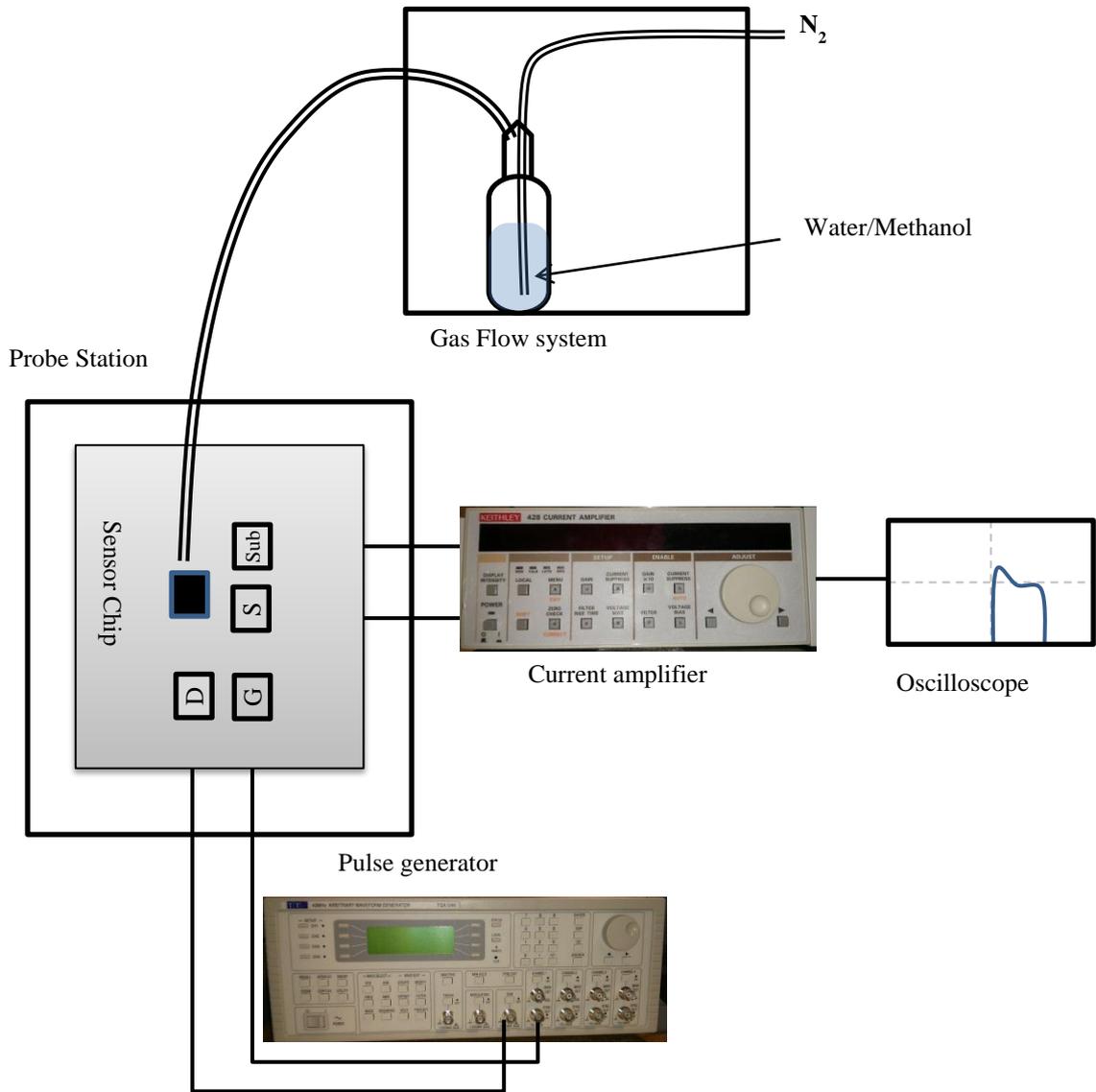


Figure 6.11. Measurement setup for short pulse measurement.

6.4.2 Short Pulse Measurement Results

In this experiment, the pulse widths were set to 20 μs (shortest pulse possible from the pulse generator) and were then changed to 40 μs and 60 μs . A constant 2

minute pulse period or interval was used. As shown in the results of previous experiments (Figure 6.4), an exposure to a higher gas concentration produced a faster sensor response. Therefore, in this experiment the sensor was exposed to 40% CH₃OH with N₂.

In Figure 6.12 the sensor response is shown to be relatively independent of the pulse width. For these short pulses, the applied bias does not appear to affect the sensor response to the analyte. In all the subsequent experiments a 40 μ s pulse width and a 2 minutes interval was used. Now that a measurement biasing condition was found that did not appear to affect the sensor response; an investigation of the sensor response to different concentrations of gas analyte was undertaken.

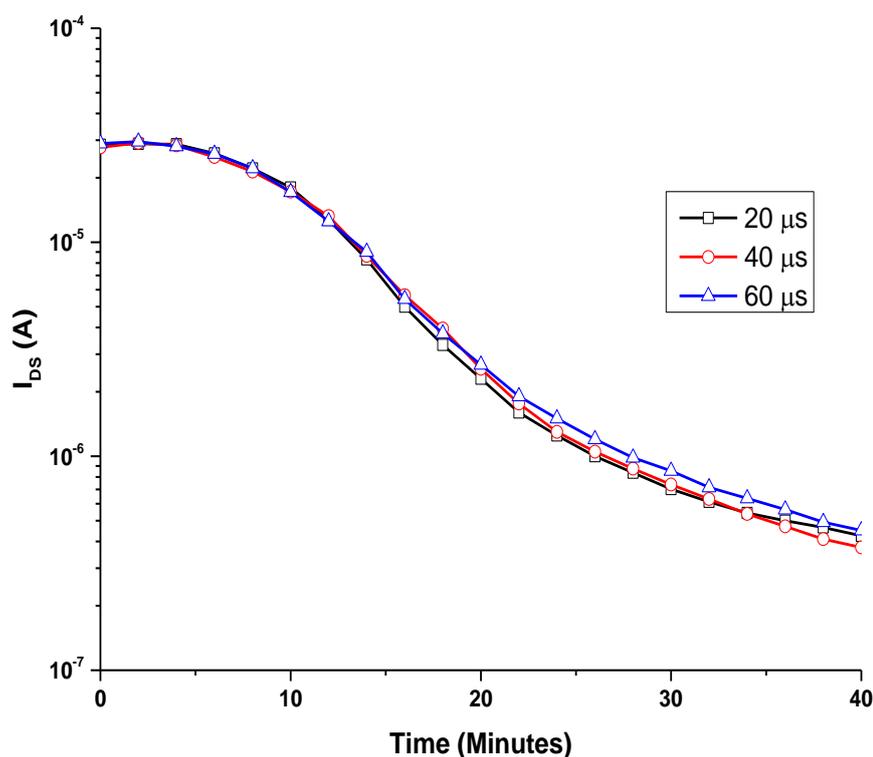


Figure 6.12. Short pulse measurement using 20 μ s, 40 μ s and 60 μ s pulse width and 2 minutes pulse interval.

6.5 Sensor Characterization using a Short Pulse

The previous measurement results provided the necessary measurement parameters to measure the sensor response without affecting the response itself. To investigate the sensor response to different analyte concentrations, the sensor was exposed to concentration of CH₃OH varying from 10% to 50% in 10% increments. The I_{DS} measurement was performed with a 40 μs pulse applied every 2 minutes interval. The bias was applied to the control gate (V_{CG} = 5 V), drain (V_D = 0.5 V), source (V_S = 0 V) and substrate (grounded) only during this 40 μs pulse period. The experiment sequences for this experiment are given below,

- i. The sensor was exposed to N₂ for 2 hours and response was measured using a 40μs pulse every 2 minutes interval.
- ii. The sensor was then exposed into 10% CH₃OH with N₂ for 1 hour and the sensor response was measured using the same pulse width and interval that was used in step (i).
- iii. The CH₃OH concentration was increased by 10% and the sensor response was measured without changing the pulse width and interval.
- iv. The measurement duration for each concentration was 1 hour.
- v. After 50% CH₃OH exposure the sensor was again exposed into 40% CH₃OH for an hour to check the reversible response of the sensor.
- vi. At the end of the experiment, the sensor was exposed to pure N₂ for an hour to refresh the sensor.

The measurement results shown in Figure 6.13 demonstrate that for a given concentration, the source-drain current (I_{DS}) was decreasing over time. The change in

I_{DS} at low concentrations (10-20%) was very small, compared to the sharp decrease in I_{DS} at higher concentrations (30-40%). Moreover, the current change was also small when the concentration was increased from 40% to 50%. After the 50% exposure, the sensor was exposed to 40% methanol to check the reversible response of the sensor. However, it was found that the response was minimal and did not return to the value expected from the first 40% response. This might be a result of the sensor reaching some form of analyte saturation. The change in the sensing polymer with increasing (10% to 40%) analyte exposure might bring the sensor to a condition after which the sensor can no longer detect any changes in the concentration. On the assumption that a saturation condition was being reached, a method of initialization or refreshing the sensor was needed.

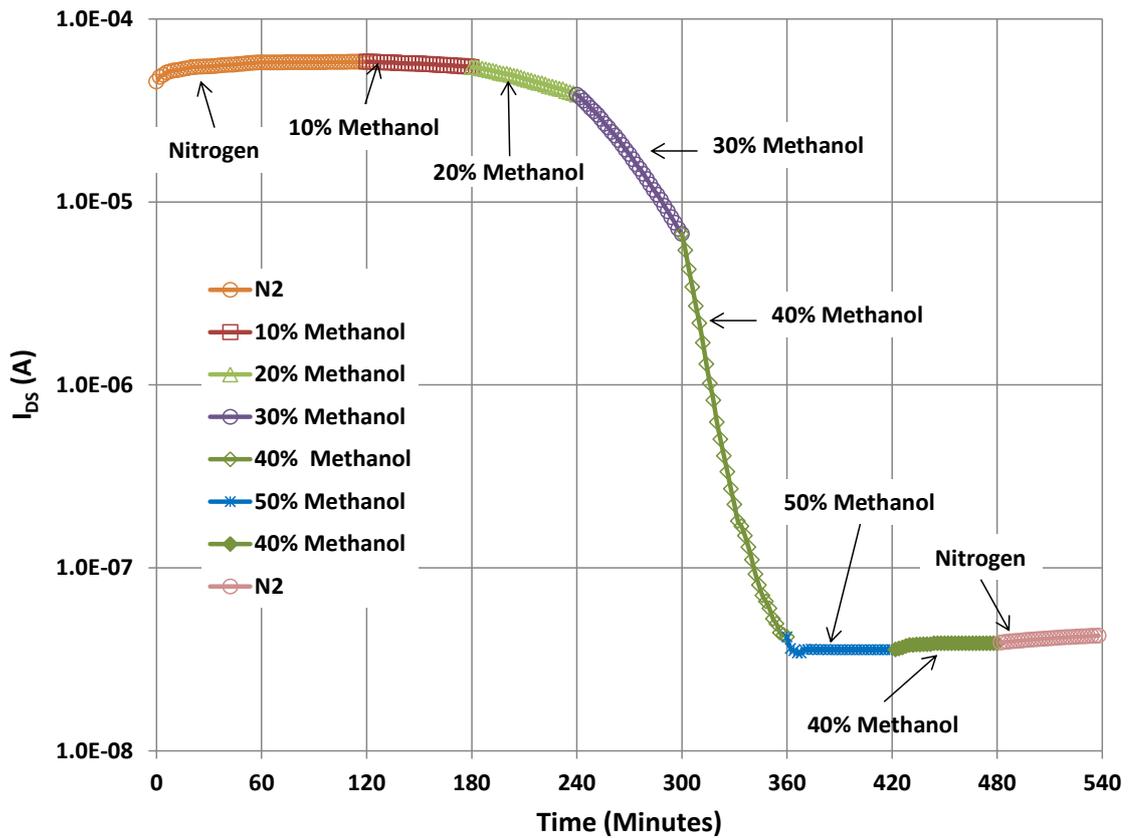


Figure 6.13. Pulse measurement with 10%-50% methanol exposure with 10% increase in concentration.

In a resistive sensor using the same polymer (Polypyrrole) and dopant, the sensor was found to need to be refreshed by exposing into nitrogen for 30 to 60 minutes [50]. To test the similar characteristic, the FGMOS sensor was exposed to N_2 for an hour after second 40% exposure. However, it was found that this was insufficient as the sensor response did not change significantly and remained in virtually the same saturation condition. Therefore, the conventional N_2 refreshing technique of conduction polypyrrole based resistive sensor was found not to be practical for refreshing this FGMOS based sensor. A different and fast refreshing mechanism for polymer based FGMOS sensor was needed.

The I-V sensor responses shown in Section 6.1.3 demonstrated that as the control gate voltage was increased, the I_{DS} was increased towards the initial sensor response (i.e. the response after 2 hours of N_2 exposure). Therefore, if a high voltage was applied to the control gate, the sensor might reach to a condition which is close to sensor response after 2 hours N_2 exposure.

6.6 Electrical Refreshing

To investigate the effect of an electrical refreshing mechanism, a high voltage was applied to the control gate for a certain time, and I_{DS} current was continuously measured. To establish an initial reference response, the sensor was exposed to N_2 for 2 hours. The I_{DS} current was measured after 2 hours by applying a constant bias on the drain ($V_D=0.5$ V) and sweeping the control gate voltage from 0 to 10V in 0.1V step (I-V measurement), while N_2 was flowing (Figure 6.14 (a)). The sensor then was exposed to 30% CH_3OH with N_2 for 30 minutes after which another I-V measurement was performed (Figure 6.15 (b)). After the gas exposure, the electrical refreshing was tested by applying a high control gate voltage ($V_{CG}=30$ V) where the I_{DS} current was continuously measured. The measurement results shown in Figure 6.13 demonstrate that, after a high bias was applied to the control gate, the I_{DS} current was found to increase rapidly and reached to saturation level within 5 seconds. This measurement was repeated 3 times to check the sensor was properly refreshed and no variation in I_{DS} was found. After this experiment, another I-V sweep measurement was performed (Figure 6.14 (c)). This result was compared with the initial reference response (response after 2 hours of N_2 exposure) and is shown in Figure 6.14. After a high bias was applied to the control gate for 5 seconds, the sensor response changed

significantly and reached a response similar to that after 2 hours initial N₂ exposure. Therefore, it was assumed that this electrical refreshing was sufficient to return the sensor to a known, initial condition.

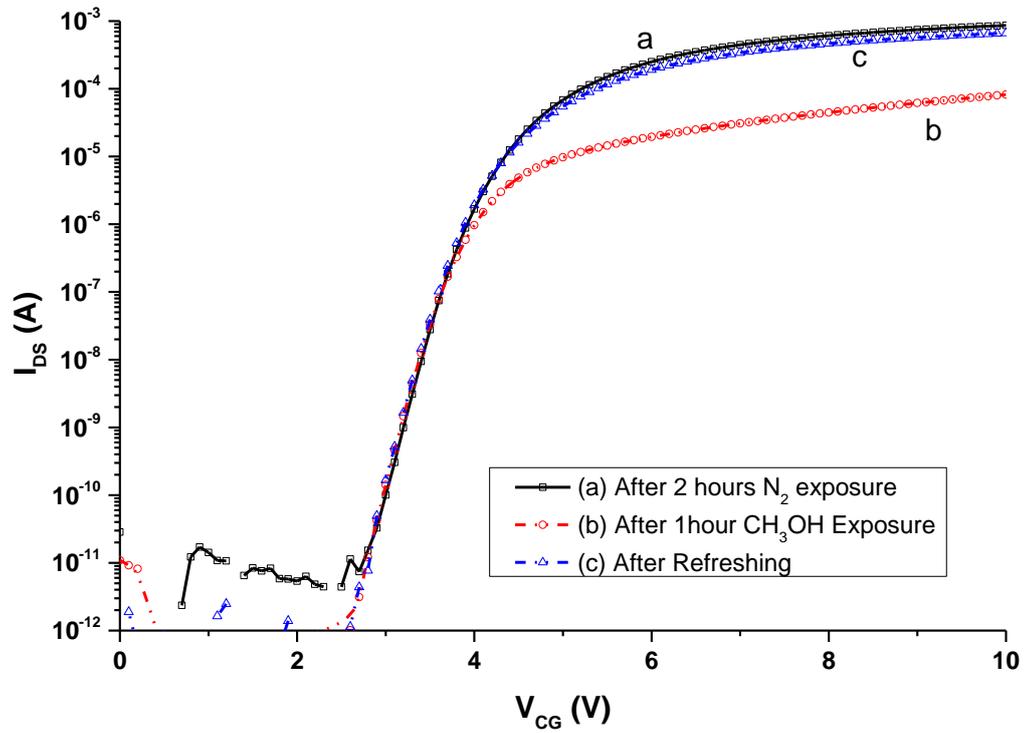


Figure 6.14. The sensor response (a) after 2 hours N₂ exposure (reference response), (b) after 30% methanol exposure, (c) After electrical refreshing with high control gate biasing.

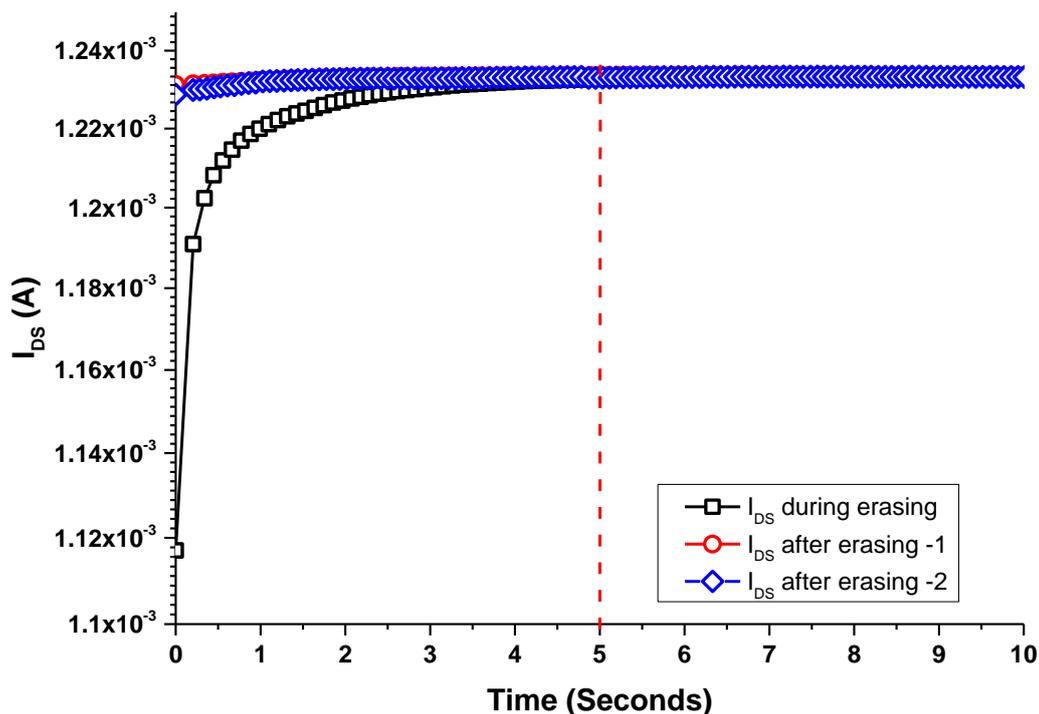


Figure 6.15. Electrical refreshing by applying a constant high voltage on the control gate ($V_{CG}=30$ V) for 10 seconds.

6.7 Pulse Measurement with Electrical Refreshing

After defining the sensor refreshing and measurement parameters, the sensor was tested again with different analyte concentrations. The sensor responses were measured for 10% to 50% concentration of CH_3OH in N_2 with a 10% increment. The sensor was electrically refreshed after each exposure. For each concentration the measurement was repeated three times to check repeatability of the measurement and sensor response. The applied potential on the control gate, drain, and source was set to $V_{CG} = 5$ V, $V_D = 0.5$ V and $V_S = 0$ V for $40 \mu\text{s}$ during which I_{DS} was measured. This

measurement was repeated every 2 minutes. The measurements procedure for this experiment are given below,

- i) The sensor was exposed into 400 sccm N_2 for two hours. The response was measured with a 40 μ s pulse once every 2 minutes.
- ii) The sensor was then exposed to 10% CH_3OH with N_2 for 1 hour and sensor response was measured with the same pulse width and interval that was used in step (i).
- iii) The gas flow was stopped and the sensor was electrically refreshed by applying $V_{CG}=30$ V and $V_D=0.5$ V for 5 seconds.
- iv) For each concentration step (ii) and (iii) was repeated three times.
- v) The CH_3OH concentration was increased by 10% and the step (ii), (iii) and (iv) for each concentration.
- vi) The measurement process continued till 50% CH_3OH concentration.

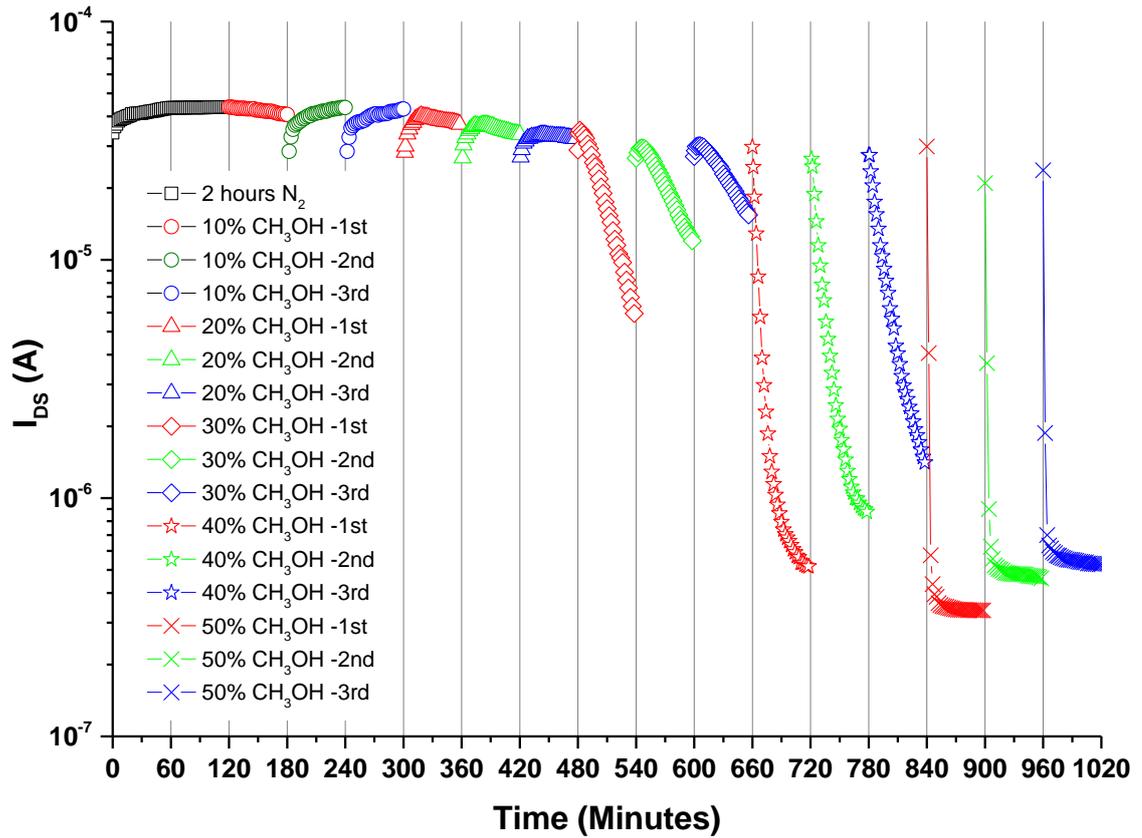


Figure 6.16. Repeated sensor response from 10% to 50% CH₃OH in N₂ with 10% increment in the concentration. After each exposure the sensor was electrically refreshed.

The measurement results are shown in

Figure 6.16 and demonstrate that for concentrations of 30% to 50% CH₃OH, the sensor responses improved significantly after electrical refreshing. However, for concentration from 10% to 20%, the response was very small. In the previous experiment, the sensor was electrically refreshed and exposed in N₂ for two hours while in the present experiment, the sensor was refreshed electrically without exposure to N₂. The results after electrical erasing are significantly different and more reliable. Electrical refreshing would also be more preferable for practical applications

of the sensor due to the complications requiring a refresh of the sensor with N₂ for few hours. The sensor also showed a more consistence shift in the response for each repeated measurement with the electrical refreshing.

6.8 Sensor Responses in Continuous, Reverse and Random Order

In the previous experiments, the analyte concentration was continuously increased from 10% to 50% with a 10% increment. In a practical application, the sensor would need to be able to detect any concentration change at any time. Therefore, in this experiment, the sensor response was measured by changing the gas concentration in a random, increasing and decreasing order. The measurement setups and parameters were same as the previous experiment. The sensor response was measured after 30 minutes of gas exposure. The sensor responses shown in Figure 6.16 demonstrate that I_{DS} for each concentration was significantly different from others after ~10 minutes of the gas exposure. In this experiment, the responses, measured after 30 minutes of exposure, should give a good variation in I_{DS} for each different concentration. The sensor responses were initially measured continuously when increasing the concentration from 10% to 50% with a 10% increment. The gas concentration was then changed randomly and responses were measured. Finally, the concentration was changed from 50% to 10% with a 10% decrease. The measurement results are shown in Figure 6.17.

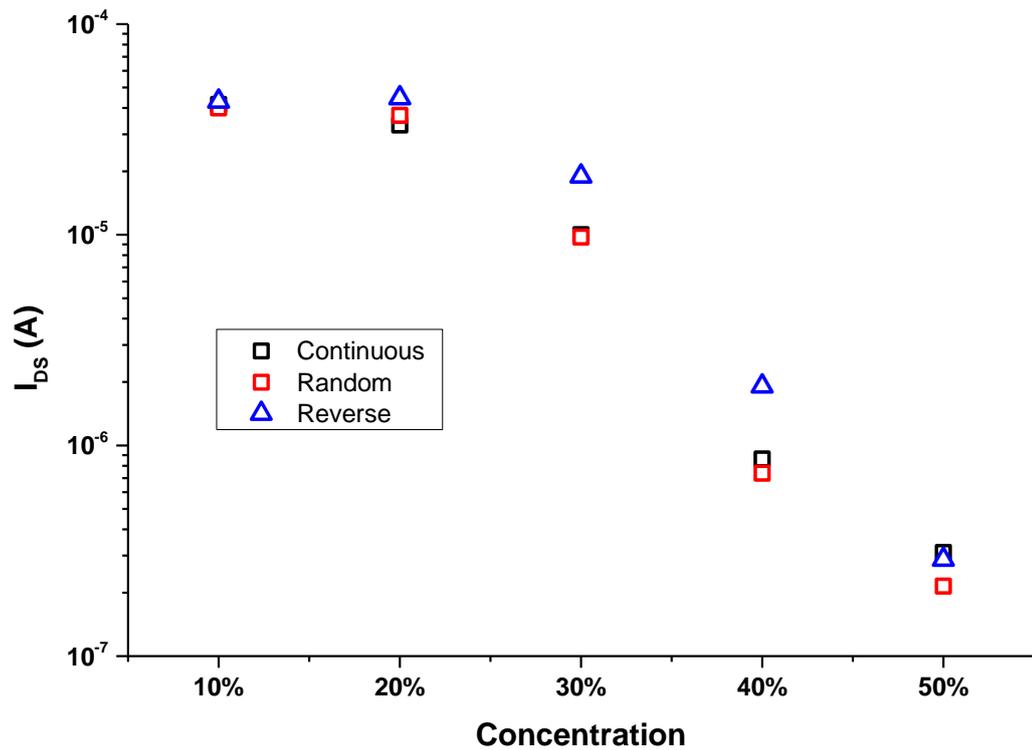


Figure 6.17. The gas concentration was changed in continuous order, the random order and reverse order.

In continuous increasing concentration measurement, the sensor shows a significant shift as the concentration increases. The random and reverse exposures show the similar response for each individual concentration. For each concentration, the responses are closely spaced and significantly separate from other concentration.

Chapter 7 – Conclusions and Future Work

A FGMOS based chemical sensor, that can be used to design a large sensor array to emulate the mammalian olfaction, was developed in this research. A new FGMOS was designed where the top metal layer of the CMOS process was used as a sensor pad. This metal layer remained exposed on top of the sensor chip and reduced the number of post processing steps that were required to expose the sensor pad for polymer deposition. A sensor chip was designed which contained a few test sensors, an 8×8 sensor array, array control circuits and an output amplifier for the sensor array. The individual sensor device was tested and results are presented in this research. A FGMOS model was developed and the results were compared with the fabricated devices. It was found that, measured characteristics of the fabricated FGMOS were significantly different than an ideal FGMOS. At present the reasons are not fully understood for the discrepancy. However, through an SEM image, it was discovered that the actual physical structure of the device was significantly different than the ideal structure used in the model. Nonetheless, the FGMOS sensor was still able to produce a stable response for charge injection onto and charge removal from the floating gate.

During the post processing, a thin layer of gold was deposited on top of the sensor pad using lift-off process. This was followed by the electrochemical deposition of a thin polymer film (polypyrrole). After depositing the polymer onto the sensor pad, the FGMOS was tested by exposing it to methanol and water vapor. The sensor response was measured with both a constant potential and with voltage pulse of different duration and duty cycle. The results suggested that the sensor response was sensitive to the applied bias during and after exposure, to the analyte concentration and to the

time of exposure as well as the measurement time. Several measurements were performed with various pulse duration and intervals to investigate those effects. It was found that for a short pulse of 40 μs in 2 minutes interval, the sensor was able to produce a response which was not affected by the applied bias.

Finally, the sensor response was measured with different concentrations of analyte gas. The measurement results demonstrated that, the sensor was able to show very good response for high concentrations of analyte gas. However, for lower concentration of analyte gas, the sensor response was very small.

This research successfully demonstrates that, a FGMOS device can be used to design a gas sensor. The same device can be used to sense many types of analyte gases. Designing a larger sensor array using this device will enable the design of a sensor chip which can be used to detect many analyte gases and can be used for electronic nose application.

7.1 Future work

The FGMOS response was found to be significantly different than an ideal FGMOS device. The model that was developed to characterize the FGMOS was not able to explain the electrical response of the FGMOS. The SEM image (shown in Figure 4.9) of the FGMOS showed that the fabricated device structure was significantly different than the ideal structure. For future work, a new FGMOS model, based on the fabricated device structure, needs to be investigated to have a better

understanding of the FGMOS. Conversely, a different device technology could be used to fabricate a device that more closely resembles an ideal structure.

The field dependent sensor response that was observed during the sensor measurement might be the results of several factors such as, bias dependent chemical reaction between the analyte gas and the polymer, diffusion or absorption of the analyte gas and/or charge by the polymer, polarization of the polymer due to the applied bias or a de-doping process in the polymer due to the presence of an analyte gas. For future work, several experiments can be performed to investigate those effects. To understand if, the analyte and/or charge diffusion or absorption in the polymer, several experiments with different bias polarity, duration and interval might yield some information. To understand the possibility of a polymer/analyte chemical reaction that could be bias dependent, selecting a suitable polymer and analyte gas pair with a known chemical interaction might shed some light on the device response. De-doping of the polymer could take place when the sensor is exposed to an analyte gas and a bias is applied on the device. This process is sensitive to the types of the dopant used in the polymer, the applied bias and the analyte gas. This effect can be investigated by changing the dopant type and/or concentration in the polymer.

The applied bias across the device might also polarize the polymer and might increase or decrease its sensitivity of the polymer. This can be investigated by measuring the sensor response with different bias voltage and exposing the sensor to analytes with molecule that are more or less polar to if there is an effect.

The sensor response was very small while it was exposed to low concentration of water and methanol vapor. This might be due to the poor sensitivity of deposited polymer. The sensitivity of the polymer depends on the type of the monomer, deposition parameters and type of dopant in the polymer. Those parameters should be investigated in future to improve the sensor response for low gas concentration.

After having a better understanding about the FGMOS characteristic and polymer interaction with the gas analyte, the FGMOS sensor should be tested with different analytes gases and polymers. Several polymers have been discovered in recent years [1], which might be sensitive to a particular gas or a group of gases. In future work, the use of different polymers with varying sensitivities should be included in the device to maximize the sensor response.

Finally, once the individual device with the different polymers is more fully understood, the sensor array can be investigated where in the ideal case, each individual sensor could be functionalized with a specific polymer.

References

- [1] H. Bai and G. Shi, "Gas Sensors Based on Conducting Polymers," *Sensors*, vol. 7, no. 3, pp. 267–307, Mar. 2007.
- [2] P. Bergveld, "The impact of MOSFET based Sensor," *Sensors and Actuators*, vol. 8, no. 2, pp. 109–127, 1985.
- [3] B. Lundberg and B. Sundqvist, "Resistivity of a composite conducting polymer as a function of temperature, pressure, and environment: Applications as a pressure and gas concentration transducer," *J. Appl. Phys.*, vol. 60, no. 3, p. 1074, Aug. 1986.
- [4] T. Ishihara and S. Matsubara, "Capacitive Type Gas Sensors," *J. Electroceramics*, vol. 2, no. 4, pp. 215–228, 1998.
- [5] H. V. Shurmer and J. W. Gardner, "Odour discrimination with an electronic nose," *Sensors Actuators B Chem.*, vol. 8, no. 1, pp. 1–11, 1992.
- [6] B. J. Polk, "ChemFET arrays for chemical sensing microsystems," in *Proceedings of IEEE Sensors*, 2002, vol. 1, pp. 732–735.
- [7] C.-S. Lee, S. K. Kim, and M. Kim, "Ion-sensitive field-effect transistor for biological sensing," *Sensors (Basel)*, vol. 9, no. 9, pp. 7111–31, Jan. 2009.
- [8] M. Liess, D. Chinn, D. Petelenz, and J. Janata, "Properties of insulated gate field-effect transistors with a polyaniline gate electrode," *Thin Solid Films*, vol. 286, no. 1, pp. 252–255, 1996.
- [9] N. Y. Shen, E. A. Minch, and E. C. Kan, "Polymer surface electrochemistry for charge-based sensing in chemoreceptive neuron MOS (CvMOS) transistors," in *Proceedings of IEEE Sensors*, 2003, vol. 2, pp. 914–919.
- [10] O. Fujita and Y. Amemiya, "A floating-gate analog memory device for neural networks," *IEEE Trans. Electron Devices*, vol. 40, no. 11, pp. 2029–2035, 1993.
- [11] N. Y. Shen, C. Lee, and E. C. Kan, "Fast and sensitive electret polymer characterization by extended floating gate MOSFET," *IEEE Trans. Dielectr. Electr. Insul.*, vol. 12, no. 5, pp. 1082–1087, Oct. 2005.
- [12] C. Tao, B. Chen, S. William, and S. Pandey, "A novel floating-gate biosensing device with controlled charge-modulation," *Life Sci. Syst. Appl. Work.*, pp. 257–260, Nov. 2007.

- [13] R. Pohle, O. von Sicard, M. Fleischer, B. Jakoby, M. J. Vellekoop, H.-P. Frerichs, C. Wilbertz, and I. Freund, "Gate pulsed readout of floating gate FET gas sensors," *Euroensors XXIV*, vol. 5, pp. 13–16, Jan. 2010.
- [14] C. Wilbertz, H.-P. Frerichs, I. Freund, and M. Lehmann, "Suspended-Gate- and Lundstrom-FET integrated on a CMOS-chip," *Sensors Actuators A Phys.*, vol. 123–124, no. September 2004, pp. 2–6, Sep. 2005.
- [15] K. Cao, "A Chemical Sensor Design Using a Standard CMOS Process," University of Manitoba, 2007.
- [16] M. A. Reyes Barranca, S. Mendoza-Acevedo, L. M. Flores-Nava, A. Avila-García, E. N. Vazquez-Acosta, J. A. Moreno-Cadenas, and G. Casados-Cruz, "Using a Floating-Gate MOS Transistor as a Transducer in a MEMS Gas Sensing System," *Sensors*, vol. 10, no. 11, pp. 10413–10434, Nov. 2010.
- [17] D. Kahng and S. M. Sze, "A floating-gate and its application to memory devices," *Bell Syst. Tech. J.*, vol. 46, no. 4, pp. 1288–1295, 1967.
- [18] A. Thomsen and M. A. Brooke, "A floating-gate MOSFET with tunneling injector fabricated using a standard double-polysilicon CMOS process," *IEEE Electron Device Lett.*, vol. 12, no. 3, pp. 111–113, Mar. 1991.
- [19] P. E. Cottrell, R. R. Troutman, and T. H. Ning, "Hot-electron emission in n-channel IGFETs," *IEEE J. Solid-State Circuits*, vol. 14, no. 2, pp. 442–455, Apr. 1979.
- [20] S. Mahapatra, S. Shukuri, and J. Bude, "CHISEL Flash EEPROM — Part II: Reliability," *IEEE Trans. Electron Devices*, vol. 49, no. 7, pp. 1302–1307, 2002.
- [21] R. H. Fowler and L. Nordheim, "Electron Emission in Intense Electric Fields," *Proc. R. Soc. A Math. Phys. Eng. Sci.*, vol. 119, no. 781, pp. 173–181, May 1928.
- [22] S. T. Wang, "On the I-V characteristics of floating-gate MOS transistors," *IEEE Trans. Electron Devices*, vol. 26, no. 9, pp. 1292–1294, 1979.
- [23] O. Fujita and Y. Amemiya, "A floating-gate analog memory device for neural networks," *IEEE Trans. Electron Devices*, vol. 40, no. 11, pp. 2029–2035, 1993.
- [24] K. Cao, "A Chemical Sensor Design Using a Standard CMOS Process," University of Manitoba, 2007.
- [25] Y. Huang, S. Wagner, and J. C. Sturm, "Nonvolatile Amorphous-Silicon Thin-Film-Transistor Memory Structure for Drain-Voltage Independent Saturation

- Current,” *IEEE Trans. Electron Devices*, vol. 58, no. 9, pp. 2924–2927, Sep. 2011.
- [26] M. Y. Li, C. M. Liu, H. Kuan, D. Wang, C. C. Tsai, H. R. Yeng, and J. Chen, Y, “TSMC 0.35um Mixed Signal Polycide 3.3/5V Design Rule,” 1999.
- [27] K. Keiji Kanazawa, A. F. Diaz, W. D. Gill, P. M. Grant, G. B. Street, G. Piero Gardini, and J. F. Kwak, “Polypyrrole: An electrochemically synthesized conducting organic polymer,” *Synth. Met.*, vol. 1, no. 3, pp. 329–336, Apr. 1980.
- [28] G. Li and P. Miao, *Theoretical Background of Electrochemical Analysis*. 2013, pp. 11–12.
- [29] S. B. Prakash, M. Urdaneta, M. Christophersen, E. Smela, and P. Abshire, “In situ electrochemical control of electroactive polymer films on a CMOS chip,” *Sensors Actuators B Chem.*, vol. 129, no. 2, pp. 699–704, Feb. 2008.
- [30] D. M. Lee, E. L. Dodson, and G. V Clatterbaugh, “Selective Electroless Nickel and Gold Plating of Individual Integrated Circuits for Thermocompression Gold Stud Bump Flip-Chip Attachment,” in *IPC APEX EXPO Proceedings*.
- [31] L. Santinacci, T. Djenizian, P. Schwaller, T. Suter, A. Etcheberry, and P. Schmuki, “Selective electrochemical gold deposition onto p-Si (1 0 0) surfaces,” *J. Phys. D. Appl. Phys.*, vol. 41, no. 17, p. 175301, Sep. 2008.
- [32] B. A. Brenner and G. E. Riddell, “Nickel Plating on Steel by Chemical Reduction,” *J. Res. Natl. Bur. Stand. (1934)*, vol. 37, no. July, pp. 31–34, 1946.
- [33] J. H. Lau, *Flip chip technologies*. McGraw-Hill, 1996, p. 565.
- [34] M. Datta, S. A. Merritt, and M. Dagenais, “Electroless remetalization of aluminum bond pads on CMOS driver chip for flip-chip attachment to vertical cavity surface emitting lasers (VCSEL’s),” *IEEE Trans. Components Packag. Technol.*, vol. 22, no. 2, pp. 299–306, Jun. 1999.
- [35] J. W. Ko, H. C. Koo, D. W. Kim, S. M. Seo, T. J. Kang, Y. Kwon, J. L. Yoon, J. H. Cheon, Y. H. Kim, J. J. Kim, and Y. J. Park, “Electroless Gold Plating on Aluminum Patterned Chips for CMOS-Based Sensor Applications,” *J. Electrochem. Soc.*, vol. 157, no. 1, p. D46, 2010.
- [36] K. Murakami, M. Hino, M. Hiramatsu, K. Osamura, and T. Kanadani, “Effect of Zincate Treatment on Adhesion of Electroless Nickel-Phosphorus Coating for Commercial Pure Aluminum,” *Mater. Trans.*, vol. 47, no. 10, pp. 2518–2523, 2006.

- [37] H. Liu, N. Li, S. Bi, and D. Li, "Gold Immersion Deposition on Electroless Nickel Substrates," *J. Electrochem. Soc.*, vol. 154, no. 12, p. D662, 2007.
- [38] G. A. Luuratsema, "Spin Coating For Rectangular Substrates," University of California, Berkeley, 1997.
- [39] K. Potje-Kamloth, "Chemical Gas Sensors Based on Organic Semiconductor Polypyrrole," *Crit. Rev. Anal. Chem.*, vol. 32, no. 2, pp. 121–140, Apr. 2002.
- [40] R. H. M. van de Leur, A. van der Waal, S. Metals, and M. Technology, "Gas and vapour detection using polypyrrole," *Synth. Met.*, vol. 102, no. 1–3, pp. 1330–1331, Jun. 1999.
- [41] R. Cabala, V. Meister, and K. Potje-Kamloth, "Effect of competitive doping on sensing properties of polypyrrole," *J. Chem. Soc. Faraday Trans.*, vol. 93, no. 1, pp. 131–137, Jan. 1997.
- [42] E. Kriván, G. Peintler, and C. Visy, "Matrix rank analysis of spectral studies on the electropolymerisation and discharge process of conducting polypyrrole/dodecyl sulfate films," *Electrochim. Acta*, vol. 50, no. 7, pp. 1529–1535, 2005.
- [43] V. Khomenko, E. Frackowiak, and F. Béguin, "Determination of the specific capacitance of conducting polymer/nanotubes composite electrodes using different cell configurations," *Electrochim. Acta*, vol. 50, no. 12, pp. 2499–2506, 2005.
- [44] U. Johanson, M. Marandi, T. Tamm, and J. Tamm, "Comparative study of the behavior of anions in polypyrrole films," *Electrochim. Acta*, vol. 50, no. 7, pp. 1523–1528, 2005.
- [45] M. M. Chehimi, M.-L. Abel, C. Perruchot, M. Delamar, S. F. Lascelles, and S. P. Armes, "The determination of the surface energy of conducting polymers by inverse gas chromatography at infinite dilution," *Synth. Met.*, vol. 104, no. 1, pp. 51–59, 1999.
- [46] S. Zafar, J. C. Poler, E. A. Irene, X. Xu, G. Haines, R. Kuehn, and J. J. Wortman, "Tunneling Current in Thin Silicon Dioxide Films," *MRS Proc.*, vol. 342, p. 325, Feb. 1994.
- [47] L. S. Juang, "TSMC 0.35um Mixed Signal 2P3M Polycide 3.3V/5V Spice Models," 1999.
- [48] P. N. Bartlett and S. K. Ling-Chung, "Conducting polymer gas sensors Part III: Results for four different polymers and five different vapours," *Sensors and Actuators*, vol. 20, no. 3, pp. 287–292, Dec. 1989.

- [49] H. S. Kang, H.-S. Kang, J. K. Lee, J. W. Lee, J. Joo, J. M. Ko, M. S. Kim, and J. Y. Lee, "Humidity-dependent characteristics of thin film poly(3,4-ethylenedioxythiophene) field-effect transistor," *Synth. Met.*, vol. 155, no. 1, pp. 176–179, Oct. 2005.
- [50] J. M. Slater, E. J. Watt, N. J. Freeman, I. P. May, D. J. Weir, and P. May, "Gas and vapour detection with poly(pyrrole) gas sensors," *Analyst*, vol. 117, no. 8, p. 1265, Jan. 1992.